Anderson transitions

Ferdinand Evers

Institut für Nanotechnologie, Forschungszentrum Karlsruhe, 76021 Karlsruhe, Germany and Institut für Theorie der Kondensierten Materie, Universität Karlsruhe, 76128 Karlsruhe, Germany

Alexander D. Mirlin

Institut für Nanotechnologie, Forschungszentrum Karlsruhe, 76021 Karlsruhe, Germany; Institut für Theorie der Kondensierten Materie, Universität Karlsruhe, 76128 Karlsruhe, Germany; and Petersburg Nuclear Physics Institute, 188300 St. Petersburg, Russia

(Published 17 October 2008)

The physics of Anderson transitions between localized and metallic phases in disordered systems is reviewed. The term "Anderson transition" is understood in a broad sense, including both metal-insulator transitions and quantum-Hall-type transitions between phases with localized states. The emphasis is put on recent developments, which include multifractality of critical wave functions, criticality in the power-law random banded matrix model, symmetry classification of disordered electronic systems, mechanisms of criticality in quasi-one-dimensional and two-dimensional systems and survey of corresponding critical theories, network models, and random Dirac Hamiltonians. Analytical approaches are complemented by advanced numerical simulations.

DOI: 10.1103/RevModPhys.80.1355 PACS number(s): 71.30.+h, 73.43.−f, 72.15.Rn, 73.20.Fz

CONTENTS

I. INTRODUCTION

It has been known since the seminal work of Anderson (1958) that disorder can localize a quantum particle inspite of quantum tunneling processes and even if the particle is not localized classically. For a given energy and disorder strength the quantum states are either all localized or all delocalized. This implies the existence of transitions between localized and metallic phases in disordered electronic systems, known as *Anderson transitions*. Great progress in understanding the corresponding physics was achieved in the 1970s and 1980s, due to the developments of scaling theory and field-theoretical approaches to localization, which demonstrated connections between the Anderson transition and conventional second-order phase transitions. These results were summarized in several review articles (Lee and Ramakrishnan, 1985; Kramer and MacKinnon, 1993) and in the context of the quantum Hall transitions (Huckestein, 1995), as well as by Efetov (1997).

During the last 10 years considerable progress has been made in several research directions. This has advanced our understanding of the Anderson localization phenomenon and the associated quantum phase transition physics in disordered electronic systems and allows us to view it nowadays in a considerably broader and more general context. These advances have motivated us in writing the present review. While the paper will also include a brief overview of earlier results, the main emphasis will be on recent developments and, in particular, on novel types of critical systems. In this paper we understand the term "Anderson transition" in a broad sense, including not only metal-insulator transitions but also critical points separating phases with localized states (most prominently, quantum-Hall-type transitions). We focus on noninteracting systems and only briefly touch the interaction issues in Secs. VI.C.10 and VII.A. We now list the key developments in the field that took place during the last decade and constitute the main subject of the paper.

A. Symmetry classification and universality classes

Within the early classification scheme, three universality classes for the Anderson transition were identified—orthogonal, unitary, and symplectic—in correspondence with the Wigner-Dyson classification of random matrix theory (RMT) ensembles. Two basic symmetries of this scheme are the invariance of the Hamiltonian under time reversal and spin rotations. More recent research has shown, however, that this picture is in fact by far incomplete for two reasons: (i) there exist more symmetry classes of disordered systems, and (ii) in many cases, the symmetry class does not uniquely determine the universality class of the transition.

1. Additional symmetries

It has been understood that a complete set of random matrix theories includes, in addition to the three Wigner-Dyson classes, three chiral ensembles and four Bogoliubov–de Gennes ensembles. The additional ensembles are characterized by one of the additional symmetries—the *chiral* or the *particle-hole* one. The field theories (σ models) associated with these new symmetry classes have in fact been considered in the 1980s (Hikami, 1983; Oppermann, 1987, 1990; Wegner, 1989). However, it was only after their physical significance had been better understood that the new symmetry classes were studied systematically. For the chiral ensembles, important contributions in this direction were made by Gade and Wegner (1991), Gade (1993), Slevin and Nagao (1993), and Verbaarschot and Zahed (1993). The particle-hole symmetric ensembles were identified several years later (Altland and Zirnbauer, 1997). Zirnbauer has also established a relation between random matrix theories, σ models, and Cartan's classification of symmetric spaces (Sec. IV), which provides the mathematical basis for the completeness statement of the new random matrix classification (Zirnbauer, 1996; Heinzner *et al.*, 2005).

Among other things, these developments have led theorists to predict two novel quantum Hall effects, the spin quantum Hall effect (SQHE) (Senthil *et al.*, 1998; Kagalovsky *et al.*, 1999), Sec. VI.D, and the thermal quantum Hall effect (TQHE) (Senthil *et al.*, 1999; Chalker *et al.*, 2002), Sec. VI.E. Both should occur in materials with paired fermions where the particle-hole symmetry is realized.

2. From symmetry classes to universality classes

The classification of fixed points governing localization transitions in disordered metals has turned out to be much richer than that of symmetries of random matrix ensembles (or field theories). The first prominent example of this was in fact given more than 20 years ago by Pruisken (1984) who showed that the quantum Hall transition is described by a σ model with an additional, topological, term. However, it is only recently that a variety of criticality types—particularly rich in two-dimensional (2D) systems—was fully appreciated.

(i) In several symmetry classes, the field theory (σ model) allows for inclusion of the topological θ term (responsible for the quantum Hall criticality) or the Wess-Zumino (WZ) term.

(ii) The phase diagram may depend on the type of disorder. The class D represents a prominent example, with three different network-model realizations yielding vastly different phase diagrams, Sec. VI.E.

(iii) In some cases, the field theory may possess a line of fixed points, since the coupling constant corresponding to the conductivity is truly marginal. This situation is in particular realized in the chiral symmetry classes BDI, AIII, and CII, Sec. VI.F.

(iv) In some cases, the symmetry of the σ model may be enhanced under renormalization, so that the ultimate fixed-point theory may have a different form. A paradigm for this behavior is provided by the S^2 sphere σ model with $\theta=\pi$ topological term (describing a spin-$\frac{1}{2}$ antiferromagnet) which flows into a SU(2) Wess-Zumino-Witten (WZW) model. It was conjectured that a similar mechanism may be relevant to some σ models of localization, including the critical theory of the integer quantum Hall effect (IQHE).

(v) It is possible that the same critical theory is shared by systems belonging to different symmetry classes. This type of "superuniversality" has been proposed to occur in disordered wires with critical states, Secs. V.E and V.F.

(vi) It was recently discovered that Griffiths effects can render the conventional renormalization-group (RG) analysis of a σ model insufficient. In the framework of the RG calculations the result can be recovered if infinitely many relevant couplings are kept, Sec. VI.F.2.

3. Many-channel disordered wires

Common wisdom has it that all states in one-dimensional disordered systems are localized. However, for several symmetry classes wires with critical states and even such with perfectly transmitting eigenchannels were identified recently. The emergence of criticality depends crucially on whether the number of channels is even or odd. These developments make a survey of disordered wires (Sec. V) a natural part of this paper.

B. Multifractality of wave functions

It was appreciated by the early 1990s that wave functions at the Anderson transition exhibit strong amplitude fluctuations that can be characterized as wave-function multifractality. The corresponding results have been summarized in review papers (Janßen, 1994; Huckestein, 1995) published about a decade ago. In more recent years considerable progress in understanding wave-

function statistics in metallic samples (Mirlin, 2000b) and at criticality (Mudry *et al.*, 1996; Evers and Mirlin, 2000; Evers *et al.*, 2001) has been achieved. Multifractality implies the presence of infinitely many relevant operators, which is a peculiarity of the Anderson transition, and the spectrum of multifractal exponents constitutes an important characteristic of the corresponding fixed point. Understanding the general properties of the statistics of critical wave functions and their multifractality (Sec. II.C) was complemented by a detailed study—analytical and numerical—for a number of localization critical points, such as conventional Anderson transitions in various dimensionalities, Dirac fermions in a random vector potential, IQHE, SQHE, and symplectic-class Anderson transition in 2D, as well as the power-law random banded matrix (PRBM) model.

In several situations, characterization of a critical point by its multifractality spectrum has turned out to be particularly important. Specifically, much of recent research activity has been devoted to conformal theories governing Anderson critical points in 2D systems. Further, in systems of the new symmetry classes, peculiar critical points have been found that correspond to strong disorder (Carpentier and LeDoussal, 2001; Motrunich *et al.*, 2002), such that critical wave functions show at the same time some kind of localization. Entrance of a system into such a strong-coupling regime manifests itself as a phase transition in the multifractality spectrum (the "freezing transition").

Finally, the notion of multifractality was recently extended onto a boundary of a critical system, yielding an independent set of surface critical exponents. The importance of this notion has been confirmed by analytical and numerical studies of the surface multifractality for several models at criticality (Sec. II.C.8).

C. Quantitative understanding of critical behavior

For several types of Anderson transitions, detailed studies using both analytical and numerical tools have been performed during the last few years. As a result, a fairly comprehensive quantitative understanding of the localization critical phenomena has been achieved. The following developments played a particularly important role in this context.

1. Power-law random banded matrix model

The PRBM model, which can be viewed as a 1D system with long-range hopping, has been analytically solved on its critical line (Mirlin and Evers, 2000). This allowed, in particular, a detailed study of the wave-function and energy-level statistics at criticality, Sec. III. The PRBM model serves as a "toy model" for the Anderson criticality. This model possesses a truly marginal coupling, thus yielding a line of critical points and allowing one to study the evolution of critical properties in the whole range from weak- to strong-coupling fixed points.

2. Network models

Formulation of quantum dynamics at the Anderson transition in terms of a network model was proposed by Shapiro (1982). Later, chiral network models, introduced by Chalker and Coddington (1988) in the IQHE context, were systematically exploited for both analytical studies and computer simulations. Such network models have played a key role in advancing our understanding of quantum Hall critical points, including the conventional IQHE and the systems of unconventional symmetries—SQHE and TQHE (Cho and Fisher, 1997a; Gruzberg *et al.*, 1999; Read and Ludwig, 2001; Chalker *et al.*, 2002). In particular, investigation of the network model of SQHE has led to an analytical understanding of the critical behavior for a number of important physical observables, Sec. VI.D.

3. Progress in numerical simulations

During the last 10 years numerical mathematicians have developed highly efficient routines for diagonalizing sparse matrices. Combined with the increase in computer power and an improved understanding of finite-size effects, this development has recently paved the way for highly accurate numerical studies of critical behavior for a variety of Anderson critical points.

4. Field theories: σ models and Dirac fermions

The development of the symmetry classification of disordered systems has allowed one to classify the corresponding field theories having a form of nonlinear σ models defined on different symmetric spaces. The RG method was used to analyze them at and near two dimensions. A complementary approach is based on the analysis of 2D disordered Dirac fermions subjected to different types of disorder (Ludwig *et al.*, 1994; Nersesyan *et al.*, 1995), Sec. VI.G. Analytical methods have allowed one to identify fixed points and determine the critical behavior for some types of disorder corresponding to unconventional symmetry classes. Interest on random Dirac fermion models has been largely motivated by their applications to disordered d-wave superconductors, see Altland *et al.* (2002) for a review. Recent breakthrough in the fabrication of monoatomic graphene sheets and corresponding transport measurements (Novoselov *et al.*, 2004, 2005; Zhang *et al.*, 2005) have greatly boosted the theoretical activity in this field.

II. ANDERSON TRANSITIONS IN CONVENTIONAL SYMMETRY CLASSES

A. Scaling theory, observables, and critical behavior

Quantum interference can completely suppress diffusion of a particle in a random potential, a phenomenon known as *Anderson localization* (Anderson, 1958). When the energy or disorder strength is varied, the system can undergo a transition from the metallic phase with delocalized eigenstates to the insulating phase,

where eigenfunctions are exponentially localized,

$$|\psi^2(\mathbf{r})| \sim \exp(-|\mathbf{r}-\mathbf{r}_0|/\xi), \tag{2.1}$$

and ξ is the localization length. The character of this transition remained, however, unclear for roughly 20 years, until Wegner conjectured, developing earlier ideas of Thouless (1974), a close connection between the Anderson transition and the scaling theory of critical phenomena (Wegner, 1976). Three years later, Abrahams, Anderson, Licciardello, and Ramakrishnan formulated a *scaling theory* of localization (Abrahams *et al.*, 1979), which describes the flow of the dimensionless conductance g with the system size L,

$$d\ln g/d\ln L = \beta(g). \tag{2.2}$$

This phenomenological theory was put on a solid basis after Wegner discovered the field-theoretical description of the localization problem in terms of a nonlinear σ model (Wegner, 1979), Sec. II.B. This paved the way for the resummation of singularities in perturbation theory at or near two dimensions (Gor'kov *et al.*, 1979; Vollhardt and Wölfle, 1980) and allowed one to cast the scaling in the systematic form of a field-theoretical RG. A microscopic derivation of the σ model (Efetov *et al.*, 1980; Jüngling and Oppermann, 1980; Schaefer and Wegner, 1980) has completed a case for it as the field theory of the Anderson localization.

To analyze the transition, one starts from the Hamiltonian $\hat{H}$ consisting of the free part $\hat{H}_0$ and the disorder potential $U(\mathbf{r})$:

$$\hat{H} = \hat{H}_0 + U(\mathbf{r}), \quad \hat{H}_0 = \hat{\mathbf{p}}^2/2m. \tag{2.3}$$

The disorder is defined by the correlation function $\langle U(\mathbf{r})U(\mathbf{r}')\rangle$; we assume it to be of the white-noise type for definiteness,

$$\langle U(\mathbf{r})U(\mathbf{r}')\rangle = (2\pi\rho\tau)^{-1}\delta(\mathbf{r}-\mathbf{r}'). \tag{2.4}$$

Here ρ is the density of states, τ the mean free time, $\langle\cdots\rangle$ denotes the disorder average, and we set $\hbar=1$. It may be shown that models with finite-range and/or anisotropic disorder correlations are equivalent with respect to the long-time and long-distance behavior (hydrodynamics) to the white-noise model with renormalized parameters (tensor of diffusion coefficients) (Wölfle and Bhatt, 1984).

More convenient for numerical simulations is the lattice version of Eqs. (2.3) and (2.4) known as the Anderson tight-binding model,

$$\hat{H} = t\sum_{\langle ij\rangle} c_i^\dagger c_j + \sum_i u_i c_i^\dagger c_i, \tag{2.5}$$

where the sum $\langle ij\rangle$ goes over nearest-neighbor sites and the random site energies u_i are chosen from some distribution $\mathcal{P}(u)$; the standard choice is the uniform distribution over an interval $[-W/2;W/2]$ (box distribution).

The physical observables whose scaling at the transition point is of primary importance is the localization length ξ on the insulating side (say, $E<E_c$) and the dc conductivity σ on the metallic side ($E>E_c$),

$$\xi \propto (E_c-E)^{-\nu}, \quad \sigma \propto (E-E_c)^s. \tag{2.6}$$

The corresponding critical indices ν and s satisfy the scaling relation $s=\nu(d-2)$, first derived by Wegner (1976).

On a technical level, the transition manifests itself in a change of the behavior of the diffusion propagator,

$$\Pi(\mathbf{r}_1,\mathbf{r}_2;\omega) = \langle G^R_{E+\omega/2}(\mathbf{r}_1,\mathbf{r}_2)G^A_{E-\omega/2}(\mathbf{r}_2,\mathbf{r}_1)\rangle, \tag{2.7}$$

where $\langle\cdots\rangle$ denotes the disorder averaging and G^R, G^A are retarded and advanced Green's functions,

$$G^{R,A}_E(\mathbf{r},\mathbf{r}') = \langle\mathbf{r}|(E-\hat{H}\pm i\eta)^{-1}|\mathbf{r}'\rangle, \quad \eta\to+0. \tag{2.8}$$

In the delocalized regime Π has the familiar diffusion form (in the momentum space),

$$\Pi(\mathbf{q},\omega) = 2\pi\rho(E)/(Dq^2-i\omega), \tag{2.9}$$

where ρ is the density of states (DOS) and D is the diffusion constant, related to the conductivity via the Einstein relation $\sigma=e^2\rho D$. In the insulating phase, the propagator ceases to have the Goldstone form (2.9) and becomes massive,

$$\Pi(\mathbf{r}_1,\mathbf{r}_2;\omega) \simeq \frac{2\pi\rho}{-i\omega}\mathcal{F}(|\mathbf{r}_1-\mathbf{r}_2|/\xi), \tag{2.10}$$

with the function $\mathcal{F}(\mathbf{r})$ decaying exponentially on the scale of the localization length, $\mathcal{F}(r/\xi)\sim\exp(-r/\xi)$. It is worth emphasizing that the localization length ξ obtained from the averaged correlation function $\Pi=\langle G^RG^A\rangle$, Eq. (2.7), is in general different from the one governing the exponential decay of the typical value $\Pi_{\rm typ}=\exp\langle\ln G^RG^A\rangle$. For example, in quasi-1D systems the two lengths differ by a factor of 4. However, this is usually not important for the definition of the critical index ν.[1] We will return to observables that are related to critical fluctuations of wave functions and discuss the corresponding family of critical exponents in Sec. II.C.

B. Field-theoretical description

1. Effective field theory: Nonlinear σ model

In the original derivation of the σ model (Wegner, 1979; Efetov *et al.*, 1980; Jüngling and Oppermann, 1980; Schaefer and Wegner, 1980), the replica trick was used to perform the disorder averaging. Within this approach, n copies of the system are considered, with fields ϕ_α, $\alpha=1,\ldots,n$ describing the particles, and the replica limit $n\to0$ is taken in the end. The resulting σ model is defined on the $n\to0$ limit of either noncompact or compact symmetric space, depending on whether the fields ϕ_α are considered as bosonic or fermionic. As an example, for the unitary symmetry class (A), which corresponds to a system with broken time-reversal invariance, the σ-model target manifold is $\mathrm{U}(n,n)/\mathrm{U}(n)\times\mathrm{U}(n)$ in the first case and $\mathrm{U}(2n)/\mathrm{U}(n)\times\mathrm{U}(n)$ in the second case,

[1] An exception is the behavior of ξ in disordered wires of the chiral symmetry, see Eqs. (5.20) and (5.21).

with $n \to 0$. A supersymmetric formulation given by Efetov (1983) combines fermionic and bosonic degrees of freedom, with the field Φ becoming a supervector. The resulting σ model is defined on a supersymmetric coset space, e.g., $U(1,1|2)/U(1|1) \times U(1|1)$ for the unitary class. This manifold combines compact and noncompact features and represents a product of the hyperboloid $H^2 = U(1,1)/U(1) \times U(1)$ and the sphere $S^2 = U(2)/U(1) \times U(1)$ "dressed" by anticommuting (Grassmannian) variables. For a detailed presentation of the supersymmetry formalism and its applications to mesoscopic systems, see Efetov (1983, 1997); Verbaarschot *et al.* (1985); Fyodorov (1995); Fyodorov and Sommers (1997); Guhr *et al.* (1998); Mirlin (2000a, 2000b); Zirnbauer (2004). While equivalent to the replica version on the level of the perturbation theory (including its RG resummation), the supersymmetry formalism also allows for a nonperturbative treatment of the theory, which is important for the analysis of the energy level and eigenfunction statistics, properties of quasi-1D systems, topological effects, etc.

We sketch the key steps in the conventional derivation of the σ model; to be specific, we consider the unitary symmetry class. One begins by expressing the product of the retarded and advanced Green's functions in terms of the integral over a supervector field $\Phi = (S_1, \chi_1, S_2, \chi_2)$:

$$G^R_{E+\omega/2}(\mathbf{r_1},\mathbf{r_2}) G^A_{E-\omega/2}(\mathbf{r_2},\mathbf{r_1}) = \int D\Phi D\Phi^\dagger S_1(\mathbf{r_1}) S_1^*(\mathbf{r_2}) S_2(\mathbf{r_2}) S_2^*(\mathbf{r_1}) \times \exp\left\{ i \int d\mathbf{r} \Phi^\dagger(\mathbf{r}) \left[(E - \hat{H})\Lambda + \frac{\omega}{2} + i\eta \right] \Phi(\mathbf{r}) \right\}, \tag{2.11}$$

where $\Lambda = \mathrm{diag}\{1,1,-1,-1\}$. After disorder averaging, the resulting quartic term is decoupled via the Hubbard-Stratonovich transformation by introducing a 4×4 supermatrix variable $\mathcal{R}_{\mu\nu}(\mathbf{r})$ conjugate to the tensor product $\Phi_\mu(\mathbf{r})\Phi^\dagger_\nu(\mathbf{r})$. Integrating out the Φ fields, one gets the action in terms of the $\mathcal{R}$ fields,

$$S[\mathcal{R}] = \pi\rho\tau \int d^d\mathbf{r}\, \mathrm{Str}\, \mathcal{R}^2 + \mathrm{Str}\, \ln\left[E + \left(\frac{\omega}{2} + i\eta \right)\Lambda - \hat{H}_0 - \mathcal{R} \right], \tag{2.12}$$

where Str denotes the supertrace. The next step is to use the saddle-point approximation, which leads to the following equation for $\mathcal{R}$:

$$\mathcal{R}(\mathbf{r}) = (2\pi\rho\tau)^{-1} \langle \mathbf{r} | (E - \hat{H}_0 - \mathcal{R})^{-1} | \mathbf{r} \rangle. \tag{2.13}$$

The relevant set of the solutions (the saddle-point manifold) has the form

$$\mathcal{R} = \Sigma \cdot I - (i/2\tau) Q, \tag{2.14}$$

where I is the unity matrix, Σ is a constant, and the 4×4 supermatrix $Q = T^{-1}\Lambda T$ satisfies the condition $Q^2 = 1$ and belongs to the σ-model target space described above. Finally, one performs the gradient expansion of the second term in Eq. (2.12), for $\mathcal{R}$ having the form (2.14) with a slowly varying $Q(\mathbf{r})$. The expression for the propagator Π, Eq. (2.7), is then given by

$$\Pi(\mathbf{r_1},\mathbf{r_2};\omega) = \int DQ Q^{bb}_{12}(\mathbf{r_1}) Q^{bb}_{21}(\mathbf{r_2}) e^{-S[Q]}, \tag{2.15}$$

where $S[Q]$ is the σ-model action

$$S[Q] = \frac{\pi\rho}{4} \int d^d\mathbf{r}\, \mathrm{Str}[-D(\nabla Q)^2 - 2i\omega\Lambda Q]. \tag{2.16}$$

The size 4 of the matrix is due to (i) two types of Green's functions (advanced and retarded), and (ii) the necessity to introduce bosonic and fermionic degrees of freedom to represent these Green's functions in terms of a functional integral. The matrix Q consists thus of four 2×2 blocks according to its advanced-retarded structure, each of them a supermatrix in the boson-fermion space. In particular, Q^{bb}_{12} is the boson-boson element of the RA block, and so on. One can also consider an average of the product of n retarded and n advanced Green's functions, which will generate a σ model defined on a larger manifold, the base of which is a product of $U(n,n)/U(n) \times U(n)$ and $U(2n)/U(n) \times U(n)$ (these are the same structures as in the replica formalism, but now without the $n \to 0$ limit).

For other symmetry classes, the symmetry of the σ model is different but the general picture is the same. For example, for the orthogonal class (AI) the 8×8 Q matrices span the manifold whose base is the product of the noncompact space $O(2,2)/O(2) \times O(2)$ and the compact space $Sp(4)/Sp(2) \times Sp(2)$. The σ-model symmetric spaces for all the classes (Wigner-Dyson as well as unconventional) are given in Sec. IV.

2. RG in $2+\epsilon$ dimensions; ϵ expansion

The σ model is the effective low-momentum, low-frequency theory of the problem, describing the dynamics of interacting soft modes—diffusons and cooperons. Its RG treatment yields a flow equation of the form (2.2), thus justifying the scaling theory of localization. The β function $\beta(t) \equiv -dt/d\ln L$ can be calculated perturbatively in the coupling constant t inversely proportional to the dimensionless (measured in units of e^2/h) conductance, $t = 1/2\pi g$.[2] This allows one to get the ϵ expansion for the critical exponents in $2+\epsilon$ dimensions, where the transition occurs at $t_* \ll 1$. In particular, for the orthogonal symmetry class (AI) one finds (Wegner, 1989)

$$\beta(t) = \epsilon t - 2t^2 - 12\zeta(3)t^5 + O(t^6). \tag{2.17}$$

The transition point t_* is given by the zero of the $\beta(t)$,

[2]For spinful systems, g does not include summation over spin projections.

$$t_* = \epsilon/2 - (3/8)\zeta(3)\epsilon^4 + O(\epsilon^5). \quad (2.18)$$

The localization length exponent ν is determined by the derivative

$$\nu = -1/\beta'(t_*) = \epsilon^{-1} - (9/4)\zeta(3)\epsilon^2 + O(\epsilon^3), \quad (2.19)$$

and the conductivity exponent s is

$$s = \nu\epsilon = 1 - (9/4)\zeta(3)\epsilon^3 + O(\epsilon^4). \quad (2.20)$$

Numerical simulations of localization on fractals with dimensionality slightly above 2 give the behavior of ν that is in good agreement with Eq. (2.19) (Schreiber and Grussbach, 1996). For the unitary symmetry class (A), the corresponding results read

$$\beta(t) = \epsilon t - 2t^3 - 6t^5 + O(t^7), \quad (2.21)$$

$$t_* = \left(\frac{\epsilon}{2}\right)^{1/2} - \frac{3}{2}\left(\frac{\epsilon}{2}\right)^{3/2} + O(\epsilon^{5/2}), \quad (2.22)$$

$$\nu = \frac{1}{2\epsilon} - \frac{3}{4} + O(\epsilon), \quad s = \frac{1}{2} - \frac{3}{4}\epsilon + O(\epsilon^2). \quad (2.23)$$

In 2D (ϵ=0) the fixed point t_* in both cases becomes zero: $\beta(t)$ is negative for any $t>0$, implying that all states are localized. The situation is qualitatively different for the third Wigner-Dyson class—the symplectic one. The corresponding β function is related to that for the orthogonal class via $\beta_{\mathrm{Sp}}(t) = -2\beta_{\mathrm{O}}(-t/2)$, yielding[3]

$$\beta(t) = \epsilon t + t^2 - (3/4)\zeta(3)t^5 + O(t^6). \quad (2.24)$$

In 2D the β function (2.24) is positive at sufficiently small t, implying the existence of a truly metallic phase at $t<t_*$, with an Anderson transition at $t_* \sim 1$, Sec. VI.B. This peculiarity of the symplectic class represents one of the mechanisms for the emergence of criticality in 2D, see Sec. VI.A. The results for the β functions in all symmetry classes are given in Sec. IV.F.

3. Additional comments

A few interrelated comments are in order here.

(i) *ϵ expansion vs 3D exponents.* The ϵ expansion is of asymptotic character, yielding numerically accurate values for the critical exponents only in the limit of small ϵ. It is thus not surprising that, if Eqs. (2.19) and (2.20) are used to estimate the indices in 3D (ϵ=1), the best thing is to keep only the leading (one-loop) term, yielding a quite substantial error [ν=1 instead of $\nu \simeq 1.57 \pm 0.02$ (Slevin and Ohtsuki, 1999) known from numerical simulations]. Rather unexpectedly, the agreement turns out to be remarkably good for the multifractal exponents, see Sec. II.C.6. Independent of the accuracy of these numbers, the ϵ expansion plays a major role in understanding the qualitative properties of the transition.

(ii) *Composite operators.* The RG can also be used to calculate the scaling dimensions of composite operators. In particular, operators of the type $(Q\Lambda)^n$ determine multifractal fluctuations of wave functions at criticality, see Sec. II.C. Another class of operators—those with high derivatives $(\nabla Q)^{2n}$—were studied by Kravtsov *et al.* (1988) and Lerner and Wegner (1990) and found to have the scaling dimensions

$$y_n = d - 2n + 2t_* n(n-1) + O(t_*^2), \quad (2.25)$$

where t_* is given by Eq. (2.18) for the orthogonal class and Eq. (2.22) for the unitary class. The fact that the one-loop result (2.25) becomes positive for a sufficiently large number of gradients $n > t_*^{-1}$ (suggesting that the corresponding operators are relevant and might drive the system into an unknown fixed point) has launched a debate about the stability of the σ model and the one-parameter scaling. This question is not specific to the localization problem but is equally applicable to a broader class of σ models, including the O(n) model of a Heisenberg ferromagnet (Wegner, 1990; Castilla and Chakravarty, 1993). It was, however, pointed out by Brezin and Hikami (1997) and Derkachov and Manashov (1997) that since the expansion (2.25) is asymptotic and its true parameter is $t_* n$, the behavior of the one-loop result at $t_* n \gtrsim 1$ does not allow one to make any reliable conclusions.

(iii) *Order parameter.* In view of the analogy with continuous thermodynamic phase transitions, it is natural to ask what is the order parameter for the Anderson transition. While naively Eq. (2.16) suggests that it is the expectation value of Q, the latter is in fact uncritical. To describe the transition in terms of symmetry breaking, one has to introduce an order parameter function (OPF) $F(Q)$ resulting from integrating out Q fields at all points except one ($\mathbf{r_0}$), with $Q(\mathbf{r_0}) \equiv Q$ (Zirnbauer, 1986a, 1986b; Efetov, 1987). One can also introduce an OPF $F(\Phi)$ with similar properties within the supervector formalism (Mirlin and Fyodorov, 1991). It was shown (Mirlin and Fyodorov, 1994a, 1994b) that the OPF is closely related to the distribution of one-site Green's functions, in particular local density of states (LDOS), and wave-function amplitudes. In the framework of scattering theory, this suggests an interpretation of the Anderson transition as a phenomenon of spontaneous breakdown of S-matrix unitarity (Fyodorov, 2003).

(iv) *Upper critical dimension.* For conventional critical phenomena, there exists an upper critical dimension d_c above which the transition is governed by a Gaussian fixed point, with exponents being d

[3]Here $t = 1/\pi g$, where g is the total conductance of the spinful system.

independent and given by their mean-field values. As a consequence, an ϵ expansion near d_c (in the most standard case, in $4-\epsilon$ dimensions) exists, alternative to the $2+\epsilon$ expansion. One can ask whether this is also the case for the Anderson localization transition. The answer is negative: there is no conventional mean-field theory for the Anderson transition, and it was argued that the the upper critical dimension is $d_c=\infty$ (Mirlin and Fyodorov, 1994a, 1994b). The closest existing analog of the mean-field theory is the model on the Bethe lattice corresponding to $d=\infty$; see Sec. II.D.

C. Critical wave functions: Multifractality

1. Scaling of inverse participation ratios

Multifractality of wave functions, describing their strong fluctuations at criticality, is a striking feature of the Anderson transitions (Wegner, 1980; Castellani and Peliti, 1986). Multifractality as a concept was introduced by Mandelbrot (1974). Multifractal structures are characterized by an infinite set of critical exponents describing the scaling of the moments for some distribution. This feature has been observed in various complex objects, such as the energy dissipating set in turbulence, strange attractors in chaotic dynamical systems, and the growth probability distribution in diffusion-limited aggregation. For the present problem, the underlying normalized measure is $|\psi^2(\mathbf{r})|$ and the corresponding moments are the inverse participation ratios (IPRs),[4]

$$P_q = \int d^d\mathbf{r}|\psi(\mathbf{r})|^{2q}. \tag{2.26}$$

At criticality, P_q show an anomalous scaling with system size L,

$$\langle P_q\rangle = L^d\langle|\psi(\mathbf{r})|^{2q}\rangle \sim L^{-\tau_q}, \tag{2.27}$$

governed by a continuous set of exponents τ_q. One often introduces fractal dimensions D_q via $\tau_q=D_q(q-1)$. In a metal $D_q=d$, in an insulator $D_q=0$, while at a critical point D_q is a nontrivial function of q, implying wave-function multifractality. Splitting off the normal part, one defines the anomalous dimensions Δ_q,

$$\tau_q \equiv d(q-1)+\Delta_q, \tag{2.28}$$

which distinguish the critical point from the metallic phase and determine the scale dependence of the wave-function correlations. Among them, $\Delta_2\equiv-\eta$ plays the most prominent role, governing the spatial correlations of the intensity $|\psi|^2$,

$$L^{2d}\langle|\psi^2(\mathbf{r})\psi^2(\mathbf{r}')|\rangle \sim (|\mathbf{r}-\mathbf{r}'|/L)^{-\eta}. \tag{2.29}$$

Equation (2.29) can be obtained from Eq. (2.27) using the fact that the wave-function amplitudes become essentially uncorrelated at $|\mathbf{r}-\mathbf{r}'|\sim L$. Scaling behavior of higher-order correlations, $\langle|\psi^{2q_1}(\mathbf{r_1})\psi^{2q_2}(\mathbf{r_2})\cdots\psi^{2q_n}(\mathbf{r}_n)|\rangle$, can be found in a similar way, e.g.,

$$L^{d(q_1+q_2)}\langle|\psi^{2q_1}(\mathbf{r_1})\psi^{2q_2}(\mathbf{r_2})|\rangle \sim L^{-\Delta_{q_1}-\Delta_{q_2}}(|\mathbf{r_1}-\mathbf{r_2}|/L)^{\Delta_{q_1+q_2}-\Delta_{q_1}-\Delta_{q_2}}. \tag{2.30}$$

Correlations of two different (but close in energy) eigenfunctions exhibit the same scaling (Chalker, 1990),

$$\left.\begin{aligned} L^{2d}\langle|\psi_i^2(\mathbf{r})\psi_j^2(\mathbf{r}')|\rangle \\ L^{2d}\langle\psi_i(\mathbf{r})\psi_j^*(\mathbf{r})\psi_i^*(\mathbf{r}')\psi_j(\mathbf{r}')\rangle \end{aligned}\right\} \sim \left(\frac{|\mathbf{r}-\mathbf{r}'|}{L_\omega}\right)^{-\eta}, \tag{2.31}$$

where $\omega=\epsilon_i-\epsilon_j$, $L_\omega\sim(\rho\omega)^{-1/d}$, ρ is the density of states, and $|\mathbf{r}-\mathbf{r}'|<L_\omega$. For conventional classes, where the DOS is uncritical, the diffusion propagator (2.7) scales in the same way.

In the field-theoretical language (Sec. II.B), Δ_q are the leading anomalous dimensions of the operators $\mathrm{Tr}(Q\Lambda)^q$ [or, more generally, $\mathrm{Tr}(Q\Lambda)^{q_1}\cdots\mathrm{Tr}(Q\Lambda)^{q_m}$ with $q_1+\cdots+q_m=q$] (Wegner, 1980). Strong multifractal fluctuations of wave functions at criticality are related to the fact that $\Delta_q<0$ for $q>1$, so that the corresponding operators increase under RG. In this formalism, the scaling of correlation functions [Eq. (2.29) and its higher-order generalizations] results from an operator product expansion (Wegner, 1985; Duplantier and Ludwig, 1991; Mudry *et al.*, 1996).

2. Singularity spectrum $f(\alpha)$

The average IPR $\langle P_q\rangle$ are (up to the normalization factor L^d) the moments of the distribution function $\mathcal{P}(|\psi|^2)$ of the eigenfunction intensities. The behavior (2.27) of the moments corresponds to the intensity distribution function of the form

$$\mathcal{P}(|\psi^2|) \sim \frac{1}{|\psi^2|}L^{-d+f(-\ln|\psi^2|/\ln L)} \tag{2.32}$$

Indeed, calculating the moments $\langle|\psi^{2q}|\rangle$ with the distribution function (2.32), one finds

$$\langle P_q\rangle = L^d\langle|\psi^{2q}|\rangle \sim \int d\alpha L^{-q\alpha+f(\alpha)}, \tag{2.33}$$

where $\alpha=-\ln|\psi^2|/\ln L$. Evaluation of the integral by the saddle-point method (justified in the limit of large L) reproduces the result (2.27), with the exponent τ_q related to the singularity spectrum $f(\alpha)$ via the Legendre transformation,

[4]Strictly speaking, P_q as defined by Eq. (2.26) diverges for negative q ($q\le-1/2$ for real ψ and $q\le-3/2$ for complex ψ) because of the zeros of wave functions related to their oscillations on the scale of the wavelength. To find τ_q for such negative q, one should smooth $|\psi^2|$ by averaging over some microscopic volume (block of several neighboring sites in the discrete version).

$$\tau_q = q\alpha - f(\alpha), \quad q = f'(\alpha), \quad \alpha = \tau_q'. \tag{2.34}$$

The meaning of the function $f(\alpha)$ is as follows: it is the fractal dimension of the set of those points $\mathbf{r}$ where the eigenfunction intensity is $|\psi^2(\mathbf{r})| \sim L^{-\alpha}$. In other words, in a lattice version of the model the number of such points scales as $L^{f(\alpha)}$ (Halsey *et al.*, 1986).

General properties of τ_q and $f(\alpha)$ follow from their definitions and the wave-function normalization:

(i) τ_q is a nondecreasing, convex function ($\tau_q' \geq 0$, $\tau_q'' \leq 0$), with $\tau_0 = -d$, $\tau_1 = 0$; and

(ii) (ii) $f(\alpha)$ is a convex function [$f''(\alpha) \leq 0$] defined on the semiaxis $\alpha \geq 0$ with a maximum at point α_0 (corresponding to $q=0$ under the Legendre transformation) and $f(\alpha_0) = d$. Further, for the point α_1 (corresponding to $q=1$) we have $f(\alpha_1) = \alpha_1$ and $f'(\alpha_1) = 1$.

If one formally defines $f(\alpha)$ for a metal, it will be concentrated in a single point $\alpha = d$, with $f(d) = d$ and $f(\alpha) = -\infty$ otherwise. On the other hand, at criticality this "needle" broadens and the maximum shifts to a position $\alpha_0 > d$, see Fig. 1.

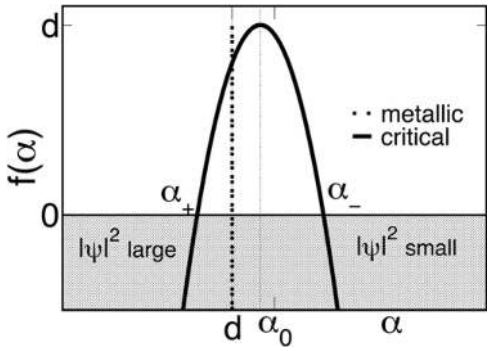

FIG. 1. Schematic plot of the multifractal spectrum $f(\alpha)$. A metal is represented by a "needle," i.e., $f(\alpha)$ having zero width, at $\alpha = d$. At criticality $f(\alpha)$ acquires a finite width and the apex shifts to $\alpha_0 > d$. The negative parts of $f(\alpha)$ (gray area) correspond to rare events—values of the wave-function amplitude that typically do not occur in a single sample.

3. Weak multifractality: Approximately parabolic spectrum

One situation in which the τ_q spectrum can be evaluated analytically is the regime of weak multifractality, when the critical point is, in a sense, close to a metal. This happens, in particular, for the Anderson transition in $2+\epsilon$ dimensions with $\epsilon \ll 1$, see Sec. II.C.6, and in the PRBM model with $b \gg 1$, see Sec. III.B. In this situation, one finds generically a spectrum of the form

$$\tau_q \simeq d(q-1) - \gamma q(q-1), \quad \gamma \ll 1, \tag{2.35}$$

i.e., the anomalous dimension $\Delta_q \simeq \gamma q(1-q)$. (We remind the readers that $\Delta_0 = \Delta_1 = 0$ by definition.) The approximation (2.35) is valid in general as long as the second term (Δ_q) is small compared to the first one, i.e., for $q \ll d/\gamma$. After the Legendre transformation Eq. (2.35) yields

$$f(\alpha) \simeq d - \frac{(\alpha - \alpha_0)^2}{4(\alpha_0 - d)}, \quad \alpha_0 = d + \gamma. \tag{2.36}$$

In some specific cases, the parabolic form of the spectrum (2.35) and (2.36) is not an approximation but rather an exact result. This happens, in particular, for the random vector potential model, see Sec. VI.G.3. Note that exact parabolicity cannot extend to all q: at $q_c = (d+\gamma)/2\gamma$ the derivative τ_q' becomes zero (i.e., the corresponding $\alpha = 0$), so that τ_q should stay constant for larger q. We discuss this issue, known as "termination" of the multifractal spectra, in Sec. II.C.7.

4. Symmetry of the multifractal spectra

Recently the multifractal exponents for the Wigner-Dyson classes were shown (Mirlin *et al.*, 2006) to satisfy an exact symmetry relation[5]

$$\Delta_q = \Delta_{1-q}, \tag{2.37}$$

connecting exponents with $q < 1/2$ (in particular, with negative q) to those with $q > 1/2$. In terms of the singularity spectrum, this implies

$$f(2d - \alpha) = f(\alpha) + d - \alpha. \tag{2.38}$$

The analytical derivation of Eqs. (2.37) and (2.38) is based on the supersymmetric σ model; it has been confirmed by numerical simulations on the PRBM model (Mildenberger, Subramaniam, *et al.*, 2007), see Fig. 2 and Sec. III, and the 2D Anderson transition of the symplectic class (Mildenberger and Evers, 2007; Obuse, Subramaniam, *et al.*, 2007), Sec. VI.B, and, most recently, on the IQHE (Evers *et al.*, 2008; Obuse, Subramaniam, *et al.*, 2008) and 3D Anderson (Rodriguez *et al.*, 2008; Vasquez *et al.*, 2008) transitions.

5. Role of ensemble averaging

a. Average vs typical spectra

It should be stressed that the definition (2.27) of τ_q is based on the ensemble-averaged IPRs $\langle P_q \rangle$. On the other hand, until recently most numerical studies of multifractality dealt with properties of a single representative wave function. This corresponds to an analysis of the typical IPR,

$$P_q^{\text{typ}} = \exp\langle \ln P_q \rangle. \tag{2.39}$$

Similar to Eq. (2.27), one can define the exponents τ_q^{typ},

[5]If the multifractal spectrum possesses a termination (nonanalyticity) point q_c, Sec. II.C.7, the status of the relation (2.37) beyond this point is not clear.

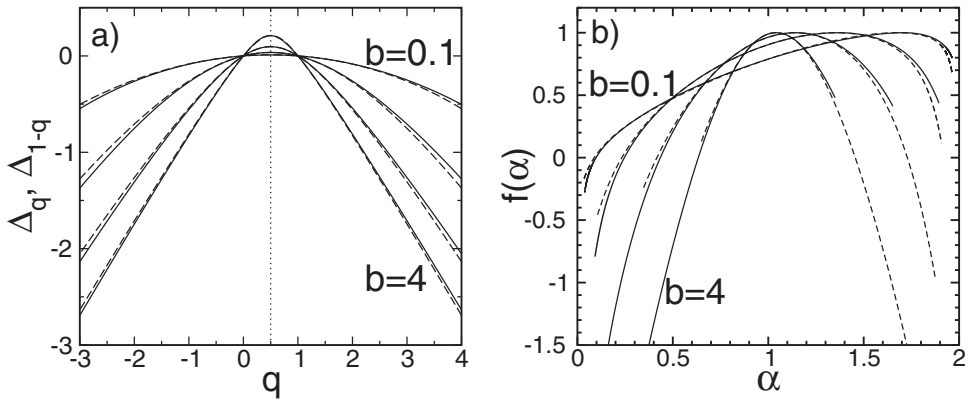

FIG. 2. Symmetry of the multifractal spectrum. (a) Multifractal exponents Δ_q for the PRBM model with $b=4$, 1, 0.3, and 0.1. The symmetry (2.37) with respect to the point $q=1/2$ is evident. A small difference between Δ_q (full line) and Δ_{1-q} (dashed line) is due to numerical errors. (b) Same data now in terms of the singularity spectrum $f(\alpha)$. Dashed lines represent $f(2-\alpha)+\alpha-1$, demonstrating the validity of Eq. (2.38) From Mildenberger, Subramaniam, *et al.*, 2007.

$$P_q^{\rm typ} \sim L^{-\tau_q^{\rm typ}}, \tag{2.40}$$

and introduce the spectrum $f^{\rm typ}(\alpha)$ as the Legendre transform of $\tau_q^{\rm typ}$. The relation between τ_q, $f(\alpha)$, on one side, and $\tau_q^{\rm typ}$, $f^{\rm typ}(\alpha)$, on the other side, was analyzed by Evers and Mirlin (2000) and Mirlin and Evers (2000).[6] The function $\tau_q^{\rm typ}$ has the form

$$\tau_q^{\rm typ} = \begin{cases} q\alpha_-, & q < q_- \\ \tau_q, & q_- < q < q_+ \\ q\alpha_+ & q > q_+, \end{cases} \tag{2.41}$$

where $\alpha_\pm$ are determined by the condition $f(\alpha)=0$, and $q_\pm$ are the corresponding values of q, with $q_-<q_+$.[7] The singularity spectrum $f^{\rm typ}(\alpha)$ is defined in the interval $[\alpha_+,\alpha_-]$, where it is equal to $f(\alpha)$. Information on the negative part of $f(\alpha)$ (on $\alpha<\alpha_+$ and $\alpha>\alpha_-$), or, equivalently, on the part of τ_q with q outside the range $[q_-,q_+]$, gets lost when one considers a single wave function. This is because, for a single eigenfunction, the average measure of the set of points with such a singularity α (i.e., the number of such points in a lattice formulation of the model) is $L^{f(\alpha)}\ll 1$, so that the ensemble averaging is of crucial importance for determining this part of the multifractal spectrum, see Fig. 1.

b. IPR distribution and tail exponents

A closely related issue is the distribution function of P_q. It was conjectured by Fyodorov and Mirlin (1995) and shown by Evers and Mirlin (2000) and Mirlin and Evers (2000) that the distribution of the IPR normalized to its typical value $P_q^{\rm typ}$ has a scale invariant form $\mathcal{P}(P_q/P_q^{\rm typ})$ at criticality. In other words, the distribution function of the IPR logarithm $\mathcal{P}(\ln P_q)$ preserves its form and only shifts along the x axis with increasing L. On the large-P_q side, this distribution develops a power-law tail,

$$\mathcal{P}(P_q/P_q^{\rm typ}) \propto (P_q/P_q^{\rm typ})^{-1-x_q}, \quad P_q \gg P_q^{\rm typ}. \tag{2.42}$$

The upper cutoff of this tail $(P_q/P_q^{\rm typ})_{\rm max}$ depends on the system size L, moving to infinity with $L\to\infty$. It is clear that the relation between $\tau_q^{\rm typ}$ and τ_q depends on the power-law exponent x_q. If $x_q>1$, the two definitions of the fractal exponents are identical, $\tau(q)=\tau^{\rm typ}(q)$. On the other hand, if $x_q<1$, the average $\langle P_q\rangle$ is determined by the upper cutoff of the power-law tail, which depends on L. As a result, $\langle P_q\rangle$ shows scaling with an exponent τ_q different from $\tau_q^{\rm typ}$. In this situation the average value $\langle P_q\rangle$ is not representative and is determined by rare realizations of disorder. Thus $x_q=1$ for $q=q_\pm$, $x_q>1$ for $q_-<q<q_+$, and $x_q<1$ otherwise. Furthermore, it was found (Mirlin and Evers, 2000) that the power-law-tail index x_q is related to the fractal exponents as follows:

$$x_q\tau_q^{\rm typ} = \tau_{qx_q}. \tag{2.43}$$

More precisely, Eq. (2.43) was proven for the case when x_q is an integer. Also, it was shown to hold for the small-b limit of the PRBM model, at $q>1/2$. The generic validity of this formula remains a conjecture. In the range of non-self-averaging IPR this formula yields

$$x_q = q_+/q, \quad q > q_+, \tag{2.44}$$

and similarly for $q<q_-$. For $q_-<q<q_+$, the behavior of x_q depends on the specific form of τ_q. In the particular case of weak multifractality, Eq. (2.35), the solution of Eq. (2.43) reads

$$x_q \simeq (q_+/q)^2, \quad q_- < q < q_+, \tag{2.45}$$

with

$$q_\pm = \pm(d/\gamma)^{1/2}. \tag{2.46}$$

[6] Evers and Mirlin (2000) and Mirlin and Evers (2000) used different notations: τ_q, $f(\alpha)$ for the typical spectra, and $\tilde\tau_q$, $\tilde f(\alpha)$ for the averaged spectra.

[7] It is assumed here that $q_\pm$ and α_- actually exist, i.e., are not infinite. To our knowledge, an example to the opposite has never been encountered for Anderson transitions.

6. Dimensionality dependence of the wave-function statistics at the Anderson transition

In this section, which is largely based on Mildenberger *et al.* (2002), we summarize the results for the Anderson transition in d dimensions, obtained by analytical and numerical means. This allows us to analyze the evolution of the critical statistics from the weak-multifractality regime in $d=2+\epsilon$ dimensions to strong multifractality at $d \gg 1$.

In $2+\epsilon$ dimensions with $\epsilon \ll 1$ the multifractality exponents can be obtained within the ϵ expansion, Sec. II.B.2. The four-loop results for the orthogonal and unitary symmetry classes are as follows (Wegner, 1987):

$$\Delta_q^{(O)} = q(1-q)\epsilon + \frac{\zeta(3)}{4} q(q-1)(q^2-q+1)\epsilon^4 + O(\epsilon^5), \tag{2.47}$$

$$\Delta_q^{(U)} = q(1-q)(\epsilon/2)^{1/2} - \frac{3}{8} q^2(q-1)^2 \zeta(3)\epsilon^2 + O(\epsilon^{5/2}). \tag{2.48}$$

Keeping only the leading (one-loop) term on the right-hand side (rhs) of Eqs. (2.47) and (2.48), we get the parabolic approximation for τ_q, Eq. (2.35), and $f(\alpha)$, Eq. (2.36), with $\gamma=\epsilon$ for the orthogonal class and $\gamma=(\epsilon/2)^{1/2}$ for the unitary class. The IPR fluctuations (Sec. II.C.5) can be studied analytically as well. In particular, in the orthogonal symmetry class, the variance σ_q of the distribution $\mathcal{P}(\ln P_q)$ is given, to the leading order in $\epsilon \ll 1$, by

$$\sigma_q = 8\pi^2 a \epsilon^2 q^2 (q-1)^2, \quad |q| \ll q_+, \tag{2.49}$$

where $a \simeq 0.003\,87$ for the periodic boundary conditions. The values $q_\pm$ of q beyond which the typical and the average IPR scale differently are given by Eq. (2.46) with $d \simeq 2$ and the above values of γ. The power-law exponent x_q of the IPR distribution is given by Eqs. (2.44) and (2.45). At $q \gg q_+$ the variance σ_q is governed by the slowly decaying power-law tail, yielding

$$\sigma_q \simeq x_q^{-1} \simeq q/q_+. \tag{2.50}$$

Numerical simulation results of the wave-function statistics in 3D and 4D for the orthogonal symmetry class are shown in Figs. 3–5 in comparison with the one-loop analytical results of the $2+\epsilon$ expansion. Figure 3 demonstrates that the critical IPR distribution $\mathcal{P}(\ln P_q)$ acquires the scale-invariant form [as also found by Cuevas *et al.* (2002)]. The corresponding variance is shown in Fig. 4; in 3D it is described well by analytical formulas with $\epsilon=1$. The evolution from the weak to strong multifractality with increasing d is nicely seen in Fig. 5(a) for $f(\alpha)$. As is demonstrated in the inset, the one-loop result of the $2+\epsilon$ expansion with $\epsilon=1$ describes the 3D singularity spectrum with remarkable accuracy (though with detectable deviations). In particular, the position of the maximum $\alpha_0=4.03\pm0.05$ is close to its value $\alpha_0=d+\epsilon$ implied by Eq. (2.36). As expected, in 4D the deviations from parabolic shape are much more pronounced and $\alpha_0=6.5\pm0.2$ differs noticeably from 6.

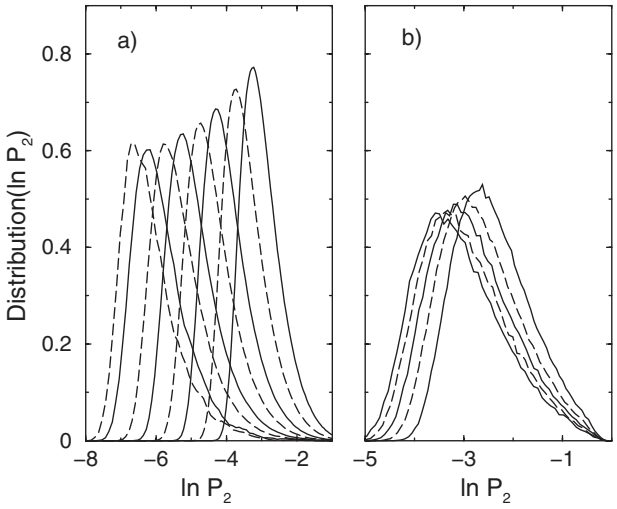

FIG. 3. IPR distribution at the Anderson transition (GOE): (a) 3D (system sizes $L=8$, 11, 16, 22, 32, 44, 64, and 80) and (b) 4D ($L=8$, 10, 12, 14, and 16) From Mildenberger *et al.*, 2002.

Evolution of the fractal dimension $D_q \equiv \tau_q/(q-1)$ with d is shown in Fig. 5(b). It is seen that the fractal dimensions D_q with $q \gtrsim 1$ decrease with increasing d. As an example, for $q=2$ we have $D_2 \simeq 2-2\epsilon$ in $2+\epsilon$ dimensions, $D_2=1.3\pm0.05$ in 3D, and $D_2=0.9\pm0.15$ in 4D. This confirms the expectation based on the Bethe-lattice results (Sec. II.D) that $\tau_q \to 0$ at $d \to \infty$ for $q>1/2$. Such behavior of the multifractal exponents is a manifestation of a sparse character of critical eigenstates at $d \gg 1$, formed by rare resonance spikes. In combination with

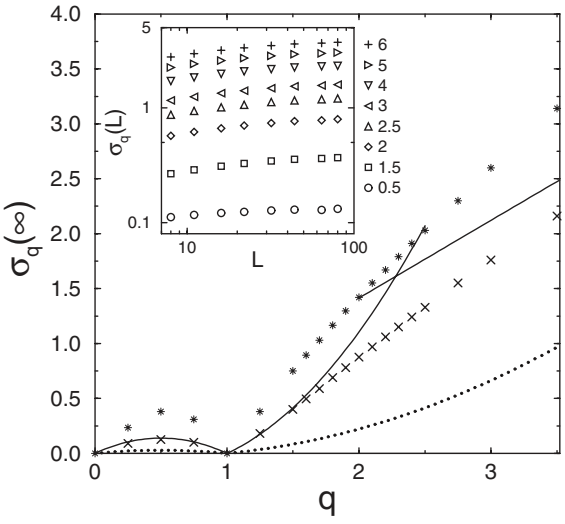

FIG. 4. The rms deviation σ_q of $\ln P_q$ extrapolated to $L \to \infty$ in 3D ($\times$) and 4D ($*$). The dotted line is the analytical result (2.49) for $\epsilon=0.2$; the full lines represent Eqs. (2.49) and (2.50) with $\epsilon=1$. Inset: Evolution of σ_q with L in 3D for values of $q=0.5$, 1.5, 2, 2.5, 3, 4, 5, and 6. The leading finite size correction of all data has the form L^{-y} with $y=0.25-0.5$ for 3D and $y=0.1-0.4$ in 4D. From Mildenberger *et al.*, 2002.

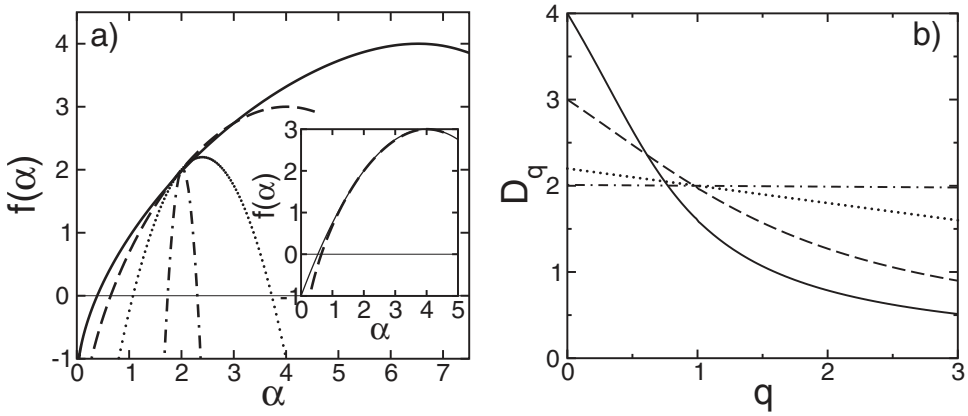

FIG. 5. Dimensionality dependence of the multifractal spectra. (a) Singularity spectrum $f(\alpha)$ in 3D (dashed line) and 4D (full line). To illustrate the evolution of the spectrum from $d=2$ to $d=4$, analytical results for $d=2+\epsilon$ are shown for $\epsilon=0.2$ (dotted) and $\epsilon=0.01$ (dot-dashed). Inset: Comparison between $f(\alpha)$ for 3D and the one-loop result of the $2+\epsilon$ expansion with $\epsilon=1$ (solid). (b) Fractal dimensions D_q in 3D (dashed line) and 4D (full line). Analytical results for $d=2+\epsilon$ with $\epsilon=0.2$ (dotted line) and $\epsilon=0.01$ (dot-dashed) are also shown. From Mildenberger *et al.*, 2002.

Eq. (2.37) this implies the limiting form of the multifractal spectrum at $d\to\infty$,

$$\tau_q = \begin{cases} 0, & q \geq 1/2, \\ 2d(q-1/2), & q \leq 1/2. \end{cases} \tag{2.51}$$

This corresponds to $f(\alpha)$ of the form

$$f(\alpha) = \alpha/2, \quad 0 < \alpha < 2d, \tag{2.52}$$

dropping to $-\infty$ at the boundaries of the interval $[0,2d]$. Mildenberger *et al.* (2002) gave arguments that the way the multifractality spectrum approaches this limiting form with increasing d is analogous to the behavior found in the PRBM model with $b \ll 1$, Sec. III.C.

7. Singularities in multifractal spectra: Termination and freezing

In this section, we discuss what kinds of singularities may be typically encountered in the multifractality spectra $f(\alpha)$ and τ_q. First, we recall that the spectrum $\tau_q^{\rm typ}$ of a typical eigenfunction has nonanalyticity points at $q_\pm$, corresponding to the termination of $f^{\rm typ}(\alpha)$ at its zero $\alpha_\pm$, see Sec. II.C.5. However, the ensemble-averaged spectra τ_q and $f(\alpha)$ do not have any singularity there.

Singularities in τ_q and $f(\alpha)$ may arise, depending on the behavior of $f(\alpha)$ at $\alpha=0$ in the particular critical system under investigation. One possibility is that $f(\alpha)$ approaches the $\alpha=0$ axis continuously, with $f(\alpha)\to-\infty$ as $\alpha\to 0$ [Fig. 6(a)]. Then τ_q increases monotonically with q, without any nonanalyticities. Such a situation is realized, e.g., in the PRBM model, see Sec. III.C. An alternative option is that $f(0)$ is finite, see Fig. 6(b). This generically implies that τ_q has a discontinuity in the second derivative at $q_c \equiv f'(\alpha)|_{\alpha\to 0}$ and is strictly constant, $\tau_q=-f(0)$ at $q\geq q_c$. Such behavior of the multifractality spectrum at $q=q_c$ is called "termination." In particular, it takes place unavoidably if the spectrum is exactly parabolic, as is the case, e.g., for the random vector potential problem, see Sec. VI.G.3. From the point of view of the underlying field theory, termination implies that there is a qualitative change in properties of the operators $\mathcal{O}_q$ describing the LDOS moments. An explicit example of how this may happen is provided by the 2D Liouville field theory (Seiberg, 1990; Kogan *et al.*, 1996; Zamolodchikov and Zamolodchikov, 1996) (closely related to the random vector potential problem), where the operators $\mathcal{O}_q$ cease to be local for $q>q_c$.

A spectrum with termination may show another peculiarity. While normally $f(0)$ is negative, one can also imagine a situation with $f(0)=0$, see Fig. 6(c) (corresponding to $q_c\leq 1$). In fact, this is exactly what happens in the random vector potential problem, see Sec. VI.G.3, when the disorder strength exceeds a certain critical value. The transition into this phase is termed "freezing transition." In the "frozen" phase the wave-functions combine properties of localized and critical states: while the wave-function normalization is governed by a vicin-

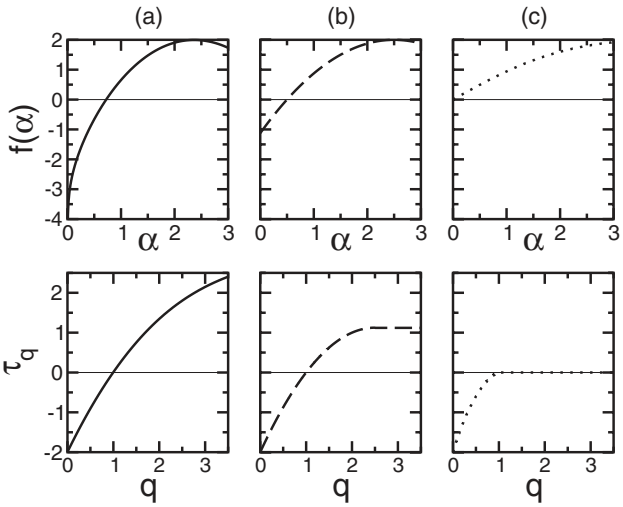

FIG. 6. Possible behavior of the singularity spectrum $f(\alpha)$ at $\alpha\to 0$: (a) no singularity, (b) termination, and (c) freezing. The corresponding behavior of τ_q is shown as well.

ity of one or few (of order unity) points, the tails away from these points show multifractal fluctuations and correlations.

8. Surface vs bulk multifractality

Recently, the concept of wave-function multifractality was extended (Subramaniam *et al.*, 2006) to the surface of a system at an Anderson transition. It was shown that fluctuations of critical wave functions at the surface are characterized by a new set of exponents τ_q^s (or, equivalently, anomalous exponents Δ_q^s), which are in general independent from their bulk counterparts,

$$L^{d-1}\langle|\psi(\mathbf{r})|^{2q}\rangle \sim L^{-\tau_q^s}, \tag{2.53}$$

$$\tau_q^s = d(q-1) + q\mu + 1 + \Delta_q^s. \tag{2.54}$$

Here μ is introduced for generality, in order to account for possible nontrivial scaling of the average value $\langle|\psi(\mathbf{r})|^2\rangle \propto L^{-d-\mu}$ at the boundary in unconventional symmetry classes. For the Wigner-Dyson classes, $\mu=0$. The normalization factor L^{d-1} is chosen such that Eq. (2.53) yields the contribution of the surface to the IPR $\langle P_q\rangle = \langle \int d^d\mathbf{r}\,|\psi(\mathbf{r})|^{2q}\rangle$. The exponents Δ_q^s as defined in Eq. (2.54) vanish in a metal and govern statistical fluctuations of wave functions at the boundary, $\langle|\psi(\mathbf{r})|^{2q}\rangle/\langle|\psi(\mathbf{r})|^2\rangle^q \sim L^{-\Delta_q^s}$, as well as their spatial correlations, e.g., $L^{2(d+\mu)}\langle|\psi^2(\mathbf{r})\psi^2(\mathbf{r}')|\rangle \sim (|\mathbf{r}-\mathbf{r}'|/L)^{\Delta_2^s}$.

Wave-function fluctuations are much stronger at the edge than in the bulk. As a result, surface exponents are important even if one performs a multifractal analysis for the whole sample, without separating it into "bulk" and "surface," despite the fact that the weight of surface points is reduced by a factor $1/L$. This was analytically demonstrated by Subramaniam *et al.* (2006) using a model of a 2D weakly localized metallic system (large dimensionless conductance $g \gg 1$), which shows weak multifractality on length scales below the localization length $\xi \sim e^{(\pi g)^\beta}$, where $\beta=1$ (2) for systems with preserved (broken) time-reversal symmetry. With minor modifications, the formulas below also describe the Anderson transition in $2+\epsilon$ dimensions.

For the bulk multifractal spectrum one gets the result (2.35) with $\gamma=(\beta\pi g)^{-1} \ll 1$ (Wegner, 1980; Altshuler *et al.*, 1986; Fal'ko and Efetov, 1995a, 1995b); generalization of this result to the surface case gives

$$\tau_q^s = 2(q-1) + 1 + 2\gamma q(1-q). \tag{2.55}$$

The corresponding $f(\alpha)$ spectra have the form (here we label bulk quantities with a superscript b)

$$f^b(\alpha) = 2 - (\alpha - 2 - \gamma)^2/4\gamma, \tag{2.56}$$

$$f^s(\alpha) = 1 - (\alpha - 2 - 2\gamma)^2/8\gamma. \tag{2.57}$$

These results are illustrated in Fig. 7. When multifractality in the whole sample is analyzed, the lowest of the τ_q exponents "wins." Surface effects become dominant outside the range $q_-^{bs} < q < q_+^{bs}$, where $q_\pm^{bs} \simeq \pm\gamma^{-1/2}$ are the

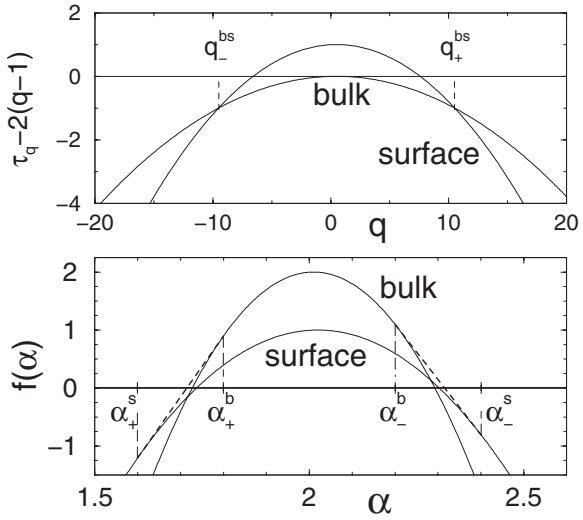

FIG. 7. Surface and bulk multifractal spectra τ_q and $f(\alpha)$ for a 2D metal with $\gamma=0.01$. For details see text. From Subramaniam *et al.*, 2006.

roots of the equation $\tau_q^b = \tau_q^s$. The lower panel of Fig. 7 shows how this is translated into the $f(\alpha)$ representation. The total singularity spectrum is given by the bulk function $f^b(\alpha)$ only for $\alpha_+^b < \alpha < \alpha_-^b$, where $\alpha_\pm^b - 2 \simeq \mp 2\gamma^{1/2}$. Outside this range surface effects are important. Specifically, $f(\alpha)$ is equal to the surface spectrum $f^s(\alpha)$ for $\alpha < \alpha_+^s$ and $\alpha > \alpha_-^s$, where $\alpha_\pm^s - 2 \simeq \mp 4\gamma^{1/2}$, while in the intermediate intervals $\alpha_+^s < \alpha < \alpha_+^b$ and $\alpha_-^b < \alpha < \alpha_-^s$ its dependence on α becomes linear (shown by dashed lines). The latter behavior is governed by intermediate (between bulk and surface) points with a distance from the surface $r \sim L^\beta$, $0 < \beta < 1$; their τ_q spectrum is found to be $\tau_q^{(\beta)}(\alpha) = \beta\tau_q^b + (1-\beta)\tau_q^s$. Note that in this case the surface effects modify $f(\alpha)$ in the whole range below $f(\alpha) \simeq 1$. Therefore the surface exponents affect the multifractal spectrum of the sample not only for rare realizations of disorder [governing the negative part of $f(\alpha)$] but already in a typical sample.

Boundary multifractality was also explicitly studied, analytically as well as numerically, for several other systems at criticality: the 2D spin quantum Hall transition (Subramaniam *et al.*, 2006), the Anderson transition in a 2D system with spin-orbit coupling (Obuse, Subramaniam, *et al.*, 2007), and the PRBM model (Mildenberger, Subramaniam, *et al.*, 2007), see Secs. VI.D.5, IV.B, and III.E, respectively.[8]

Obuse, Subramaniam, *et al.* (2007) generalized the notion of surface multifractality to a corner of a critical system. It was shown that in 2D conformal invariance leads to the following dependence of the corresponding anomalous exponent Δ_q^θ on the opening angle θ:

$$\Delta_q^\theta = (\pi/\theta)\Delta_q^s. \tag{2.58}$$

More carefully, for $\theta < \pi$ the spectrum will terminate at some q_θ [see Sec. II.C.7, and Fig. 6(b)], even if the sur-

[8]See also the Note added in proof for more recent developments.

face spectrum showed no singularity, as in Fig. 6(a). Equation (2.58) holds then for $q \le q_\theta$; for larger q the exponent τ_q is constant.

9. Manifestations of multifractality in other observables

The multifractal structure of wave functions at criticality manifests itself also in other physical characteristics of the system. In particular, one can open the system by attaching a local lead at some point $\mathbf{r}$. The system can then be characterized by the Wigner delay time t_W (energy derivative of the scattering phase shift), whose statistical properties in chaotic and disordered systems have become a subject of recent research activity (Fyodorov and Sommers, 1997; Kottos, 2005). At criticality, the moments of the inverse delay time show a scaling behavior (Fyodorov, 2003; Mendez-Bermudez and Kottos, 2005; Ossipov and Fyodorov, 2005; Mirlin *et al.*, 2006),

$$\langle t_W^{-q} \rangle \propto L^{-\gamma_q}. \tag{2.59}$$

It was shown that for all Wigner-Dyson classes the exponents γ_q are linked to the wave-function exponents τ_q by an exact relation (Ossipov and Fyodorov, 2005; Mirlin *et al.*, 2006),

$$\gamma_q = \tau_{1+q}. \tag{2.60}$$

If a second local lead is attached to the system, the statistics of the two-point conductance $g(\mathbf{r},\mathbf{r}')$ can be studied. Specifically, one can analyze the scaling of the moments $\langle g^q(\mathbf{r}',\mathbf{r})\rangle$ with the distance $|\mathbf{r}-\mathbf{r}'|$ between the contacts (Zirnbauer, 1994, 1999; Janßen *et al.*, 1999),

$$\langle g^q(\mathbf{r},\mathbf{r}')\rangle \sim |\mathbf{r}-\mathbf{r}'|^{-X_q}. \tag{2.61}$$

For the case of the unitary symmetry class (A), a relation linking the exponents X_q to the wave-function anomalous dimensions Δ_q [and based on a result by Klesse and Zirnbauer (2001)] was obtained (Evers *et al.*, 2001),

$$X_q = \begin{cases} \Delta_q + \Delta_{1-q}, & q < 1/2 \\ 2\Delta_{1/2}, & q > 1/2. \end{cases} \tag{2.62}$$

In view of Eq. (2.37), the first line of Eq. (2.62) can be equivalently written as $X_q = 2\Delta_q$, which has been proposed by Janßen *et al.* (1999).

A relation between the exponents X_q and Δ_q was also derived for the case of the SQH transition (Sec. VI.D.5), belonging to the unconventional symmetry class C. In contrast to critical points of the Wigner-Dyson classes, the DOS ρ in this case is critical, i.e., it has a nontrivial scaling dimension $\rho \propto L^{-x_\rho}$ with $x_\rho > 0$. It was shown by Mirlin *et al.* (2003) [see also Bernard and LeClair (2002b)] that in this case

$$X_q = \begin{cases} 2qx_\rho + 2\Delta_q, & q \le q_0 \\ X_{q_0}, & q > q_0, \end{cases} \tag{2.63}$$

where q_0 is the point at which $2qx_\rho + 2\Delta_q$ reaches its maximum. It is plausible that the relation (2.63) [which reduces to Eq. (2.62) for the Wigner-Dyson classes] holds in fact for critical points of all symmetry classes.

D. Anderson transition in $d=\infty$: Bethe lattice

The Bethe lattice (BL) is a treelike lattice with a fixed coordination number. Since the number of sites at a distance r increases exponentially with r on the BL, it effectively corresponds to the limit of high dimensionality d. As mentioned in Sec. II.B.3, the BL models are the closest existing analogs of the mean-field theory for an Anderson transition.

The Anderson tight-binding model (2.5) on the BL was first studied by Abou-Chacra *et al.* (1973), where the existence of the metal-insulator transition was proven and the position of the mobility edge was determined. The analytical results were confirmed by numerical simulations (Abou-Chacra and Thouless, 1974; Girvin and Jonson, 1980); similar behavior was also found in a network model (Chalker and Siak, 1990). Further, the BL versions of the σ model (2.16) (Efetov, 1985, 1987; Zirnbauer, 1986a, 1986b) and tight-binding model (Mirlin and Fyodorov, 1991) were studied within the supersymmetry formalism, which allowed one to determine the critical behavior. It was found that the localization length diverges in the way usual for BL models, $\xi \propto |E - E_c|^{-1}$, where E is a microscopic parameter driving the transition. When reinterpreted within the effective-medium approximation (Efetov, 1990; Fyodorov *et al.*, 1992), this yields the conventional mean-field value of the localization length exponent, $\nu = 1/2$. On the other hand, the critical behavior of other observables is very peculiar. The inverse participation ratios P_q with $q > 1/2$ have a finite limit at $E \to E_c$ when the critical point is approached from the localized phase and then jump to zero. By comparison with the scaling formula $P_q \propto \xi^{-\tau_q}$ this can be interpreted as $\tau_q = 0$ for all $q \ge 1/2$. Further, in the delocalized phase the diffusion coefficient vanishes exponentially when the critical point is approached,

$$D \propto \Omega^{-1} \ln^3 \Omega, \tag{2.64}$$

$$\Omega \sim \exp\{\text{const} \times |E - E_c|^{-1/2}\}, \tag{2.65}$$

which can be thought as corresponding to the infinite value $s = \infty$ of the critical index s. The distribution of the LDOS $v \equiv \rho(r)/\langle\rho\rangle$ (normalized to its average value for convenience) was found to be of the form

$$\mathcal{P}(v) \propto \Omega^{-1/2} v^{-3/2}, \quad \Omega^{-1} \ll v \ll \Omega, \tag{2.66}$$

and exponentially small outside this range. Equation (2.66) implies for the moments of the LDOS

$$\langle v^q \rangle \propto \Omega^{|q-1/2|-1/2}. \tag{2.67}$$

The physical reason for the unconventional critical behavior was unraveled by Mirlin and Fyodorov (1994a, 1994b). It was shown that the exponential largeness of the factor Ω reflects the spatial structure of the BL: the correlation volume V_ξ (number of sites within a distance ξ from the given one) on such a lattice is exponentially large. On the other hand, for any finite dimensionality d the correlation volume has power-law behavior,

$V_d(\xi) \propto \xi^d \propto |E-E_c|^{\nu d}$, where $\nu \simeq 1/2$ at large d. Thus the scale Ω cannot appear for finite d and, assuming some matching between the BL and large-d results, will be replaced by $V_d(\xi)$. Then Eq. (2.67) yields the following high-d behavior of the anomalous exponents Δ_q governing the scaling of the LDOS moments (Sec. II.C):

$$\Delta_q \simeq d(1/2 - |q - 1/2|), \tag{2.68}$$

or, equivalently, the results (2.51) and (2.52) for the multifractal spectra τ_q, $f(\alpha)$. These formulas describe the strongest possible multifractality.

The critical behavior of the conductivity, Eq. (2.64), is governed by the same exponentially large factor Ω. When it is replaced by the correlation volume $V_d(\xi)$, the power-law behavior at finite $d \gg 1$ is recovered, $\sigma \propto |E-E_c|^s$ with $s \simeq d/2$. The result for the exponent s agrees (within its accuracy, i.e., to the leading order in d) with the scaling relation $s = \nu(d-2)$.

E. Level statistics at criticality

We restrict ourselves here to a brief account of key results on the critical level statistics; more detailed exposition and a list of references can be found in Mirlin (2000b). The primary quantity is the two-level correlation function (the superscript c standing for the connected part)

$$R_2^{(c)}(s) = \langle \rho \rangle^{-2} \langle \rho(E - \omega/2)\rho(E + \omega/2) \rangle - 1, \tag{2.69}$$

where $\rho(E) = V^{-1}\,\mathrm{Tr}\,\delta(E-\hat{H})$ is the fluctuating DOS, V the system volume, $s = \omega/\Delta$, and $\Delta = 1/\langle \rho \rangle V$ the mean level spacing. In a metallic system $R_2^{(c)}(s)$ is given, as a first approximation, by the RMT [Wigner-Dyson statistics; see Mirlin (2000b) for analysis of deviation and limits of applicability], while in the insulating limit the levels are uncorrelated, $R_2^{(c)}(s) = \delta(s)$ (Poisson statistics). At a critical point the level statistics takes an intermediate scale-invariant form (Altshuler *et al.*, 1988; Shklovskii *et al.*, 1993). Specifically, $R_2^{(c)}(s)$ (and higher-order correlation functions) is independent under rescaling of the sample, although it does depend on the sample shape and the boundary conditions, see Fig. 8.

A closely related quantity is the variance $\langle \delta N(\mathcal{E})^2 \rangle$ of the number of levels $N(\mathcal{E})$ in a spectral window of width $\mathcal{E}$,

$$\langle \delta N(\mathcal{E})^2 \rangle = \int_{-\langle N(\mathcal{E}) \rangle}^{\langle N(\mathcal{E}) \rangle} ds [\langle N(\mathcal{E}) \rangle - |s|] R_2^{(c)}(s). \tag{2.70}$$

In the RMT limit the level number variance increases logarithmically, $\langle \delta N^2 \rangle = (2/\pi^2\beta)\ln\langle N \rangle$ at $\langle N \rangle \gg 1$, while in the Poisson limit $\langle \delta N^2 \rangle = \langle N \rangle$. At criticality, $\langle \delta N^2 \rangle$ shows an intermediate linear behavior

$$\langle \delta N^2 \rangle = \chi \langle N \rangle, \tag{2.71}$$

with a coefficient $0 < \chi < 1$ called spectral compressibility. The parameter χ is a universal characteristic of the critical theory, i.e., it has a status analogous to critical indices. Evolution of χ from the "quasimetallic" ($\chi \ll 1$) to "quasi-insulating" (χ close to 1) criticality can be analyzed for the family of critical PRBM theories, see Sec. III. It is expected that similar evolution takes place for the Anderson transition in d dimensions when d changes from $d = 2+\epsilon$ to $d \gg 1$, see a related discussion of the wave-function statistics in Sec. II.C.6. The quasimetallic $d = 2+\epsilon$ limit can be studied analytically with the result $\chi = t^*/\beta$, where the critical coupling t^* is given by Eq. (2.18) or (2.22), depending on the symmetry class. The approach of the critical statistics to the Poisson limit at large d was demonstrated in recent numerical work (Garcia-Garcia and Cuevas, 2007), where systems of dimensionality up to $d=6$ were studied (with χ reaching the value $\simeq 0.8$ in 6D).

In systems of unconventional symmetry classes already the one-point correlation function (average DOS) is nontrivial and acquires, in analogy with the two-level correlation function discussed above, a scale-invariant form at criticality. In particular, this will be shown in Sec. VI.D.6 for the SQH transition (class C).

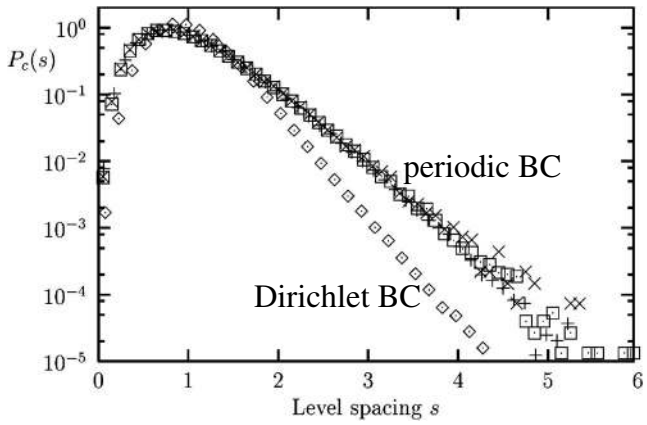

FIG. 8. Critical level spacing distribution of 2D symplectic systems for periodic (PBC) and Dirichlet (DBC) boundary conditions and various system sizes L. PBC: $L=20$ ($\diamond$); DBC: $L=40,80,120$ ($+, \square, \times$). Adapted from Schweitzer and Potempa, 1999; see also Schweitzer and Zharekeshev, 1997.

III. CRITICALITY IN THE POWER-LAW RANDOM BANDED MATRIX (PRBM) MODEL

A. Definition and generalities

The PRBM model is defined (Mirlin *et al.*, 1996) as the ensemble of random $L \times L$ Hermitean matrices $\hat{H}$ (real for $\beta=1$ or complex for $\beta=2$). The matrix elements H_{ij} are independently distributed Gaussian variables with zero mean $\langle H_{ij} \rangle = 0$ and with variance

$$\langle |H_{ij}|^2 \rangle \equiv J_{ij} = a^2(|i-j|), \tag{3.1}$$

$$a^2(r) = [1 + (r/b)^{2\alpha}]^{-1}. \tag{3.2}$$

At $\alpha=1$ the model undergoes an Anderson transition from the localized ($\alpha > 1$) to the delocalized ($\alpha < 1$)

phase. Below, we concentrate on the critical value $\alpha=1$, when $a(r)$ decrease as $a(r)\propto 1/r$ at $r\gg b$.

In a straightforward interpretation, the PRBM model describes a 1D sample with random long-range hopping, the hopping amplitude decaying as $1/r^{\alpha}$ with the distance. Also, such an ensemble arises as an effective description in a number of physical contexts, see Evers and Mirlin (2000) for relevant references. At $\alpha=1$ the PRBM model is critical for an arbitrary value of b and shows all key features of the Anderson critical point, including multifractality of eigenfunctions and nontrivial spectral compressibility. The existence of the parameter b which labels the critical point is a distinct feature of the PRBM model: Eq. (3.1) defines a whole family of critical theories parametrized by b. The limit $b\gg 1$ represents a regime of weak multifractality, analogous to the conventional Anderson transition in $d=2+\epsilon$ with $\epsilon\ll 1$. This limit allows for a systematic analytical treatment via mapping onto a supermatrix σ model and a weak-coupling expansion (Mirlin *et al.*, 1996; Evers and Mirlin, 2000; Mirlin, 2000b; Mirlin and Evers, 2000). The opposite limit $b\ll 1$ is characterized by strongly fluctuating eigenfunctions, similar to the Anderson transition in $d\gg 1$, where the transition takes place in the strong disorder ("strong coupling" in the field-theoretical language) regime. It is also accessible to an analytical treatment using a real-space RG method (Mirlin and Evers, 2000) introduced earlier for related models by Levitov (1990).

In addition to the feasibility of the systematic analytical treatment of both the weak- and strong-coupling regimes, the PRBM model is well suited for numerical simulations in a broad range of couplings. For these reasons, it has attracted considerable interest in the last few years as a model for investigating various properties of the Anderson critical point, see Secs. III.E and III.F.

B. Weak multifractality, $b\gg 1$

The quasimetallic regime $b\gg 1$ can be studied (Mirlin *et al.*, 1996; Evers and Mirlin, 2000; Mirlin, 2000b; Mirlin and Evers, 2000) via mapping onto the supermatrix σ model, cf. Sec. II.B.1,

$$S[Q]=\frac{\pi\rho\beta}{4}\,\mathrm{Str}\left[\pi\rho\sum_{rr'}J_{rr'}Q(r)Q(r')-i\omega\sum_{r}Q(r)\Lambda\right]. \tag{3.3}$$

In momentum (k) space and in the low-k limit, the action takes the form

$$S[Q]=\beta\,\mathrm{Str}\left[-\frac{1}{t}\int\frac{dk}{2\pi}|k|Q_kQ_{-k}-\frac{i\pi\rho\omega}{4}Q_0\Lambda\right], \tag{3.4}$$

where $Q_k=\Sigma_r e^{ikr}Q(r)$ and $Q(r)$ is a 4×4 ($\beta=2$) or 8×8 ($\beta=1$) supermatrix field constrained by $Q^2(r)=1$, see Sec. II.B.1, ρ is the DOS given by the semicircle law

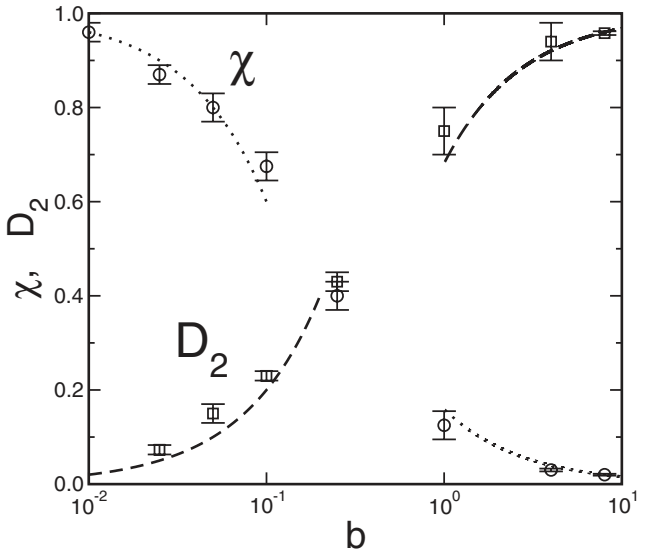

FIG. 9. Crossover from the quasimetallic ($b\gg 1$) to the quasi-insulating ($b\ll 1$) behavior in the PRBM ensemble: fractal dimension D_2 vs parameter b (□). Data points are numerical simulations, while the dashed lines represent $b\gg 1$ and $b\ll 1$ analytical asymptotics, $D_2=1-1/\pi b$ [Eq. (3.7)] and $D_2=2b$ [Eq. (3.20)]. Also shown is the spectral compressibility χ (○). The dotted lines indicate the analytical results for $b\gg 1$ and $b\ll 1$, Eqs. (3.28) and (3.30). From Mirlin and Evers, 2000.

$$\rho(E)=(1/2\pi^2 b)(4\pi b-E^2)^{1/2},\quad |E|<2\sqrt{\pi b}, \tag{3.5}$$

and $t\ll 1$ is the coupling constant,

$$1/t=(\pi/4)(\pi\rho)^2b^2=(b/4)(1-E^2/4\pi b). \tag{3.6}$$

The main difference between the action (3.4) and that of the diffusive σ model, Eq. (2.16), is in the replacement of the diffusion operator $(\pi\rho/8)Dk^2$ by $|k|/t$. Consequently, all calculations within the weak coupling expansion of the σ model are generalized to the PRBM case by substituting $\Pi(k)=t/8|k|$ for the diffusion propagator $\Pi(k)=1/\pi\rho Dk^2$. The $1/|k|$ behavior of $\Pi(k)$ implies that the kinetics is superdiffusive, also known as Lévy flights, and leads to criticality in 1D (Bouchaud and Georges, 1990). In particular, calculating the average IPR $\langle P_q\rangle$, one finds the fractal dimensions

$$\tau_q\simeq(q-1)(1-qt/8\pi\beta),\quad q\ll 8\pi\beta/t, \tag{3.7}$$

i.e., weak-multifractality results (2.35) and (2.36) for τ_q and $f(\alpha)$ with $d=1$ and $\gamma=t/8\pi\beta$. Below, we focus on the band center, $E=0$, where $\gamma=1/2\pi\beta b$.

These results are in good agreement with numerical simulations, see Figs. 9 and 10. Deviations from the asymptotic (parabolic) form in Fig. 10, which are pronounced at $b=1$, are a precursor of the crossover to the small-b regime (Sec. III.C), where the parabolic approximation breaks down completely.

The IPR fluctuations are also found (Evers and Mirlin, 2000; Mirlin and Evers, 2000) by generalizing the results obtained for metallic samples (Fyodorov and

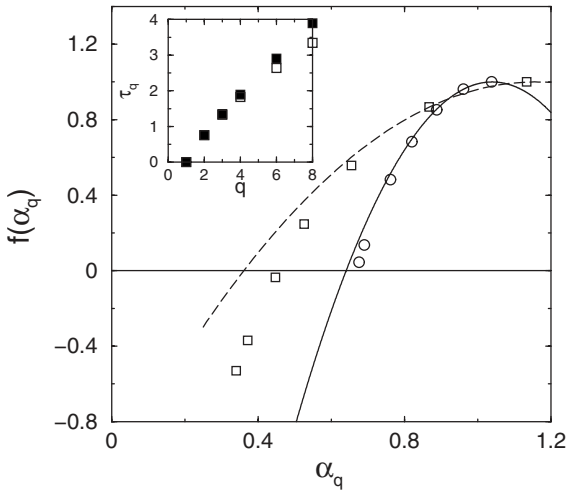

FIG. 10. Multifractal spectrum $f(\alpha)$ for $b=1$ (□) and $b=4$ (○). Lines indicate parabolic approximation (2.36). Inset: exponents τ_q (□), $\tau_q^{\rm typ}$ (■) for $b=1$. From Mirlin and Evers, 2000.

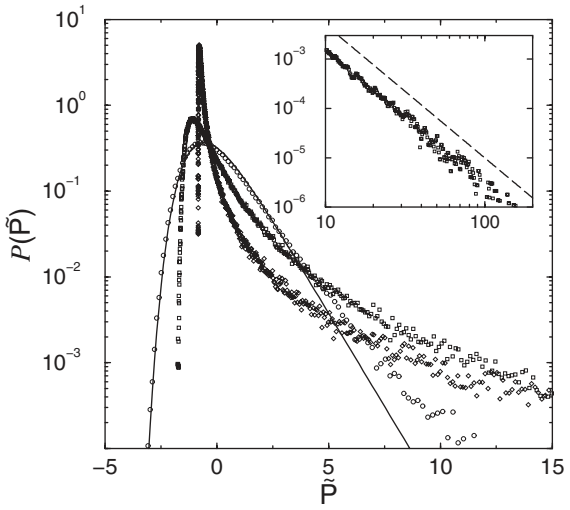

FIG. 12. Distribution function $\mathcal{P}(\tilde{P}_q)$ at $q=2$ (○), 4 (□), and 6 (◇) at $b=4$ for systems of size $L=4096$. The solid line represents the analytical result Eq. (3.9). Inset: Asymptotic of $\mathcal{P}(\tilde{P}_4)$. Dashed line indicates power law with exponent $x_4=1.7$. From Mirlin and Evers, 2000.

Mirlin, 1995; Prigodin and Altshuler, 1998; Mirlin, 2000b). In particular, the IPR variance is given for $q \ll q_+(b) \equiv (2\beta\pi b)^{1/2}$ by

$$\mathrm{var}(P_q)/\langle P_q\rangle^2 = q^2(q-1)^2/24\beta^2 b^2, \tag{3.8}$$

cf. Eq. (2.49). Calculating higher cumulants, one can restore the corresponding scale-invariant distribution,

$$\mathcal{P}(\tilde{P}) = e^{-\tilde{P}-\mathbf{C}} \exp(-e^{-\tilde{P}-\mathbf{C}}), \tag{3.9}$$

$$\tilde{P} = \left[\frac{P_q}{\langle P_q\rangle} - 1\right]\frac{2\pi\beta b}{q(q-1)}, \tag{3.10}$$

where $\mathbf{C}\simeq 0.5772$ is the Euler constant. Equation (3.9) is valid for $P_q/\langle P_q\rangle - 1 \ll 1$. At $P_q/\langle P_q\rangle - 1 \sim 1$ the exponential falloff (3.9) crosses over to a power-law tail

$$\mathcal{P}(P_q) \sim (P_q/\langle P_q\rangle)^{-1-x_q}, \tag{3.11}$$

$$x_q = 2\pi\beta b/q^2, \quad q^2 < 2\pi\beta b, \tag{3.12}$$

see the discussion of general properties of the IPR distribution in Sec. II.C.5.

The analytical results on the IPR distribution are confirmed by numerical simulations. Figure 11(a) demonstrates the scale invariance of the distribution. Figure 12 shows results for the distribution of the IPRs P_q with $q=2$, 4, and 6 at $b=4$ [the corresponding value of q_+ being $q_+=(8\pi)^{1/2}\simeq 5$]. It can be seen that at $q=2$ the analytical formula (3.9) nicely describes the "main body" of the distribution, with the upward deviations at large $\tilde{P}$ indicating the crossover to the power-law tail (3.11). The asymptotic behavior (3.11) is outside the reach of numerical simulations for $q=2$, however, since the condition of its validity $\tilde{P} \gg 2\pi\beta/q(q-1) \simeq 12.5$ corresponds to

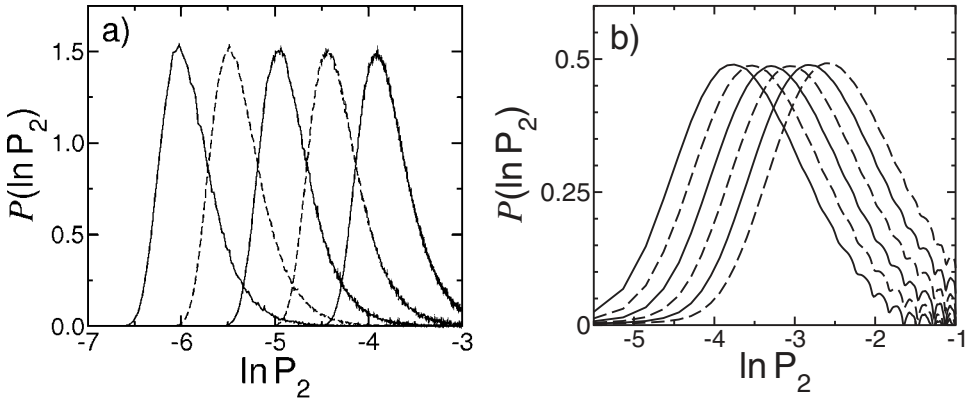

FIG. 11. Scale invariance of the IPR distribution in the PRBM model. (a) Evolution of the distribution $\mathcal{P}(\ln P_2)$ for $b=1$ with the system size L (from right to left: $L=256$, 512, 1024, 2048, and 4096). The scale invariance of the IPR distribution is clearly seen. (b) Distribution flow of $\ln P_2$ calculated from the kinetic equation (3.17) at $t=b\ln r=1.2\cdots 1.7$ (from right to left). Oscillations near $\ln P_2=-1.5$ are numerical artifacts due to rounding errors. From Mirlin and Evers, 2000.

small values of the distribution function $\mathcal{P}(\tilde{P}) \ll 10^{-5}$, its clear resolution would require a much larger statistical ensemble. The situation changes, however, with increasing q (see the data for $q=4$, 6 in Fig. 12). Equation (3.9) becomes inapplicable (since the condition of its validity $q \ll q_+$ is no longer met), and the power-law asymptotic behavior (3.11) becomes clearly seen. In particular, the inset of Fig. 12 shows the tail for $q=4$; the extracted value of the index $x_4 \simeq 1.7$ is in good agreement with the prediction of the $b \gg 1$ theory, $x_4 = \pi/2$.

C. Strong multifractality, $b \ll 1$

In the quasi-insulating case $b \ll 1$ the problem can be studied (Mirlin and Evers, 2000) via the RG method earlier developed for related problems by Levitov (1990, 1999). The idea of the method is as follows. One starts from the diagonal part of the matrix $\hat{H}$, each eigenstate with an energy $E_i = H_{ii}$ being localized on a single site i. Then one includes into consideration nondiagonal matrix elements H_{ij} with $|i-j|=1$. Most of these matrix elements are essentially irrelevant, since their typical value is $\sim b$, while the energy difference $|E_i - E_j|$ is typically of order unity. Only with a small probability ($\sim b$) is $|E_i - E_j|$ also of the order of b, so that the matrix element strongly mixes the two states, which are then said to be in resonance. In this case one is led to consider a two-level problem,

$$\hat{H}_{\text{two level}} = \begin{pmatrix} E_i & V \\ V & E_j \end{pmatrix}, \quad V = H_{ij}. \tag{3.13}$$

The corresponding eigenfunctions and eigenenergies are

$$\psi^{(+)} = \begin{pmatrix} \cos\theta \\ \sin\theta \end{pmatrix}, \quad \psi^{(-)} = \begin{pmatrix} -\sin\theta \\ \cos\theta \end{pmatrix}, \tag{3.14}$$

$$E_\pm = (E_i + E_j)/2 \pm |V|\sqrt{1+\tau^2}, \tag{3.15}$$

where $\tan\theta = -\tau + \sqrt{1+\tau^2}$ and $\tau = (E_i - E_j)/2V$.

In the next RG step the matrix elements H_{ij} with $|i-j|=2$ are taken into account, then those with $|i-j|=3$, and so forth. Each time a resonance is encountered, the Hamiltonian is reexpressed in terms of the new states. Since the probability of a resonance at a distance r is $\sim b/r$, the typical scale r_2 at which a resonance state formed at a scale r_1 will be again in resonance satisfies

$$\ln(r_2/r_1) \sim 1/b, \tag{3.16}$$

so that r_2 is much larger than r_1. Therefore when considering the resonant two-level system at the scale r_2, one can treat the r_1-resonance state as pointlike.

This leads to the following evolution equation for the IPR distribution (for $\beta=1$):

$$\frac{\partial}{\partial \ln r} f(P_q, r) = \frac{2b}{\pi} \int_0^{\pi/2} \frac{d\theta}{\sin^2\theta \cos^2\theta} \Bigg[-f(P_q,r) + \int dP_q^{(1)} dP_q^{(2)} f(P_q^{(1)},r) f(P_q^{(2)},r) \times \delta(P_q - P_q^{(1)} \cos^{2q}\theta - P_q^{(2)} \sin^{2q}\theta) \Bigg]. \tag{3.17}$$

Equation (3.17) is a kind of kinetic equation (in time $t = b \ln r$), with the two terms in the square brackets describing scattering-out and scattering-in processes.

Multiplying Eq. (3.17) by P_q and then integrating over P_q, we get the evolution equation for $\langle P_q \rangle$,

$$\partial \langle P_q \rangle / \partial \ln r = -2bT(q) \langle P_q \rangle, \tag{3.18}$$

$$T(q) = \frac{1}{\pi} \int_0^{\pi/2} \frac{d\theta}{\sin^2\theta \cos^2\theta} (1 - \cos^{2q}\theta - \sin^{2q}\theta) = \frac{2}{\sqrt{\pi}} \frac{\Gamma(q-1/2)}{\Gamma(q-1)} \equiv \frac{1}{2^{2q-3}} \frac{\Gamma(2q-1)}{\Gamma(q)\Gamma(q-1)}. \tag{3.19}$$

Integrating Eq. (3.18) from $r=1$ to $\sim L$, we find the multifractal behavior $\langle P_q \rangle \sim L^{-\tau_q}$ with exponents

$$\tau_q = 2bT(q). \tag{3.20}$$

It is assumed here that $q > 1/2$, which is the condition for the existence of the integral in Eq. (3.19). For $q < 1/2$ the resonance approximation breaks down; exponents can be found from the symmetry relation (2.37). The function $T(q)$ is shown in Fig. 13(a). Its asymptotics are

$$T(q) \simeq -1/\pi(q-1/2), \quad q \to 1/2; \tag{3.21}$$

$$T(q) \simeq (2/\sqrt{\pi}) q^{1/2}, \quad q \gg 1. \tag{3.22}$$

We see that the fractal exponents are proportional to $b \ll 1$. This is characteristic of wave functions that are very small, typically, with rare and strong peaks (resonances). In the limit $b \to 0$ the fractal exponents tend to their insulator value $\tau_q = 0$ for all $q > 1/2$.

Legendre transformation of Eq. (3.20) produces the $f(\alpha)$ spectrum of the form

$$f(\alpha) = 2bF(A), \quad A = \alpha/2b, \tag{3.23}$$

where $F(A)$ is the Legendre transform of $T(q)$. The function $F(A)$ is shown in Fig. 13(a) (inset); its asymptotics are

$$F(A) \simeq -1/\pi A, \quad A \to 0; \tag{3.24}$$

$$F(A) \simeq A/2, \quad A \to \infty. \tag{3.25}$$

Furthermore, it changes sign at $A_+ \simeq 0.5104$, corresponding to $q_+ \simeq 2.4056$. These analytical findings are fully supported by numerical simulations, see Fig. 13(b). Equa-

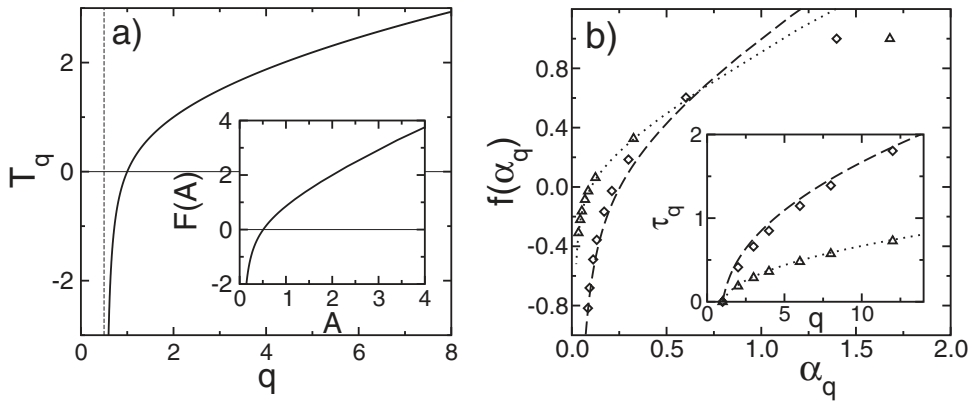

FIG. 13. Strong multifractality in the PRBM model. (a) The function $T(q)$ characterizing exponents $\tau(q)$ via $\tau(q)=2bT(q)$ at $b \ll 1$. Dashed line indicates pole position. Inset: Legendre transform $F(A)$ describing multifractal spectrum via $f(\alpha)=2bF(\alpha/2b)$. (b) $f(\alpha)$ for $b=0.25$ ($\diamond$) and $b=0.1$ ($\triangle$). Inset: Exponent $\tau(q)$. Dashed and dotted lines indicate analytical results, Eqs. (3.23) and (3.20). From Mirlin and Evers, 2000.

tions (3.20)–(3.25) are valid for $q>1/2$, which corresponds to $\alpha<1$. The other part of the spectrum can be obtained via the symmetry relation (2.37) and (2.38), as is also confirmed by numerical results, see Figs. 2, 17, and 18.

We return now to the IPR distribution function. Figure 11(b) shows results of numerically integrating Eq. (3.17) for $q=2$ with the initial condition $f(P_2)=\delta(P_2-1)$ at $t=0$. It can be seen that at sufficiently large t the distribution of $\ln P_2$ acquires a limiting form, shifting with t without changing its shape. This conclusion of scale invariance of the IPR distribution is also supported by analytical arguments: the fixed-point distribution is of the form

$$f(P_q,r) = r^{\tau_q^{\rm typ}} f_0(P_q r^{\tau_q^{\rm typ}}) \tag{3.26}$$

with $\tau_q^{\rm typ}$ as defined in Sec. II.C.5. In agreement with a general discussion in Sec. II.C.5 the distribution is found to have a power-law tail, $f_0(\tilde{P}_q) \sim \tilde{P}_q^{-x_q-1}$, with the index x_q given by Eqs. (2.43) and (2.44). All formulas of this section remain valid for the case $\beta=2$, with a replacement $b \to (\pi/2\sqrt{2})b$.

D. Levels statistics

In the $b \gg 1$ regime the two-level correlation function (2.69) is obtained by an appropriate generalization of earlier findings for diffusive samples. In particular, for the $\beta=2$ ensemble at the band center, the level correlation function has the form[9] (Kravtsov and Muttalib, 1997; Mirlin, 2000b; Mirlin and Evers, 2000)

$$R_2^{(c)}(s) = \delta(s) - \frac{\sin^2(\pi s)}{(\pi s)^2}\frac{(\pi s/4b)^2}{\sinh^2(\pi s/4b)}. \tag{3.27}$$

The correlation function (3.27) follows the RMT result $R_2^{(c)}(s)=\delta(s)-\sin^2(\pi s)/(\pi s)^2$ up to the scale $s \sim b$ (playing the role of the Thouless energy here), and then decays exponentially. The spectral compressibility is given by

$$\chi \simeq 1/2\pi\beta b, \quad b \gg 1. \tag{3.28}$$

In the opposite limit, $b \ll 1$, the evolution equation for $R_2(\omega,r)$ can be written down in analogy with Eq. (3.17) (Mirlin and Evers, 2000), with the result (for $\beta=1$)

$$R_2^{(c)}(s) = \delta(s) - \mathrm{erfc}(|s|/2\sqrt{\pi}b), \tag{3.29}$$

where $\mathrm{erfc}(x)=(2/\sqrt{\pi})\int_x^\infty \exp(-t^2)dt$ is the error function. This yields the spectral compressibility

$$\chi \simeq 1 - 4b, \quad b \ll 1. \tag{3.30}$$

The results for the $\beta=2$ case are qualitatively similar,

$$R_2^{(c)}(s) = \delta(s) - \exp(-s^2/2\pi b^2), \tag{3.31}$$

$$\chi \simeq 1 - \pi\sqrt{2}b, \quad b \ll 1. \tag{3.32}$$

Thus in the limit of small b the level repulsion is efficient in a narrow region $|s| \lesssim b$ only, and the spectral compressibility tends to the Poisson value $\chi=1$. The physical reason for the reduced range of the level repulsion is quite transparent. Consider two nearby in energy states separated by a typical distance $r \sim L$ in the coordinate space. If their energy difference $s \lesssim b$, two such states form a resonance pair, so that their levels will repel. On the other hand, if $s \gg b$, these two states are not in resonance, their wave functions remain weakly overlapping, and the level repulsion between them is inefficient.

These results are fully supported by numerical data. Figure 14(a) represents the level correlation function $R_2(s)$ at $b=0.1$, in agreement with Eq. (3.29). The level number variance $\mathrm{var}[N(\mathcal{E})]$ is plotted versus the average $\langle N(\mathcal{E})\rangle$ in Fig. 14(b); the data show an extended plateau

[9]The precise form of the level correlation function R_2 depends on the boundary conditions, which are chosen here to be periodic. The value of the spectral compressibility χ is independent of the boundary conditions.

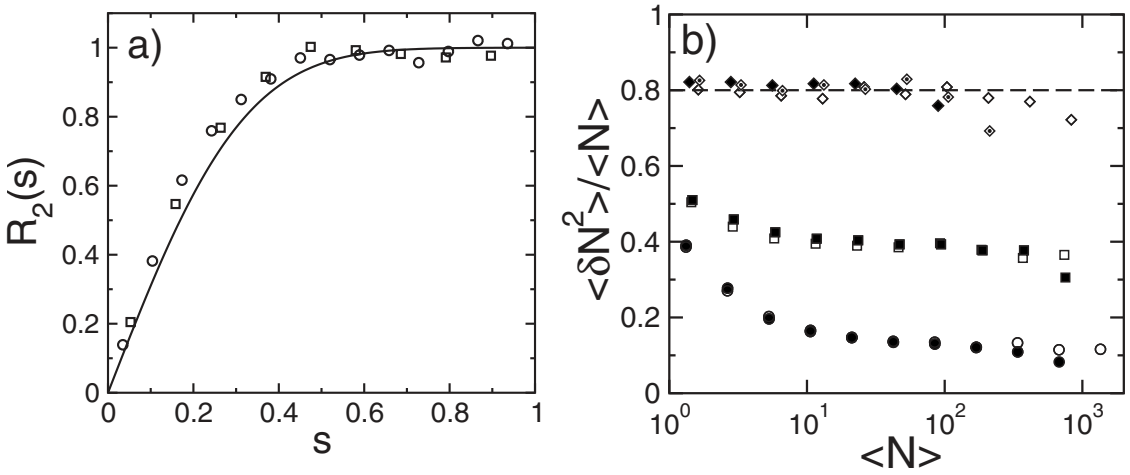

FIG. 14. Level statistics in the PRBM model. (a) Two-level correlation function $R_2(s)$ for two system sizes $L=256$ (○) and $L=512$ (□) at $b=0.1$. The solid line indicates the theoretical result (3.29). (b) Variance of the number of levels $\langle \delta N^2 \rangle$ as a function of the energy width for the interval parametrized by the mean level number $\langle N \rangle$. Traces correspond to $b=1$ (open ∘: $L=4096$, closed: $L=2048$), $b=0.25$ (open □: $L=4096$, closed: $L=2048$) and $b=0.05$ (open ◇: $L=4096$, ◇ with dot: $L=1024$, closed: $L=512$). The dashed line indicates the analytical prediction Eq. (3.30). From Mirlin and Evers, 2000.

region in $\mathrm{var}[N(\mathcal{E})]/\langle N(\mathcal{E})\rangle$ determining χ. The upper bound for this region is set by the matrix size L, while the lower bound is $\sim b$. The numerically obtained spectral compressibility in a broad range of b is shown in Fig. 9; in the large-b and small-b regions it agrees well with the corresponding analytical asymptotics.

E. Boundary criticality

The presentation in this section follows Mildenberger, Subramaniam, *et al.*, 2007. In the spirit of Sec. II.C.8, we consider the critical PRBM model with a boundary at $i=0$, which means that the matrix element H_{ij} is zero whenever one of the indices is negative. Implementation of the boundary is, however, not unique. An important point is that this degree of freedom affects the boundary criticality. One should specify what happens with a particle which "attempts to hop" from a site $i\geq 0$ to a site $j<0$, which is outside of the Hilbert space. One possibility is that such hops are simply discarded, so that the variance $\langle |H_{ij}|^2\rangle \equiv J_{ij}$ is given by $J_{ij}=[1+(i-j)^2/b^2]^{-1}$ for $i,j\geq 0$. More generally, the particle may be reflected by the boundary with certain probability p and "land" on the site $-j>0$. This leads to the following formulation of the model:

$$J_{ij}=\frac{1}{1+|i-j|^2/b^2}+\frac{p}{1+|i+j|^2/b^2}. \tag{3.33}$$

While the above probability interpretation restricts p to the interval $[0,1]$, the model is defined for all p in the range $-1<p<\infty$. The reflection parameter p is immaterial in the bulk, where $i,j\gg|i-j|$ and the second term in Eq. (3.33) can be neglected. Therefore the bulk exponents τ_q^{b} depend on b only (and not on p), and their analysis in Secs. III.B and III.C remains applicable without changes. On the other hand, as discussed below, the surface exponents τ_q^{s} are a function of two parameters, b and p.

Equation (3.33) describes a semi-infinite system with one boundary at $i=0$. For a finite system of length L (implying that the relevant coordinates are restricted to $0\leq i,j\leq L$) another boundary term, $p'/[1+(i+j-2L)^2/b^2]$, needs to be included on the right-hand side of Eq. (3.33). In general, the parameter p' of this term may be different from p. This term, however, does not affect the boundary criticality at the $i=0$ boundary, so it is discarded below.

The regime of weak criticality, $b\gg 1$, can be studied via a mapping onto the supermatrix σ model as in the bulk case, see Sec. III.B. This results again in an approximately parabolic spectrum, which, however, differs by a constant factor R_p from its bulk counterpart,

$$\Delta_q^{\mathrm{s}}=[q(1-q)/2\pi\beta b]R_p\equiv\Delta_q^{\mathrm{b}}R_p. \tag{3.34}$$

This factor is determined from solution of the classical Lévy flight problem with boundaries,

$$\frac{\partial W_i(t)}{\partial t}+\pi\rho\sum_{j=0}^{\infty}[\delta_{ij}J_0^{(i)}-J_{ij}]W_j(t)=0, \tag{3.35}$$

where $J_0^{(i)}=\Sigma_{k=0}^{\infty}J_{ik}$, with the initial condition $W_i(0)=\delta_{ir}$, where r is near the boundary. Specifically, the return probability $W_r(t)$ decays with time as $1/t$, and the corresponding prefactor yields the fractal exponents,

$$\Delta_q^{\mathrm{s}}/q(1-q)=\beta^{-1}tW_r(t)|_{t\to\infty}. \tag{3.36}$$

The evolution equation (3.35) was solved numerically; the results obtained for R_p are shown in Fig. 15. For $p=1$ the evolution equation can be obtained from its bulk counterpart (defined on the whole axis $-\infty<i<\infty$) by folding the system on the semiaxis $i>0$ according to $W_i(t)+W_{-i}(t)\to W_i(t)$, leading to the analytical result

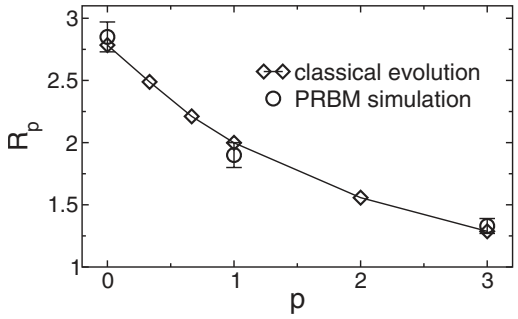

FIG. 15. The ratio $R_p=\Delta_q^s(b,p)/\Delta_q^b(b)$ of the surface and bulk anomalous exponents for large b, as a function of the reflection parameter p. Diamonds represent the results of the σ-model analysis with a numerical solution of the corresponding classical evolution equation (3.35). Circles represent a direct computer simulation of the PRBM model with $b=8$. The ratio R_p has been evaluated for the range $0<q<1$, where numerical accuracy of the anomalous exponents is the best. Within this interval the obtained R_p is q independent (within numerical errors) in agreement with Eq. (3.34). From Mildenberger, Subramaniam, *et al.*, 2007.

$$R_1 = 2. \tag{3.37}$$

As in the bulk case, the regime of small b can be studied via the real-space RG method (Sec. III.C). The multifractal exponents are found to be

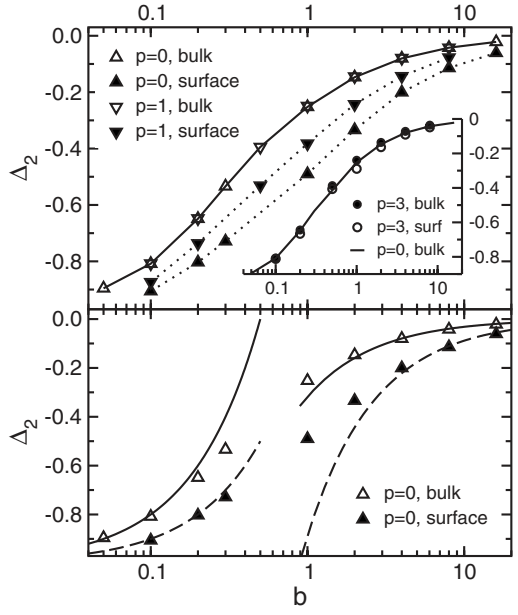

FIG. 16. Surface vs bulk criticality in the PRBM model: evolution from the quasimetallic ($b\gg1$) to the quasi-insulating ($b\ll1$) regime. Upper panel: Anomalous exponent $\Delta_2\equiv D_2-1$ as a function of b from numerical simulations in the bulk and at the boundary for the reflection parameter $p=0$ and 1. Inset: Data for $p=3$ compared to the $p=0$ bulk values. Lower panel: Surface and bulk data for $p=0$ compared with analytical results for small and large b (using $R_0=2.78$), Eqs. (3.7), (3.34), (3.20), and (3.38). From Mildenberger, Subramaniam, *et al.*, 2007.

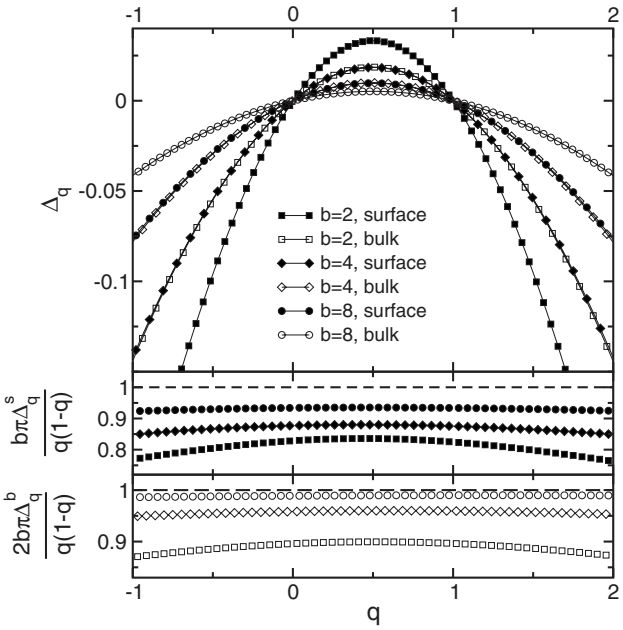

FIG. 17. Surface vs bulk multifractality in the PRBM model for large b. Upper panel: Boundary and bulk multifractal spectra Δ_q^s and Δ_q^b at $b=2$, 4, and 8 for the reflection parameter $p=1$. In accordance with Eq. (3.37), the surface multifractality spectrum is enhanced by a factor close to 2 compared to the bulk. Middle panel: Surface spectrum divided by the analytical $b\gg1$ result, Eq. (3.34). With increasing b, the numerical data converge towards the analytical result (dashed line). Lower panel: Analogous plot for the bulk spectrum. From Mildenberger, Subramaniam, *et al.*, 2007.

$$\tau_q^s = (1+p)^{1/2} b\, T(q) = [(1+p)^{1/2}/2]\tau_q^b, \tag{3.38}$$

with $T(q)$ given by Eq. (3.19), i.e., they differ from the bulk exponents by the factor $(1+p)^{1/2}/2$. In full analogy with the bulk formula (3.20), the result (3.38) is valid for $q>1/2$, where the multifractal exponent τ_q is small. The results can, however, be extended to the range $q<1/2$ using the relation (2.37). For all q the relation obtained between the surface and bulk multifractal spectra can be formulated in the following way:

$$\tau_q^s(b,p) = \tau_q^b[b \to b(1+p)^{1/2}/2]. \tag{3.39}$$

These predictions were corroborated by numerical simulations of the PRBM model. Figure 16 shows the dependence of the anomalous dimension $\Delta_2\equiv D_2-1$ on b in the bulk and at the boundary, for three different values of p. In Fig. 17 the whole multifractal spectra Δ_q are shown for fixed large values of b. Specifically, the anomalous dimensions Δ_q^s and Δ_q^b are presented for $b=2$, 4, and 8, with the reflection parameter chosen to be $p=1$. For all curves the q dependence is approximately parabolic, as predicted by the large-b theory, Eq. (3.34), with the prefactor inversely proportional to b. It can also be seen in Fig. 17 that the bulk multifractality spectrum for $b=4$ and the surface spectrum for $b=8$ are almost identical, in agreement with Eq. (3.37). The same is true for the relation between the bulk spectrum for $b=2$ and

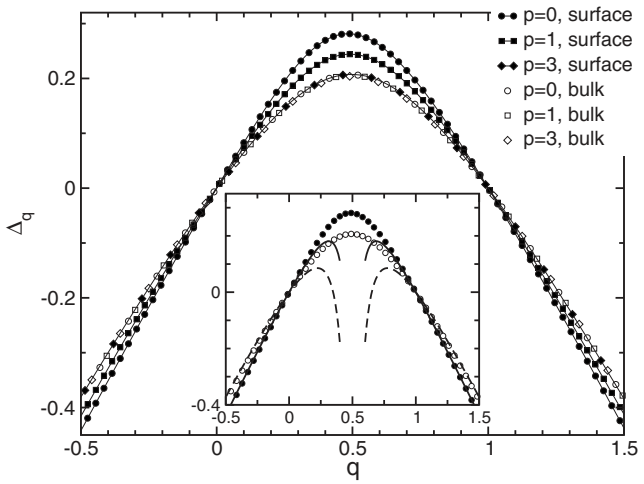

FIG. 18. Numerically determined boundary and bulk anomalous dimensions Δ_q at $b=0.1$ for $p=0$, 1, and 3. As expected, the bulk anomalous dimension is independent of p. In accordance with Eq. (3.39), for $p=3$ surface and bulk dimensions have the same values. Inset: The $p=0$ data compared to the analytical results, surface [solid line, Eq. (3.38)] and bulk [dashed line, Eq. (3.20)]. Analytical data have been calculated for $q \geq 0.6$ and mirrored for $q \leq 0.4$ using the symmetry relation $\Delta_q = \Delta_{1-q}$. In the vicinity of $q=1/2$, at $|q-1/2| \lesssim 1/\ln b^{-1}$, the analytical result (3.20) breaks down. From Subramaniam, Mildenberger *et al.*, 2007.

the surface spectrum for $b=4$. The ratio of the large-b surface and bulk anomalous dimensions $R_p = \Delta_q^{\mathrm{s}}/\Delta_q^{\mathrm{b}}$ is in good agreement with the σ-model predictions for R_p, as shown in Fig. 15. In Fig. 18 the surface and bulk multifractal spectra are shown for the case of small b. While the spectra are strongly nonparabolic in this limit, they clearly exhibit the symmetry $q \to 1-q$, Eq. (2.37). The data are in good agreement with the real-space RG results.

F. Further related activities

As a model of the Anderson critical point, the PRBM ensemble has recently attracted a lot of interest. We briefly mention some of these works. Research directions include the following: relation to the system of interacting fermions in 1D (Luttinger liquid) (Kravtsov and Tsvelik, 2000), a generalization of the model to two dimensions (Potempa and Schweitzer, 2002), wave-function statistics (Cuevas *et al.*, 2002; Varga, 2002; Cuevas, 2003a, 2003b), level correlations (Cuevas, 2005; Garcia-Garcia, 2006), virial expansion for level statistics of almost diagonal random matrices (Yevtushenko and Kravtsov, 2003, 2004; Kravtsov *et al.*, 2006), chiral PRBM and possible applications to quantum chromodynamics (Garcia-Garcia and Takahashi, 2004); and manifestations of multifractality in scattering characteristics of an open system (Mendez-Bermudez and Kottos, 2005; Mendez-Bermudez and Varga, 2006). Rotationally invariant random matrix ensembles with level statistics similar to that in the critical PRBM ensembles have been studied by Muttalib *et al.* (1993, 2001); Moshe *et al.* (1994); Garcia-Garcia and Verbaarschot (2003); a relation between these ensembles and the PRBM model has been discussed by Kravtsov and Muttalib (1997); Mirlin (2000b).

IV. SYMMETRIES OF DISORDERED SYSTEMS

In this section we review the symmetry classification of disordered systems based on the relation to the classical symmetric spaces, established by Zirnbauer (1996); Altland and Zirnbauer (1997). For a detailed presentation of the scheme and underlying mathematical structures the reader is referred to Caselle and Magnea (2004). A mathematical proof of the completeness of the classification has been given by Heinzner *et al.* (2005).

A. Wigner-Dyson classes

The random matrix theory (RMT) was introduced into physics by Wigner (1951). Developing Wigner's ideas, Dyson (1962) put forward a classification scheme of ensembles of random Hamiltonians. This scheme takes into account the invariance of the system under time reversal and spin rotations, yielding three symmetry classes: unitary, orthogonal, and symplectic.

If the time-reversal invariance (T) is broken, the Hamiltonians are arbitrary Hermitian matrices,

$$H = H^{\dagger}, \tag{4.1}$$

with no further constraints. This set of matrices is invariant with respect to rotations by unitary matrices; hence the name "unitary ensemble." In this situation, the presence or absence of spin rotation invariance (S) is not essential: if the spin is conserved, H is simply a spinless unitary-symmetry Hamiltonian times the unit matrix in the spin space. In the RMT one usually considers an ensemble of matrices with independent, Gaussian-distributed random entries—the Gaussian unitary ensemble (GUE). While disordered systems have much richer physics than the Gaussian ensembles, their symmetry classification is inherited from the RMT.

We now turn to systems with preserved time-reversal invariance. The latter is represented by a antiunitary operator $T=KC$, where C is the operator of complex conjugation and K is unitary. Time-reversal invariance thus implies $H=KH^{\mathrm{T}}K^{-1}$ (we used the Hermiticity, $H^{*}=H^{\mathrm{T}}$). Since acting twice with T should leave the physics unchanged, one infers that $K^{*}K=p$, where $p=\pm 1$. As shown by Wigner, the two cases correspond to systems with integer ($p=+1$) and half-integer ($p=-1$) angular momentum. If $p=1$, a representation can be chosen where $K=1$, so that

$$H = H^{\mathrm{T}}. \tag{4.2}$$

The set of Hamiltonians thus spans the space of real symmetric matrices in this case. This is the orthogonal symmetry class; its representative is the Gaussian orthogonal ensemble (GOE). For disordered electronic

systems this class is realized when spin is conserved, as the Hamiltonian reduces to that for spinless particles (times unit matrix in the spin space).

If T is preserved but S is broken, we have $p=-1$. In the standard representation, K is realized by the second Pauli matrix $K=i\sigma_y$ so that the Hamiltonian satisfies

$$H = \sigma_y H^{\mathrm{T}} \sigma_y. \tag{4.3}$$

It is convenient to split the $2N\times 2N$ Hamiltonian in 2×2 blocks (quaternions) in spin space. Each of them is of the form $q=q_0\sigma_0+iq_1\sigma_x+iq_2\sigma_y+iq_3\sigma_z$ (where σ_0 is the unit matrix and $\sigma_{x,y,z}$ the Pauli matrices), with real q_μ, which defines a real quaternion. This set of Hamiltonians is invariant with respect to the group of unitary transformations conserving σ_y, $U\sigma_y U^T=\sigma_y$, which is the symplectic group Sp($2N$). The corresponding symmetry class is thus called symplectic, and its RMT representative is the Gaussian symplectic ensemble (GSE).

B. Relation to symmetric spaces

Before discussing the relation to the families of symmetric spaces, we remind the reader how the latter are constructed (Helgason, 1978; Caselle and Magnea, 2004). Let G be one of the compact Lie groups SU(N), SO(N), Sp($2N$), and $\mathfrak{g}$ the corresponding Lie algebra. Further, let θ be an involutive automorphism $\mathfrak{g}\to\mathfrak{g}$ such that $\theta^2=1$ but θ is not identically equal to unity. It is clear that θ splits $\mathfrak{g}$ in two complementary subspaces, $\mathfrak{g}=\mathfrak{K}\oplus\mathfrak{P}$, such that $\theta(X)=X$ for $X\in\mathfrak{K}$ and $\theta(X)=-X$ for $X\in\mathfrak{P}$. It is easy to see that the following Lie algebra multiplication relations hold:

$$[\mathfrak{K},\mathfrak{K}]\subset\mathfrak{K},\quad [\mathfrak{K},\mathfrak{P}]\subset\mathfrak{P},\quad [\mathfrak{P},\mathfrak{P}]\subset\mathfrak{K}. \tag{4.4}$$

This implies, in particular, that $\mathfrak{K}$ is a subalgebra, whereas $\mathfrak{P}$ is not. The coset space G/K (where K is the Lie group corresponding to $\mathfrak{K}$) is then a compact symmetric space. The tangent space to G/K is $\mathfrak{P}$. One can also construct an associated noncompact space. For this purpose, one first defines the Lie algebra $\mathfrak{g}^*=\mathfrak{K}\oplus i\mathfrak{P}$, which differs from $\mathfrak{g}$ in that the elements in $\mathfrak{P}$ are multiplied by i. Going to the corresponding group and dividing K out, one gets a noncompact symmetric space G^*/K.

The groups G themselves are also symmetric spaces and can be viewed as coset spaces $G\times G/G$. The corresponding noncompact space is G^{C}/G, where G^{C} is the complexification of G (which is obtained by taking the Lie algebra $\mathfrak{g}$, promoting it to the algebra over the field of complex numbers, and then exponentiating).

The connection with symmetric spaces is now established in the following way (Zirnbauer, 1996; Altland and Zirnbauer, 1997). Consider first the unitary symmetry class. Multiplying a Hamiltonian matrix by i, we get an anti-Hermitean matrix $X=iH$. Such matrices form the Lie algebra $\mathfrak{u}(N)$. Exponentiating it, one gets the Lie group U(N), which is the compact symmetric space of class A in Cartan's classification. For the orthogonal class, $X=iH$ is purely imaginary and symmetric. The set of such matrices is a linear complement $\mathfrak{P}$ of the algebra $\mathfrak{K}=\mathfrak{o}(N)$ of imaginary antisymmetric matrices in the algebra $\mathfrak{g}=\mathfrak{u}(N)$ of anti-Hermitean matrices. The corresponding symmetric space is $G/K=\mathrm{U}(N)/\mathrm{O}(N)$, which is termed AI in Cartan's classification. For the symplectic ensemble the same consideration leads to the symmetric space U(N)/Sp(N), which is the compact space of the class AII. If we do not multiply H by i but instead proceed with H in the analogous way, we end up with associated noncompact spaces G^*/K. To summarize, the linear space $\mathfrak{P}$ of Hamiltonians can be considered as a tangent space to the compact G/K and noncompact G^*/K symmetric spaces of the appropriate symmetry class.

This correspondence is summarized in Table I, where the first three rows represent the Wigner-Dyson classes, the next three the chiral classes (Sec. IV.C), and the last four the Bogoliubov–de Gennes classes (Sec. IV.D). The last two columns of the table specify the symmetry of the corresponding σ model. In the supersymmetric formulation, the base of the σ-model target space $\mathcal{M}_B\times\mathcal{M}_F$ is the product of a noncompact symmetric space $\mathcal{M}_B$ corresponding to the bosonic sector and a compact ("fermionic") symmetric space $\mathcal{M}_F$. (In the replica formulation, the space is $\mathcal{M}_B$ for bosonic or $\mathcal{M}_F$ for fermionic replicas, supplemented with the limit $n\to 0$.) The Cartan symbols for these symmetric spaces are given in the sixth column, and the compact components $\mathcal{M}_F$ are listed in the last column. It should be stressed that the symmetry classes of $\mathcal{M}_B$ and $\mathcal{M}_F$ are different from the symmetry class of the ensemble (i.e., of the Hamiltonian) and in most cases are also different from each other. Following common convention, when we refer to a system as belonging to a particular class, we mean the symmetry class of the Hamiltonian.

It is also worth emphasizing that the orthogonal groups appearing in $\mathcal{M}_F$ are O(N) rather than SO(N). This difference (which was irrelevant when discussing the symmetry of the Hamiltonians, as it does not affect the tangent space) is important here, since it influences topological properties of the manifold. As detailed in Secs. V and VI the topology of the σ-model target space often crucially affects the localization properties of the theory.

C. Chiral classes

The Wigner-Dyson classes are the only ones allowed if one looks for a symmetry that is translationally invariant in energy, i.e., is not spoiled by adding a constant to the Hamiltonian. However, additional discrete symmetries may arise at some particular value of energy (which can be chosen as zero without loss of generality), leading to novel symmetry classes. As the vicinity of a special point in the energy space governs the physics in many cases (i.e., the band center in lattice models at half filling, or zero energy in gapless superconductors), these ensembles are of much interest. They can be subdivided

TABLE I. Symmetry classification of disordered systems. First column: Symbol for the symmetry class of the Hamiltonian. Second column: Names of the corresponding RMT. Third column: Presence (+) or absence (–) of the time-reversal (T) and spin-rotation (S) invariance. Fourth and fifth columns: Families of the compact and noncompact symmetric spaces for the corresponding symmetry class. The Hamiltonians span the tangent space to these symmetric spaces. Sixth column: Symmetry class of the σ model; the first symbol corresponds to the noncompact (bosonic) and the second to the compact (fermionic) sector of the base of the σ-model manifold. The compact component $\mathcal{M}_F$ (which is particularly important for theories with nontrivial topological properties) is given in the last column.

Hamiltonian class	RMT	T S	Compact symmetric space	Noncompact symmetric space	σ-model $B\|F$	σ-model compact sector $\mathcal{M}_F$
Wigner-Dyson classes						
A	GUE	– ±	$\mathrm{U}(N)\times\mathrm{U}(N)/\mathrm{U}(N)\equiv\mathrm{U}(N)$	$\mathrm{GL}(N,\mathbb{C})/\mathrm{U}(N)$	AIII|AIII	$\mathrm{U}(2n)/\mathrm{U}(n)\times\mathrm{U}(n)$
AI	GOE	+ +	$\mathrm{U}(N)/\mathrm{O}(N)$	$\mathrm{GL}(N,\mathbb{R})/\mathrm{O}(N)$	BDI|CII	$\mathrm{Sp}(4n)/\mathrm{Sp}(2n)\times\mathrm{Sp}(2n)$
AII	GSE	+ –	$\mathrm{U}(2N)/\mathrm{Sp}(2N)$	$\mathrm{U}^*(2N)/\mathrm{Sp}(2N)$	CII|BDI	$\mathrm{O}(2n)/\mathrm{O}(n)\times\mathrm{O}(n)$
Chiral classes						
AIII	chGUE	– ±	$\mathrm{U}(p+q)/\mathrm{U}(p)\times\mathrm{U}(q)$	$\mathrm{U}(p,q)/\mathrm{U}(p)\times\mathrm{U}(q)$	A|A	$\mathrm{U}(n)$
BDI	chGOE	+ +	$\mathrm{SO}(p+q)/\mathrm{SO}(p)\times\mathrm{SO}(q)$	$\mathrm{SO}(p,q)/\mathrm{SO}(p)\times\mathrm{SO}(q)$	AI|AII	$\mathrm{U}(2n)/\mathrm{Sp}(2n)$
CII	chGSE	+ –	$\mathrm{Sp}(2p+2q)/\mathrm{Sp}(2p)\times\mathrm{Sp}(2q)$	$\mathrm{Sp}(2p,2q)/\mathrm{Sp}(2p)\times\mathrm{Sp}(2q)$	AII|AI	$\mathrm{U}(n)/\mathrm{O}(n)$
Bogoliubov–de Gennes classes						
C		– +	$\mathrm{Sp}(2N)\times\mathrm{Sp}(2N)/\mathrm{Sp}(2N)\equiv\mathrm{Sp}(2N)$	$\mathrm{Sp}(2N,\mathbb{C})/\mathrm{Sp}(2N)$	DIII|CI	$\mathrm{Sp}(2n)/\mathrm{U}(n)$
CI		+ +	$\mathrm{Sp}(2N)/\mathrm{U}(N)$	$\mathrm{Sp}(2N,\mathbb{R})/\mathrm{U}(N)$	D|C	$\mathrm{Sp}(2n)$
BD		– –	$\mathrm{SO}(N)\times\mathrm{SO}(N)/\mathrm{SO}(N)\equiv\mathrm{SO}(N)$	$\mathrm{SO}(N,\mathbb{C})/\mathrm{SO}(N)$	CI|DIII	$\mathrm{O}(2n)/\mathrm{U}(n)$
DIII		+ –	$\mathrm{SO}(2N)/\mathrm{U}(N)$	$\mathrm{SO}^*(2N)/\mathrm{U}(N)$	C|D	$\mathrm{O}(n)$

into two groups—chiral and Bogoliubov–de Gennes ensembles—considered here and in Sec. IV.D, respectively.

The chiral ensembles appeared in both contexts of particle physics and physics of disordered electronic systems about 15 years ago (Gade and Wegner, 1991; Gade, 1993; Slevin and Nagao, 1993; Verbaarschot and Zahed, 1993). The corresponding Hamiltonians have the form

$$H=\begin{pmatrix}0 & h\\ h^\dagger & 0\end{pmatrix}, \tag{4.5}$$

i.e., they possess the symmetry

$$\tau_z H\tau_z=-H, \tag{4.6}$$

where τ_z is the third Pauli matrix in a certain "isospin" space. In the condensed matter context, such ensembles arise, in particular, when one considers a tight-binding model on a bipartite lattice with randomness in hopping matrix elements only. In this case, H has the block structure (4.5) in the sublattice space.

In addition to chiral symmetry, a system may possess time-reversal and/or spin-rotation invariance. In complete analogy with the Wigner-Dyson classes, IV.A, one gets three chiral classes (unitary, orthogonal, and symplectic). The corresponding symmetric spaces, the Cartan notations for symmetry classes, and the σ-model manifolds are given in rows 4–6 of Table I.

D. Bogoliubov–de Gennes classes

As found by Altland and Zirnbauer (1997), the Wigner-Dyson and chiral classes do not exhaust all possible symmetries of disordered electronic systems. The remaining four classes arise most naturally in superconducting systems. The quasiparticle dynamics in such systems can be described by the Bogoliubov–de Gennes Hamiltonian of the form

$$\hat{H}=\sum_{\alpha\beta}^{N}h_{\alpha\beta}c_\alpha^\dagger c_\beta+\frac{1}{2}\sum_{\alpha\beta}^{N}(\Delta_{\alpha\beta}c_\alpha^\dagger c_\beta^\dagger-\Delta_{\alpha\beta}^*c_\alpha c_\beta), \tag{4.7}$$

where $c^\dagger$ and c are fermionic creation and annihilation operators, and the $N\times N$ matrices h, Δ satisfy $h=h^\dagger$ and $\Delta^T=-\Delta$, due to Hermiticity. Combining $c_\alpha^\dagger, c_\alpha$ in a spinor $\psi_\alpha^\dagger=(c_\alpha^\dagger, c_\alpha)$, one gets a matrix representation of the Hamiltonian $\hat{H}=\psi^\dagger H\psi$, where

$$H=\begin{pmatrix}h & \Delta\\ -\Delta^* & -h^T\end{pmatrix},\quad h=h^\dagger,\quad \Delta=-\Delta^T. \tag{4.8}$$

The minus signs in the definition of H result from the fermionic commutation relations between $c^\dagger$ and c. The Hamiltonian structure (4.8) corresponds to the condition

$$H=-\tau_x H^T\tau_x \tag{4.9}$$

(in addition to the Hermiticity $H=H^\dagger$), where τ_x is the Pauli matrix in the particle-hole space. Alternatively, one can perform a unitary rotation of the basis, defining $\tilde{H}=g^\dagger Hg$ with $g=(1+i\tau_x)/\sqrt{2}$. In this basis, the defining condition of class D becomes $\tilde{H}=-\tilde{H}^T$, so that $\tilde{H}$ is purely imaginary. The matrices $X=iH$ thus form the Lie algebra $\mathfrak{so}(2N)$, corresponding to the Cartan class D. This symmetry class describes disordered superconducting systems in the absence of other symmetries.

TABLE II. Compact symmetric spaces arranged in a form of a matrix, with the corresponding Cartan symbols. First row: U, Sp, and O groups. Second (third, fourth) row: Symmetric spaces G/K (which are not groups themselves) with K the unitary (symplectic, orthogonal) group.

$U(N)$	A	$Sp(2N)$	C	$SO(N)$	BD
$U(p+q)/U(p)\times U(q)$	AIII	$Sp(2N)/U(N)$	CI	$SO(2N)/U(N)$	DIII
$U(2N)/Sp(2N)$	AII	$Sp(2p+2q)/Sp(2p)\times Sp(2q)$	CII		
$U(N)/O(N)$	AI			$SO(p+q)/SO(p)\times SO(q)$	BDI

The symmetry class will be changed if time-reversal and/or spin rotation invariance are present. The difference with respect to the Wigner-Dyson and chiral classes is that now one gets four different classes rather than three. This occurs because the spin-rotation invariance has an impact even in the absence of time-reversal invariance, since it combines with the particle-hole symmetry in a nontrivial way. Indeed, if spin is conserved, the Hamiltonian has the form

$$\hat{H} = \sum_{ij}^{N} [h_{ij}(c_{i\uparrow}^{\dagger}c_{j\uparrow} - c_{j\downarrow}c_{i,\downarrow}^{\dagger}) + \Delta_{ij}c_{i,\uparrow}^{\dagger}c_{j,\downarrow}^{\dagger} + \Delta_{ij}^{*}c_{i\downarrow}c_{j\uparrow}], \tag{4.10}$$

where h and Δ are $N\times N$ matrices satisfying $h=h^{\dagger}$ and $\Delta=\Delta^{T}$. Similar to Eq. (4.8), we introduce the spinors $\psi_i^{\dagger}=(c_{i\uparrow}^{\dagger},c_{i\downarrow})$ and obtain the following matrix form of the Hamiltonian:

$$H = \begin{pmatrix} h & \Delta \\ \Delta^{*} & -h^{T} \end{pmatrix}, \quad h=h^{\dagger}, \quad \Delta=\Delta^{T}. \tag{4.11}$$

The Hamiltonian exhibits a symmetry property

$$H = -\tau_y H^{T} \tau_y. \tag{4.12}$$

The matrices $H=iX$ now form the Lie algebra $\mathfrak{sp}(2N)$, which is the symmetry class C.

If time reversal invariance is present, one gets two more classes (CI and DIII). The symmetric spaces for the Hamiltonians and the σ models corresponding to the Bogoliubov—de Gennes classes are given in the last four rows of Table I.

E. Additional comments

(i) In addition to Table I, where the symmetry classes are ordered according to the discrete symmetries of the underlying physical systems, we include Table II with a more mathematical ordering. There, the first row is formed by compact symmetric spaces that are groups and the rest is a matrix of symmetric spaces G/K arranged according to the type (U, Sp, or O) of the groups G and K. This ordering illustrates the completeness of the classification scheme: all entries in the matrix are filled, except for two, as there is no symmetric spaces of the O/Sp and Sp/O types. Also, we show in Sec. VI that this ordering is relevant to types of 2D critical behavior that the corresponding systems may show. In particular, the first row are the classes where different types of the QHE (IQHE, SQHE, and TQHE) take place. The second row is formed by the classes allowing for the Wess-Zumino type of criticality, while the third row are the systems which allow for a $\mathbb{Z}_2$ topological term. The diagonal of the matrix is occupied by three chiral classes.

(ii) Strictly speaking, one should distinguish between the orthogonal group $SO(N)$ with even and odd N, which form different Cartan classes: $SO(2N)$ belongs to class D, while $SO(2N+1)$ to class B. In the conventional situation of a disordered superconductor, the matrix size is even due to the particle-hole space doubling, see Sec. IV.D. It was found, however, that the class B can arise in p-wave vortices (Ivanov, 2002a, 2002b). In the same sense, the class DIII should be split into DIII-even and DIII-odd; the last one represented by the symmetric space $SO(4N+2)/U(2N+1)$ can appear in vortices in the presence of time-reversal symmetry.

F. Perturbative β functions for σ models of different symmetry classes

Perturbative β functions for σ models on all types of symmetric spaces were in fact calculated (Hikami, 1981; Wegner, 1989) long before the physical significance of the chiral and Bogoliubov–de Gennes classes has been fully appreciated. In Table III we present results for all β functions, $\beta(t)=-dt/d\ln L$, in $d=2+\epsilon$ dimensions up to four-loop order. Here t is the coupling constant inversely proportional to the dimensionless conductance g, and the Anderson localization problem corresponds to the replica limit $N=p=0$. The corresponding results for the Wigner-Dyson classes have already been shown in Sec. II.B.2. For each symmetry class of disordered electronic systems, the perturbative β function can be equivalently obtained from either compact or noncompact σ models on the appropriate manifolds. As an example, the β function for the Wigner-Dyson orthogonal class can be found using the replica limit of the compact σ model of the type CII or of the noncompact σ model of the type BDI.

It is seen that for the classes A, AI, C, CI the β function is negative in 2D in the replica limit $N=p=0$ (at

TABLE III. Perturbative β functions, $\beta(t)=-dt/d\ln L$, up to the four-loop order for the σ models in $d=2+\epsilon$ dimensions with symmetric spaces as target manifolds (Hikami, 1981; Wegner, 1989). First column: Cartan symbol for the σ-model symmetric space. Second column: Compact σ-model manifold. (The associated noncompact spaces can be found in Table I.) Third column: Symmetry class of random Hamiltonians described by the replica version of the compact σ model (c) and of its noncompact counterpart (*nc*). The last five columns give the coefficients of the terms from t to t^5 in the β functions for compact σ models. The β functions for the corresponding noncompact σ models are obtained by the substitution $\beta(t)\to-\beta(-t)$, i.e., by flipping the sign of the terms with even powers of t. The following notations are used: $a=\frac{3}{16}\zeta(3)$, $c_5(N,p)=-(\frac{2}{3}N^2(N-p)+5p^2(N-p)+16a)p(N-p)+(-\frac{2}{3}+16a)p(N-p)+(\frac{7}{6}+16a)N^2+(\frac{1}{3}-64a)N+64a)$; $c_4(N,p)=-[\frac{1}{3}pN^2(N-p)+5p^2(N-p)^2+\frac{11}{6}N^2+11p(N-p)+6]$; $c_3(N)=-(\frac{19}{48}N^4+\frac{119}{48}N^3+\frac{380}{48}N^2+\frac{578}{48}N+\frac{376}{48})$; $c_2(N)=-[\frac{19}{3}N^3-(\frac{43}{3}-8a)N^2+(9+8a)N-1]$; and $c_1(N)=-[(\frac{19}{48}+a)(N-2)^3-a(N-3)(N-4)(N+2)]$.

σ-model class	Compact σ-model manifold	Hamiltonian $c\|nc$	t	t^2	t^3	t^4	t^5
AIII	$U(N)/U(p)\times U(N-p)$	A	ϵ	$-N$	$-2[1+p(N-p)]$	$-\frac{1}{2}N[3p(N-p)+7]$	$c_4(N,p)$
BDI	$O(N)/O(p)\times O(N-p)$	AII|AI	ϵ	$-(N-2)$	$-[2p(N-p)-N]$	$-[\frac{3}{2}pN(N-p)-\frac{5}{4}N^2+p(N-p)+\frac{1}{2}N]$	$c_5(N,p)$
CII	$Sp(2N)/Sp(2p)\times Sp(2N-2p)$	AI|AII	ϵ	$\frac{1}{2}(N-2)$	$-\frac{1}{4}[2p(N-p)-N]$	$\frac{1}{8}[\frac{3}{2}pN(N-p)-\frac{5}{4}N^2+p(N-p)+\frac{1}{2}N]$	$\frac{1}{16}c_5(N,p)$
AI	$U(N)/O(N)$	CII|BDI	ϵ	$-N$	$-N(\frac{1}{2}N+1)$	$-N(\frac{3}{8}N^2+\frac{5}{4}N+1)$	$-\frac{N}{2}c_2(-N/2)$
AII	$U(2N)/Sp(2N)$	BDI|CII	ϵ	$-2N$	$-2N(N-1)$	$-N(3N^2-5N+2)$	$Nc_2(N)$
CI	$Sp(2N)/U(N)$	C|BD	ϵ	$-(N+1)$	$-\frac{1}{2}(N^2+3N+4)$	$-\frac{1}{8}(3N^3+14N^2+35N+28)$	$c_3(N)$
DIII	$O(2N)/U(N)$	BD|C	ϵ	$-(2N-2)$	$-(2N^2-6N+8)$	$-(3N^3-14N^2+35N-28)$	$c_3(-2N)$
A	$U(N)\times U(N)/U(N)$	AIII	ϵ	$-N$	$-\frac{1}{2}N^2$	$-N^3[\frac{3}{8}+(\frac{19}{48}+a)N]$	$aN^2(N-2)(N+2)$
C	$Sp(2N)\times Sp(2N)/Sp(2N)$	CI|DIII	ϵ	$-(N+1)$	$-\frac{1}{2}(N+1)^2$	$-\frac{3}{8}(N+1)^3$	$-\frac{N+1}{8}c_1(-2N)$
BD	$O(N)\times O(N)/O(N)$	DIII|CI	ϵ	$-(N-2)$	$-\frac{1}{2}(N-2)^2$	$-\frac{3}{8}(N-2)^3$	$(N-2)c_1(N)$

least, for small t). This indicates that normally all states are localized for such systems in 2D. (This conclusion can in fact be changed in the presence of topological or Wess-Zumino terms, see Sec. VI.A.) Above 2D, these systems undergo the Anderson transition that can be studied within the $2+\epsilon$ expansion, see Sec. II.B.2. For the classes AIII, BDI, and CII (chiral unitary, orthogonal, and symplectic classes, respectively) the $\beta(t)\equiv 0$ in 2D, implying a line of fixed points, see Sec. VI.F. Finally, in the classes AII, D, and DIII the β function is positive at small t, implying the existence of a metal-insulator transition at strong coupling in 2D. The 2D Anderson transitions in the Wigner-Dyson symplectic class AII and in the Bogoliubov–de Gennes class D are discussed in Secs. VI.B and VI.E, respectively.

V. QUASI-1D SYSTEMS: DISORDERED WIRES

Under usual conditions, electronic states in disordered wires are localized with localization length $\xi\sim Nl$, where l is the mean-free path and N the number of conducting channels (Berezinsky, 1974; Thouless, 1977; Efetov and Larkin, 1983). This is, however, not the complete story, and that is why we include quasi-1D systems in this review on localization-delocalization transitions and criticality. In fact, one route to delocalization and criticality in systems of 1D geometry—long-range $1/r$ hopping—was discussed in Sec. III. In this section we consider possible types of delocalization in disordered wires which are related to the symmetries of the problem. We show that in many cases there are close connections between such phenomena in quasi-1D and 2D systems (Sec. VI).

Two approaches to quasi-1D disordered electronic systems have been developed. The first one is the supersymmetric σ-model approach, see Sec. II.B.1. For the wire geometry, the σ-model field Q depends on the longitudinal coordinate only. As a result, the problem becomes a kind of imaginary-time quantum mechanics on the σ-model manifold, with the longitudinal coordinate playing the role of the (imaginary) time. This has allowed one to get a number of exact results for Wigner-Dyson symmetry classes, including the asymptotics of the density-density correlation function and the value of the localization length (Efetov and Larkin, 1983), a detailed description of the wave-function statistics (Fyodorov and Mirlin, 1994), average conductance, and its variance (Zirnbauer, 1992; Mirlin *et al.*, 1994). For reviews of results for statistical properties of various quantities in disordered wires obtained within the σ-model approach, see Efetov (1997) and Mirlin (2000b).

The second approach is based on the description of a wire in terms of its transfer matrix M. The evolution of the corresponding distribution $\mathcal{P}(M)$ with the wire length is described by the Dorokhov-Mello-Pereyra-Kumar (DMPK) equation (Dorokhov, 1982; Mello *et al.*, 1988). At variance with the σ-model approach, which allows one to address any observable, the DMPK approach is designed to study the transport properties. On

TABLE IV. Transfer matrix spaces. First column: Symmetry class of the Hamiltonian. Second and third columns: Symmetric space for the transfer matrix and the corresponding Cartan symmetry class. Last three columns: Multiplicities of the ordinary (m_o), long (m_l), and short (m_s) roots.

Hamiltonian class	Transfer matrix symmetric space	Transfer matrix class	m_o	m_l	m_s
Wigner-Dyson classes					
A	$\mathrm{U}(p+q)/\mathrm{U}(p)\times\mathrm{U}(q)$	AIII	2	1	$2\lvert p-q\rvert$
AI	$\mathrm{Sp}(2N,\mathbb{R})/\mathrm{U}(N)$	CI	1	1	0
AII	$\mathrm{SO}^*(2N)/\mathrm{U}(N)$ N even	DIII−e	4	1	0
	N odd	DIII−o			4
chiral classes					
AIII	$\mathrm{GL}(N,\mathbb{C})/\mathrm{U}(N)$	A	2	0	0
BDI	$\mathrm{GL}(N,\mathbb{R})/\mathrm{O}(N)$	AI	1	0	0
CII	$\mathrm{U}^*(2N)/\mathrm{Sp}(2N)$	AII	4	0	0
Bogoliubov–de Gennes classes					
C	$\mathrm{Sp}(2p,2q)/\mathrm{Sp}(2p)\times\mathrm{Sp}(2q)$	CII	4	3	$4\lvert p-q\rvert$
CI	$\mathrm{Sp}(2N,\mathbb{C})/\mathrm{Sp}(2N)$	C	2	2	0
BD	$\mathrm{O}(p,q)/\mathrm{O}(p)\times\mathrm{O}(q)$	BDI	1	0	$\lvert p-q\rvert$
DIII	$\mathrm{SO}(N,\mathbb{C})/\mathrm{SO}(N)$ N even	D	2	0	0
	N odd	B			2

the other hand, the advantage of the DMPK approach is that it allows one to study wires with an arbitrary number N of channels (not necessarily $N\gg 1$ as required for the diffusive σ model) and provides detailed information on the whole distribution of transmission eigenvalues. The two approaches are thus complementary; their equivalence for transport properties of many-channel wires (when both of them are applicable) was shown by Brouwer and Frahm (1996). A review of the results of the DMPK method for Wigner-Dyson symmetry classes was given by Beenakker (1997).

Peculiar transport properties of disordered wires of unconventional symmetry classes have been mainly studied within the DMPK approach. Below we describe this method and present key results. Whenever appropriate, we also make contact with results obtained within the σ-model formalism.

A. Transfer matrix and DMPK equations

In the transfer matrix approach, one imagines the wire attached to two clean electrodes, where one can define asymptotic states. This allows one to formulate a scattering problem. The transfer matrix M relates the amplitudes in N incoming and N outgoing channels to the right of the wire to the corresponding amplitudes on its left,

$$\begin{pmatrix} R^{\mathrm{out}} \\ R^{\mathrm{in}} \end{pmatrix} = M \begin{pmatrix} L^{\mathrm{in}} \\ L^{\mathrm{out}} \end{pmatrix}. \tag{5.1}$$

(In fact, for symmetry classes A, C, and BD with broken time-reversal symmetry the number of incoming and outgoing channels can differ. We discuss this in Sec. V.D.) The requirement for current conservation $|R^{\mathrm{out}}|^2 - |R^{\mathrm{in}}|^2 = |L^{\mathrm{in}}|^2 - |L^{\mathrm{out}}|^2$ implies that M is an element of the pseudounitary group $G=\mathrm{U}(N,N)$. The transfer matrix can be presented in the form (Cartan decomposition)

$$M = \begin{pmatrix} u & 0 \\ 0 & u' \end{pmatrix} \begin{pmatrix} \cosh\hat{x} & \sinh\hat{x} \\ \sinh\hat{x} & \cosh\hat{x} \end{pmatrix} \begin{pmatrix} v & 0 \\ 0 & v' \end{pmatrix}, \tag{5.2}$$

where $\hat{x}=\mathrm{diag}(x_1,\ldots,x_N)$ are radial coordinates, while the left and right matrices (angular coordinates) are elements of $K=\mathrm{U}(N)\times\mathrm{U}(N)$. If the Hamiltonian possesses some additional (time-reversal, spin-rotation, chiral, particle-hole) symmetries, the group G of the transfer matrices will change correspondingly, with K the maximal compact subgroup of G. The coset spaces G/K (which play the central role for the DMPK equations, see below) are noncompact symmetric spaces; they are listed for all symmetry classes of the Hamiltonian in Table IV. The dimensionless conductance of the wire is expressed in terms of the radial coordinates x_n as $G = d\Sigma_{n=1}^{N} T_n$, where $T_n = 1/\cosh^2 x_n$ are transmission eigenvalues and d is the degeneracy (1, 2, or 4) depending on the symmetry class.

When an additional thin slice with a transfer matrix T is attached to the wire, the new transfer matrix is obtained by simple multiplication $M'=TM$. For a given distribution function of the elementary transfer matrices T, one then gets a stochastic process on the space of transfer matrices. It is assumed in the derivation of the DMPK equations that the distribution of T is fully invariant with respect to the subgroup K (isotropy assumption), which corresponds to a complete mixture of channels at each elementary step. (This model assumption is justified by the fact that the mixing of channels in

a realistic wire takes place on a scale much shorter than the localization length.) As a result, the stochastic process develops in fact on the coset space G/K, describing a Brownian motion on this manifold. In view of the rotational symmetry, the distribution function depends on radial coordinates x_i only. The corresponding evolution equation, which is the DMPK equation, has the form

$$\frac{d\mathcal{P}}{dL} = \frac{1}{2\ell\gamma}\sum_{i=1}^{N}\frac{\partial}{\partial x_i}J(x)\frac{\partial}{\partial x_i}J^{-1}(x)\mathcal{P}, \tag{5.3}$$

where ℓ is the mean-free path; the Jacobian $J(x)$ of transformation to the radial coordinates and the parameter γ are specified below.

For the Wigner-Dyson and Bogoliubov–de Gennes classes the radial coordinates x_i satisfy[10] $0<x_1<x_2<\cdots<x_N$ and the Jacobian $J(x)$ is

$$J(x) = \prod_{i<j}^{N}\prod_{\pm}|\sinh(x_i \pm x_j)|^{m_o}\prod_{k}^{N}|\sinh 2x_k|^{m_l} \times \prod_{l}^{N}|\sinh x_l|^{m_s}. \tag{5.4}$$

Here m_o, m_s, and m_l are the multiplicities of the ordinary, short, and long roots for the corresponding symmetric space (Helgason, 1978; Caselle, 1996; Caselle and Magnea, 2004). The root multiplicities for all symmetry classes are listed in Table IV. The first factor in Eq. (5.4) is responsible for the repulsion between eigenvalues x_i, analogous to the energy level repulsion in RMT. The last two factors govern (when the corresponding multiplicities are nonzero) the repulsion between an eigenvalue x_i and its mirror $-x_i$, and the repulsion between x_i and zero, respectively. For the chiral classes, the variation domain of the coordinates x_i does not restrict their sign, $x_1<x_2<\cdots<x_N$, and the Jacobian is

$$J(x) = \prod_{i<j}^{N}|\sinh(x_i - x_j)|^{m_o}. \tag{5.5}$$

(For these classes $m_s=m_l=0$.) For the Wigner-Dyson and chiral classes the multiplicity m_o of the ordinary roots is the familiar parameter β of the RMT, equal to 1, 2, and 4 for the orthogonal, unitary, and symplectic symmetry classes, respectively. Further, the parameter γ in the DMPK equation is given by

$$\gamma = \begin{cases} m_o(N-1)+m_l+1, & \text{WD and BdG,} \\ \frac{1}{2}[2+m_o(N-1)], & \text{chiral.} \end{cases} \tag{5.6}$$

In the short-wire regime, $L \ll \gamma\ell$, where the conductance is large, $g \gg 1$, the DMPK equation yields Ohm's law for the average conductance, the quasi-1D universal conductance fluctuations, and the weak-localization corrections in the form of a $1/g$ series. Our interest here is in the opposite, long-wire limit, $L \gg \gamma\ell$, where localization or critical properties of the problem manifest themselves. This will be the subject of the remaining part of Sec. V. We also mention that at the crossover scale, $L \sim \gamma\ell$, an analytical treatment is most complicated. An approximate scheme has, however, been developed by Muttalib and Wölfle (1999); Gopar *et al.* (2002); Muttalib *et al.* (2003) that allows one to understand key properties of the conductance distribution in this regime.

B. Conventional localization in 1D geometry

We begin by considering the standard quasi-1D localization in Wigner-Dyson classes ($m_l=1$, $m_o=\beta$, $m_s=0$). In the long-wire limit the transmission eigenvalues satisfy the hierarchy $1 \gg T_1 \gg T_2 \gg \cdots$, i.e., the consecutive x_i are separated by intervals much larger than unity. One can thus approximate the hyperbolic sine functions in Eq. (5.4) by exponentials. As a result, all variables in the DMPK equation (5.3) fully decouple; the resulting Fokker-Planck equation for each of x_k is given by

$$\frac{d\mathcal{P}(x_k)}{dL} = \frac{1}{2\gamma\ell}\frac{\partial^2\mathcal{P}}{\partial x_k^2} - \frac{1}{\xi_k}\frac{\partial\mathcal{P}}{\partial x_k}, \tag{5.7}$$

where $\xi_k^{-1}=[1+\beta(k-1)]/\gamma\ell$. Equation (5.7) is of the advection-diffusion type, with $1/2\gamma\ell$ playing the role of the diffusion constant and $1/\xi_k$ the drift velocity. The solution has a Gaussian form with $\langle x_k\rangle = L/\xi_k$ and $\mathrm{var}(x_k) = L/\gamma\ell$. This implies that the logarithm of the conductance $g \simeq d/\cosh^2 x_1$ has a Gaussian distribution with the following average and variance (Beenakker, 1997):

$$-\langle \ln g\rangle = 2L/\gamma\ell, \quad \mathrm{var}(\ln g) = 4L/\gamma\ell. \tag{5.8}$$

For an atypically large g this distribution is cut at $g\sim 1$. The average conductance is found to be determined by this cutoff (i.e., by rare events of $g\sim 1$), $-\ln\langle g\rangle = L/2\gamma l$. Defining the typical and the average localization length via

$$-\langle \ln g\rangle = 2L/\xi_{\mathrm{typ}}, \quad -\ln\langle g\rangle = 2L/\xi_{\mathrm{av}}, \tag{5.9}$$

we thus find

$$\xi_{\mathrm{typ}} = \gamma\ell, \quad \xi_{\mathrm{av}} = 4\gamma\ell. \tag{5.10}$$

These results are in full agreement with those obtained within the σ-model formalism (Mirlin, 2000b), which corresponds to $N \gg 1$, so that $\gamma = \beta N$.

Similar behavior is also found in the Bogoliubov–de Gennes classes C and CI (Brouwer, Furusaki, *et al.*, 2000). The same derivation yields Eq. (5.7) with $\xi_k^{-1}=[3+4(k-1)]/\gamma\ell$ for class C and $\xi_k^{-1}=[2+2(k-1)]/\gamma\ell$ for class CI. Thus

$$-\langle \ln g\rangle = 6L/\gamma\ell, \quad \mathrm{var}(\ln g) = 4L/\gamma\ell \ \text{(C)}; \tag{5.11}$$

$$-\langle \ln g\rangle = 4L/\gamma\ell, \quad \mathrm{var}(\ln g) = 4L/\gamma\ell \ \text{(CI)}. \tag{5.12}$$

Calculating the average conductance, one gets $-\ln\langle g\rangle = 4L/\gamma l$ (class C) and $-\ln\langle g\rangle = 2L/\gamma l$ (class CI), so that

[10] For classes D and DIII the proper variation domain of x_i is slightly different, $|x_1|<x_2<\cdots<x_N$ (Gruzberg *et al.*, 2005).

$$\xi_{\rm typ} = \gamma\ell/3, \quad \xi_{\rm av} = \gamma\ell/2 \ \text{(C)}; \tag{5.13}$$

$$\xi_{\rm typ} = \gamma\ell/2, \quad \xi_{\rm av} = \gamma\ell \ \text{(CI)}. \tag{5.14}$$

A quasi-1D model of class C was also studied within the σ-model formalism by Bundschuh *et al.* (1998). They found that $\xi_{\rm av}$ is 8 times shorter than for class A. This agrees with the result of the DMPK approach, as is seen by comparison of $\xi_{\rm av}$ in Eqs. (5.13) and (5.10).

C. Types of delocalization in disordered wires

Having discussed how conventional localization in disordered quasi-1D systems takes place in Sec. V.B, we now analyze how electrons in such a system can escape exponential localization. Table IV is useful in this respect, showing that there are two distinct mechanisms.

First, we see that in all three chiral classes (AIII, BDI, and CII), as well as in the superconducting classes with broken spin-rotation invariance (BD and DIII), the multiplicity m_l of long roots is zero. This implies that there is no repulsion between the eigenvalue x_i and its mirror $-x_i$, so that the smallest (by absolute value) x_i can be close to zero. We analyze the critical behavior that emerges in these classes in Secs. V.E and V.F.

The second type of delocalization is related to the multiplicity of short roots m_s in Table IV. In the conventional situation it is equal to zero. However, there are five classes (A, C, BD, AII, and DIII) where it can be nonzero. A nonzero value of m_s implies a repulsion of x_i from zero, which indicates the existence of exactly zero eigenvalues of the transfer matrix. These zero eigenvalues imply perfectly transmitting channels, yielding a finite conductance in the limit of infinite system length. We discuss this class of systems in Sec. V.D.

D. Models with perfectly conducting channels

In this section, we consider models with perfectly transmitting channels ($m_s \neq 0$, see Table IV). These models are in turn subdivided into two types.

In the classes A, C, and BD, the transfer matrix spaces given in the Table IV correspond to a model with p channels propagating to the left and q channels propagating to the right. While in the conventional situation $p=q$, symmetric spaces with $p \neq q$ are allowed as well. It is not difficult to understand what is the physical realization for these models if one recalls that these are exactly those classes whose 2D representatives show the quantum Hall effects, see Sec. VI. When such a 2D system is on the quantum Hall plateau of order p, there are p edge channels that propagate on its boundary. These channels are chiral in the sense that they can propagate in one direction only. The edge of such a system thus represents a wire of the corresponding symmetry class with p modes propagating in one direction and zero in the opposite. Since there is no backscattering, the conductance of such a wire is identically equal to p. Consider now parallel edges of two quantum Hall systems with counterpropagating modes separated by a potential barrier. Assuming that there are p modes in one edge and q in the other and that they are coupled by tunneling, we get a wire of the (q,p) type from the corresponding class. In the long length limit, $|p-q|$ modes will then remain perfectly conducting, while the rest will be localized. It was recently shown that graphene ribbons with zigzag edge and smooth disorder provide a physical realization of the class A with $|p-q|=1$ (Wakabayashi *et al.*, 2007).

The situation with the classes AII and DIII is much more intricate. The systems of these classes may possess a single perfectly conducting channel. As explained below, this reflects an underlying $\mathbb{Z}_2$ topological structure. A delocalization in the symplectic Wigner-Dyson class AII was obtained for the first time within the σ-model formalism by Zirnbauer (1992) and Mirlin *et al.* (1994). It was found in these works that the average conductance and its variance remain finite in the long wire limit, $\langle g\rangle \to 1/2$, $\mathrm{var}(g)\to 1/4$ due to a zero mode of the corresponding transfer operator. The physical significance of these results was not understood at this stage. Further, it was shown by Brouwer and Frahm (1996) that the above zero mode is double valued on the σ-model manifold and thus does not contribute in the case of a conventional wire with spin-orbit interaction. More recently, it was shown, however, that a model of symplectic symmetry with a perfectly conducting channel arises if one considers transport in carbon nanotubes (Ando and Suzuura, 2002; Suzuura and Ando, 2002). The problem is described by two species of Dirac fermions corresponding to two valleys in the graphene spectrum. If the scatterers are of long-range character and the intervalley scattering can be neglected, the problem acquires the symplectic (AII) symmetry, with the sublattice space taking the role of isospin (Sec. VI.G.2). Furthermore, in contrast to conventional wires of AII symmetry, where the number of channels is even, there is a single channel here. (More precisely, its partner belongs to the other node, and they do not talk to each other.) As a result, the channel remains perfectly transmitting independent of the length of the wire.

In subsequent works (Takane, 2004a, 2004b; Sakai and Takane, 2005; Caselle and Magnea, 2006) quasi-1D systems of the AII symmetry class with an odd number N of channels were studied within the DMPK approach. It was found that for any odd N a single perfectly transmitting channel remains in the limit $L \gg \gamma\ell$. As emphasized by Takane (2004c), these results are in full agreement with earlier σ-model results of Zirnbauer (1992) and Mirlin *et al.* (1994), if the latter are complemented by the following interpretation. The Fourier expansion employed by Zirnbauer (1992) and Mirlin *et al.* (1994) contained eigenfunctions of the Laplace operator in the σ-model manifold of two types—with even and odd parity (the zero mode is of the odd-parity type). For systems with an even (odd) number of channels one should keep only even-parity (odd-parity) eigenmodes and include an overall factor of 2. The original results of Zirnbauer

(1992) and Mirlin *et al.* (1994) with $\langle g\rangle$, $\langle g^2\rangle \to 1/2$ at $L\to\infty$ corresponds thus to an average over wires with even and odd number of channels.

In the problem with perfectly transmitting channels, one can determine the localization length for the remaining modes by considering the deviation δg of the conductance from its $L\to\infty$ limit. A straightforward generalization of the consideration sketched in Sec. V.B yields (Caselle and Magnea, 2006)

$$-\langle \ln \delta g\rangle = (2m_l + m_s)L/\gamma\ell\ , \tag{5.15}$$

so that $\xi_{\rm typ}=\gamma\ell/(m_l+m_s/2)$. This implies for both the AII and DIII models with an odd number of channels

$$\xi_{\rm typ} = \gamma\ell/3, \quad \xi_{\rm av} = \gamma\ell/2. \tag{5.16}$$

The qualitative different behavior of class AII (and DIII) wires with an even and odd number of channels is intimately connected with a nontrivial topology of the corresponding σ-model manifold (or, more specifically, of its compact component $\mathcal{M}_F$): the first homotopy group $\pi_1(\mathcal{M}_F)$ is equal to $\mathbb{Z}_2$. This enables a topological θ term with θ equal to 0 or π (Ostrovsky *et al.*, 2007a), in analogy with the 2D situation, see Secs. VI.A.5 and VI.B.5 for these symmetry classes. The topological term with $\theta=\pi$ is present if the number of channels is odd.

Another realization of a symplectic symmetry wire with an odd number of channels has emerged in the quantum spin Hall (QSH) effect in systems of Dirac fermions with spin-orbit coupling (Kane and Mele, 2005a, 2005b; Bernevig *et al.*, 2006). Such systems were found to possess two distinct insulating phases (with a transition between them driven by Rashba spin-orbit coupling strength), both having a gap in the bulk electron spectrum but differing by the edge properties. The topological distinction between the two insulating phases retains its validity in the presence of disorder (Sheng *et al.*, 2005; Essin and Moore, 2007; Obuse, Furusaki, *et al.*, 2007; Onoda *et al.*, 2007). While the normal insulating phase has no edge states, the QSH insulator is characterized by a pair of mutually time-reversed edge states penetrating the bulk gap. These edge states in the QSH phase, which do not get localized by disorder, represent the class AII wire with a nontrivial $\mathbb{Z}_2$ topology.

E. Chiral classes

For the chiral classes, the consideration analogous to that in Sec. V.B (Mudry *et al.*, 1999, 2000; Brouwer, Mudry, and Furusaki, 2000) yields $\langle x_k\rangle = (2k-1-N)\beta L/2\gamma\ell$. If the number of channels is even, then the smallest (by absolute value) eigenvalues x_k are separated by a large gap from zero: $-\langle x_{N/2}\rangle = \langle x_{N/2+1}\rangle = L/2\gamma\ell$. Therefore exponential localization is preserved, $-\langle \ln g\rangle = \beta L/\gamma\ell$, $\mathrm{var}(\ln g) = 4L/\gamma\ell$, yielding the localization lengths

$$\xi_{\rm typ} = 2\gamma\ell/\beta, \quad \xi_{\rm av} = 16\gamma\ell/\beta^2. \tag{5.17}$$

On the other hand, if N is odd, one of the eigenvalues is close to zero, $\langle x_{(N+1)/2}\rangle = 0$. This leads to a completely different behavior for the conductance,

$$-\langle \ln g\rangle = \left(\frac{8L}{\pi\gamma\ell}\right)^{1/2}, \quad \mathrm{var}(\ln g) = \left(4-\frac{8}{\pi}\right)\frac{L}{\gamma\ell}; \tag{5.18}$$

$$\langle g\rangle = (2\gamma\ell/\pi L)^{1/2}, \quad \mathrm{var}(g) = (8\gamma\ell/9\pi L)^{1/2}. \tag{5.19}$$

It can be seen from Eq. (5.18) that while the typical conductance decays in a stretched-exponential way, its fluctuations are very strong so that the probability to have $g\sim 1$ is small as $L^{-1/2}$ only. This determines the slow decay (5.19) of the average conductance, which is even slower than in the classical Ohm's law.

Delocalization takes place for an arbitrary odd N, including $N=1$. The single-channel model with chiral class disorder has been studied, in its various incarnations, starting from the pioneering paper by Dyson (1953). We list most salient features characterizing (in addition to the above results for the statistical properties of the conductance) this critical point.

(i) *Localization length.* If the energy E deviates from zero, chiral symmetry is broken, and exponential localization establishes. One can thus ask how the corresponding localization length diverges at $E\to 0$. It has been found that one should distinguish between average and typical observables (e.g., conductance) whose spatial dependence is governed by two parametrically different lengths (Fisher, 1995; Balents and Fisher, 1997),

$$\xi_{\rm typ} \sim |\ln E|, \quad \xi_{\rm av} \sim |\ln E|^2. \tag{5.20}$$

The scaling of $\xi_{\rm typ}$ was found previously (Eggarter and Riedinger, 1978; Ziman, 1982).

(ii) *Staggering.* An alternative way to drive the system out of criticality is to introduce a staggering M in the hopping strength which opens a gap around zero energy in the spectrum of a clean system. The corresponding localization lengths behave as follows (Fisher, 1995; Balents and Fisher, 1997; Mathur, 1997):

$$\xi_{\rm typ} \sim M^{-1}, \quad \xi_{\rm av} \sim M^{-2}. \tag{5.21}$$

(iii) *Wave function at criticality.* The Hamiltonian of a single-channel problem can be written in a Dirac form (Balents and Fisher, 1997),

$$H = -i\sigma_z\partial_x + m(x)\sigma_y, \tag{5.22}$$

where $m(x)=M+\tilde{m}(x)$ and $\tilde{m}(x)$ is the disorder (e.g., of the white-noise type). The zero-energy eigenfunction can then be found explicitly,

$$\Psi(x) = \begin{pmatrix} 1 \\ \pm 1 \end{pmatrix} \frac{\psi_{\pm}(x)}{\left[\int dx \psi_{\pm}^2(x)\right]^{1/2}},$$

$$\psi_{\pm}(x) = \exp\left[\pm \int^x dx' m(x')\right]. \quad (5.23)$$

The properties of this wave function were analyzed by Balents and Fisher (1997). The following scaling of the spatial correlation function of the moments of $\psi(x)$ at criticality ($M=0$) was found:

$$\langle |\psi(x)\psi(0)|^q \rangle \sim L^{-1}|x|^{-3/2}, \quad (5.24)$$

for all $q>0$. This result can be interpreted in terms of the following picture of wave functions at criticality (Balents and Fisher, 1997). The wave function is typically quasilocalized, showing a stretched exponential decay with respect to its principal maximum. However, with a probability $\sim x^{-3/2}$ it shows a secondary maximum of a magnitude close to the primary one and separated by a distance x.

(iv) *Density of states.* The DOS shows at criticality the Dyson singularity (Dyson, 1953; McKenzie, 1996; Titov and Brouwer, 2001),

$$\rho(E) \sim 1/|E \ln^3 E|. \quad (5.25)$$

When the system is driven away from criticality by a nonzero staggering parameter M, the singularity weakens and becomes nonuniversal, $\rho(E) \sim |E|^{-1+\delta}$ with $\delta>0$.

Finally, it has been shown that a sufficiently strong staggering M can also drive a system with even N into a critical state (Brouwer *et al.*, 1998). More specifically, the staggering shifts all variables x_k by a constant. With increasing M, the average values $\langle x_k \rangle$ consecutively cross zero; whenever this happens, the system is at criticality. Therefore, whether N is odd or even, changing M will drive the system through N transition points.

F. Bogoliubov–de Gennes classes with broken spin-rotation invariance

Analysis of the DMPK equation for the classes BD and DIII (Brouwer, Furusaki, *et al.*, 2000a) leads to results identical to those obtained for chiral classes, Eqs. (5.18) and (5.19). Furthermore, the DOS was found to show the Dyson singularity (5.25), again in full analogy with the chiral classes.

On the other hand, Motrunich *et al.* (2001) studied certain single-channel models of the classes D and DIII via a strong-disorder real-space RG. They found that generically these systems are in localized phases and the DOS diverges in a power-law fashion with a nonuniversal exponent, $\rho(E) \sim E^{-1+\delta}$ with $\delta>0$. Only at phase boundaries is the system critical and the DOS takes the Dyson form (5.25).

An apparent contradiction between the results of both papers was resolved by Gruzberg *et al.* (2005). They showed that, generically, quasi-1D systems of the classes BD and DIII are in a localized phase, in agreement with Motrunich *et al.* (2001). The terms that drive the system towards localization are usually neglected within the DMPK approach, as they are irrelevant at the short-distance (diffusive) fixed point. However, Gruzberg *et al.* (2005) found that these terms become relevant at the long-distance (critical) fixed point and drive the system away from it, into the localization fixed point. Only if the disorder is fine tuned, the system is at the critical point. On the other hand, the length at which the crossover from criticality to localization happens becomes exponentially large with increasing number of channels N. Therefore in the thick-wire limit, $N \gg 1$, the system is essentially at criticality. An analogous conclusion was also reached by Brouwer *et al.* (2003).

Motrunich *et al.* (2001) and Gruzberg *et al.* (2005) argued that critical points with Dyson singularities of all five symmetry classes (AIII, BDI, CII, BD, and DIII) belong to the same universality class. To establish this remarkable "superuniversality," Gruzberg *et al.* (2005) pointed out that all universal properties can be obtained from $N=1$ models and then constructed mappings between single-channel models of all five classes.

VI. CRITICALITY IN 2D

A. Mechanisms of criticality in 2D

As discused in Sec. II.B.2, conventional Anderson transitions in the orthogonal and unitary symmetry classes take place only if the dimensionality is $d>2$, whereas in 2D all states are localized. It is, however, well understood that there is a rich variety of mechanisms that lead to emergence of criticality in 2D disordered systems. Such 2D critical points have been found to exist for 9 out of 10 symmetry classes, namely, in all classes except for the orthogonal class AI. A summary of possible types of 2D criticality was given by Fendley (2001); we closely follow this work here. We now describe the mechanisms for the emergence of criticality; a detailed discussion of the corresponding critical points is given in Sec. VI.B–VI.G.

1. Broken spin-rotation invariance: Metallic phase

We begin with the mechanism mentioned in Sec. II.B.2 in the context of the Wigner-Dyson symplectic class (AII). In this case the β function [Eq. (2.24) with $\epsilon=0$] is positive for not too large t (i.e., sufficiently large conductance), so that the system is metallic (t scales to zero under RG). On the other hand, for strong disorder (large t) the system is an insulator, as usual, i.e., $\beta(t)<0$. Thus the β function crosses zero at some t_*, which is the point of the Anderson transition. Properties of this critical point are discussed in Sec. VI.B.

This mechanism (positive β function and thus metallic phase at small t, with a transition at some t_*) is also

realized in two of the Bogoliubov–de Gennes classes, D and DIII; see Table III. These classes correspond to systems with broken spin-rotation invariance. The unconventional sign of the β function in these classes, indicating weak antilocalization (rather then localization), is physically related to destructive interference of time-reversed paths for particles with spin $s=1/2$.

2. Chiral classes: Vanishing β function

Another peculiarity of the perturbative β function takes place for three chiral classes—AIII, BDI, and CII. Specifically, for these classes $\beta(t)\equiv 0$ to all orders of perturbation theory, as first discovered by Gade and Wegner (Gade and Wegner, 1991; Gade, 1993). As a result, the conductance is not renormalized, serving as an exactly marginal coupling. There is thus a line of critical points for these models, labeled by the conductance value. In fact, the σ models for these classes contain an additional term (Gade and Wegner, 1991; Gade, 1993) that does not affect the absence of renormalization of the conductance but is crucial for the analyzing the DOS behavior. A discussion of the chiral classes is given in Sec. VI.F.

3. Broken time-reversal invariance: Topological θ term and quantum Hall criticality

For several classes, the σ-model action allows for inclusion of a topological term, which is invisible to any order of the perturbation theory. This occurs when the second homotopy group π_2 of the σ-model manifold $\mathcal{M}$ (a group of homotopy classes of maps of the sphere S^2 into $\mathcal{M}$) is nontrivial.[11] From this point of view, only the compact sector $\mathcal{M}_F$ (originating from the fermionic part of the supervector field) of the manifold base matters. There are five classes for which $\pi_2(\mathcal{M}_F)$ is nontrivial, namely A, C, D, AII, and CII.

For the classes A, C, and D the homotopy group is $\pi_2(\mathcal{M}_F)=\mathbb{Z}$. Therefore the action $S[Q]$ may include the (imaginary) θ term,

$$iS_{\text{top}}[Q]=i\theta N[Q], \tag{6.1}$$

where an integer $N[Q]$ is the winding number of the field configuration $Q(\mathbf{r})$. Without loss of generality, θ can be restricted to the interval $[0,2\pi]$, since the theory is periodic in θ with period 2π.

The topological term (6.1) breaks the time-reversal invariance, so it may only arise in the corresponding symmetry classes. The by far most famous case is the Wigner-Dyson unitary class (A). As first understood by Pruisken (1984, 1987), the σ model of this class with the topological term (6.1) describes the integer quantum Hall effect (IQHE), with the critical point of the plateau transition corresponding to $\theta=\pi$. More recently, it was shown that counterparts of the IQHE also exist in the Bogoliubov–de Gennes classes with broken time-reversal invariance—classes C and D. They were called *spin* and *thermal* quantum Hall effects (SQHE and TQHE), respectively. Criticality at the IQHE, SQHE, and TQHE transitions is discussed in Secs. VI.C–VI.E, respectively.

4. $\mathbb{Z}_2$ topological term

For two classes, AII and CII, the second homotopy group is $\pi_2(\mathcal{M}_F)=\mathbb{Z}_2$. This allows for the θ term but θ can only take the values 0 and π. Recently it was shown (Ostrovsky *et al.*, 2007a) that the σ model of the Wigner-Dyson symplectic class (AII) with a $\theta=\pi$ topological angle arises from a model of Dirac fermions with random scalar potential, which describes, in particular, graphene with long-range disorder. As in quantum Hall systems, this topological term inhibits localization. Whether the model flows then unavoidably into the ideal metal fixed point or, else, there is also a novel attractive fixed point is a matter of ongoing research. We refer the reader to Sec. VI.B for more details.

5. Wess-Zumino term

Finally, one more mechanism for the emergence of criticality is the Wess-Zumino (WZ) term. This term may appear in σ models of the classes AIII, CI, and DIII. For these classes, the compact component $\mathcal{M}_F$ of the manifold is the group $H\times H/H=H$, where H is U(n), Sp($2n$), and O($2n$), respectively. The corresponding theories are called principal chiral models. The WZ term has the following form:

$$iS_{\text{WZ}}(g)=\frac{ik}{24\pi}\int d^2r\int_0^1 ds\,\epsilon_{\mu\nu\lambda}\text{Str}(g^{-1}\partial_\mu g)(g^{-1}\partial_\nu g)\times(g^{-1}\partial_\lambda g), \tag{6.2}$$

where k is an integer called the level of the WZW model. The definition (6.2) of the WZ term requires an extension of the σ-model field $g(\mathbf{r})\equiv g(x,y)$ to the third dimension, $0\le s\le 1$, such that $g(\mathbf{r},0)=1$ and $g(\mathbf{r},1)=g(\mathbf{r})$. Such an extension is always possible, since the second homotopy group is trivial, $\pi_2(H)=0$, for all three classes. Further, the value of the WZ term does not depend on how the extension to the third dimension is performed. [This becomes explicit when one calculates the variaton of the WZ term: it is expressed in terms of $g(\mathbf{r})$ only.] More precisely, there is a topological ambiguity in the definition of $S_{\text{WZ}}(g)$. Since the third homotopy group is nontrivial, $\pi_3(H)=\mathbb{Z}$, $S_{\text{WZ}}(g)$ is defined up to an arbitrary additive integer n times $2\pi k$. This, however, does not affect any observables, it simply adds the phase $nk\times 2\pi i$ to the action.

The WZ term arises when one bosonizes certain models of Dirac fermions (Witten, 1984) and is a manifestation of the chiral anomaly. In particular, a σ model for a system of the AIII (chiral unitary) class with the WZ term describes Dirac fermions in a random vector po-

[11] A pedagogical introduction of topological concepts in the context of condensed matter theory can be found in Altland and Simons (2006).

tential. In this case the σ-model coupling constant is truly marginal (as is typical for chiral classes) and one finds a line of fixed points. On the other hand, for the class CI there is a single fixed point. The WZ models of these classes were encountered in the course of study of dirty d-wave superconductors (Nersesyan *et al.*, 1995; Altland *et al.*, 2002) and, most recently, in the context of disordered graphene. We discuss the critical properties of these models in Sec. VI.G.3.

B. Symplectic Wigner-Dyson class (AII)

In metals with spin-orbit coupling the spin of a particle is no longer conserved. The spin-up and spin-down channels are coupled, and an electron needs to be represented as a two component spinor. If time-reversal symmetry is preserved, the system belongs to the symplectic Wigner-Dyson class AII. The one-loop quantum correction at large conductance g takes then the form of weak antilocalization, see Secs. II.B.2 and VI.A.1. At lower g the one-loop β function is not sufficient anymore, and higher-order terms lead to localization, with the Anderson transition taking place at some g_*. While the β function has been calculated up to the four-loop order, see Eq. (2.24), this does not help to get quantitative predictions for critical properties. In particular, an attempt to use the four-loop β function to extract the localization length exponent (Wegner, 1989) yields $\nu = \frac{1}{5}[\frac{3}{4}\zeta(3)]^{1/3} \approx 0.193$, which is an order of magnitude smaller than the numerical result (see below) and even violates the Harris criterion $\nu \geq 2/d$ (Chayes *et al.*, 1986). This is not surprising: the considered Anderson transition takes place at strong coupling, $g_* \sim 1$, so that keeping the first few terms of the perturbative expansion is an uncontrolled procedure. In this situation, numerical simulations are particularly important. On their basis, a detailed quantitative picture of the transition has been developed; the key findings are summarized below.

1. Microscopic models

Most numerical studies employed a tight-binding Hamiltonian. The Hamiltonian is defined on a two-dimensional square lattice with nearest-neighbor coupling

$$H = \sum_{i,\sigma} \epsilon_i c^\dagger_{i,\sigma} c_{i,\sigma} + \sum_{\langle i,j\rangle,\sigma,\sigma'} V_{i,\sigma;j,\sigma'} c^\dagger_{i,\sigma} c_{j,\sigma'}. \tag{6.3}$$

Here $c^\dagger_{i,\sigma}$ ($c_{i,\sigma}$) denote creation (annihilation) operators of an electron with spin σ on site i. The on-site energies ϵ_i are taken to be random numbers drawn from the interval $[-W/2, W/2]$ with a homogeneous distribution. There exist various versions of the model that differ by the choice of the hopping matrix $V_{i,\sigma;j,\sigma'}$.

Most studies employ the Ando model (Ando, 1989) characterized by nonrandom hopping between next neighbors only,

$$V_{i,\sigma;i+k,\sigma'} = [V_0 \exp(i\theta_k \sigma_k)]_{\sigma,\sigma'}, \quad k = x, y, \tag{6.4}$$

where σ_x, σ_y are the Pauli matrices. Conventionally, the spin-orbit energy scale is set to unity, $V_0 = 1$, and the mixing angles take constant values $\theta_k = \pi/6$. In the Evangelou-Ziman model (Evangelou and Ziman, 1987; Evangelou, 1995), the components of V that are proportional to $\sigma_{x,y,z}$ are chosen to be random with prefactors drawn independently from a box distribution of a width V_0. Recently, a third variant was introduced (Asada *et al.*, 2002, 2004)—the SU(2) model, in which the random matrix $\exp(i\theta_k \sigma_k)$ is chosen to be uniformly distributed on the SU(2) group. This last model was found particularly suitable for numerics, since finite-size corrections appear to be small.

2. Localization length exponent

The small magnitude of finite-size corrections in the SU(2) model has allowed Asada *et al.* (2002, 2004) to determine the localization length exponent with a high precision, $\nu = 2.746 \pm 0.009$. Recently, a similar result was obtained (Markos and Schweitzer, 2006) in the context of the Ando model, $\nu = 2.8 \pm 0.04$. Asada *et al.* (2004) evaluated numerically the whole β function and found that it has the expected shape, with a single zero determining the transition point.

3. Critical conductance

Since the transition takes place in the strong coupling regime, the mesoscopic conductance fluctuations at criticallity are comparable to the mean value, so that an ensemble of macroscopically identical coherent samples should be characterized by the whole distribution function $\mathcal{P}(g)$ (Shapiro, 1987). Quite generally, critical conductance distributions are scale invariant but depend on the shape of the sample (similar to the IPR distribution function, Sec. II.C.5 and the level statistics, Sec. II.E); a review of numerical results has been given by Markos (2006). The distribution $\mathcal{P}(g)$ for a square sample at the symplectic Anderson transition was determined by Ohtsuki *et al.* (2004) for the SU(2) model, see Fig. 22, and by Markos and Schweitzer (2006) for the Ando model, with essentially identical results. The average value $\langle g \rangle$ was found to be $\langle g \rangle = 1.42 \pm 0.005$ with a variance $\mathrm{var}\, g = 0.36$ (Markos and Schweitzer, 2006).

4. Multifractal spectrum

The spectrum τ_q can be calculated for the 2D symplectic transition with good accuracy because corrections to scaling turn out to be extremely small (Asada *et al.*, 2004; Mildenberger and Evers, 2007). Therefore many generic features of the critical wave-function statistics can be studied in great detail.

Results from a high-precision study of wave-function multifractality at the symplectic Anderson transition (Mildenberger and Evers, 2007) are summarized in Fig.

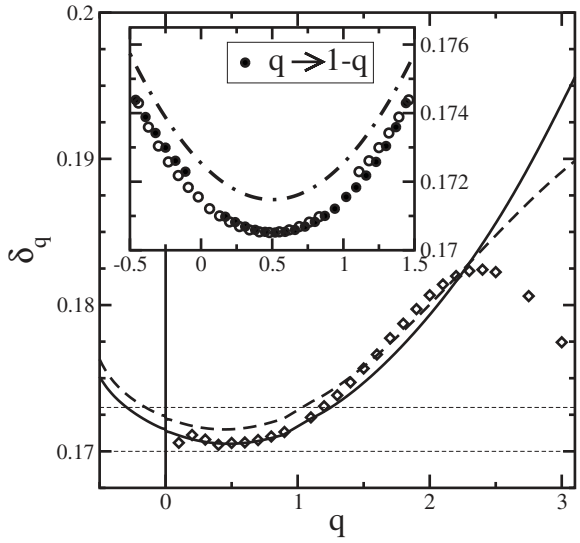

FIG. 19. Multifractal spectrum δ_q for the Ando model (dashed, $W_c=5.84$) and the SU(2) model (solid, $W_c=5.953$). To highlight deviations from parabolicity, reduced anomalous dimensions $\delta_q=\Delta_q/q(1-q)$ are plotted. Anomalous dimensions $\delta_q^{\rm typ}$ obtained from typical IPR are also shown ($\diamond$). Dashed lines indicate the estimated error (2σ) in δ_0. Inset: Blow up of the solid line behavior near $q=\frac{1}{2}$ is represented by empty circles ($\circ$). Filled symbols ($\bullet$) show original trace after reflection at $q=\frac{1}{2}$. Dot-dashed line is a fit (offset: 10^{-3}) $\delta_q=0.1705+0.0043(q-\frac{1}{2})^2$. From Mildenberger and Evers, 2007.

19. In order to highlight nontrivial features, the reduced anomalous dimensions $\delta_q=\Delta_q/q(1-q)$ are depicted. The key observations are as follows.

(i) One finds that $\delta_0\equiv\alpha_0-2=0.172\pm0.002$. This result may be used as a check on the conformal invariance, which imposes the exact condition (Janßen, 1994, 1998)

$$\pi\delta_0\Lambda_c=1. \tag{6.5}$$

Here $\Lambda_c=\xi_M/M$, where ξ_M is the localization length in a quasi-1D strip of width M at criticality. With the above value for δ_0 and with $\Lambda_c=1.844\pm0.002$ (Asada *et al.*, 2004), the left-hand side of Eq. (6.5) becomes indeed very close to unity: 0.996 ± 0.013.

(ii) The function δ_q fulfills the symmetry relation Eq. (2.37), as demonstrated in the inset of Fig. 19 where the data for the range $-0.5<q<1.5$ are displayed.

(iii) δ_q has a small but nonzero curvature, implying that the multifractal spectrum is not parabolic.

(iv) The results are essentially identical for the SU(2) and Ando models, confirming the universality of the transition. An abrupt change in the behavior of the data for the typical IPR in Fig. 19 at $q\simeq2.5$ is related to the fact that at $q>q_+$, when the average IPR probes the tail of its distribution function, the exponents τ_q and $\tau_q^{\rm typ}$ start to differ, see Eq. (2.41). In this range of q the statistical uncertainty in determination of τ_q also increases, explaining some deviation between the data for both models.

Similar results for the multifractality spectrum were obtained by Obuse, Subramaniam, *et al.* (2007). In this work, the multifractality was also studied at the boundary and at the corner of the system. It was found that the multifractal exponents fulfill the relation (2.58), thus providing further evidence for the conformal invariance at this critical point.

5. Symplectic-class theories with $\mathbb{Z}_2$ topology

As explained in Sec. VI.A.4, the σ model of the symplectic class allows for inclusion of a topological term with $\theta=\pi$. Microscopic realization of such a nontrivial topology was first identified by Ostrovsky *et al.* (2007a) where the model of Dirac fermions in disordered graphene was studied (see Sec. VI.G). It was found that for the case of long-range impurities, when two valleys in the spectrum are decoupled and the problem reduces to that of a single species of Dirac fermions in a random potential, the field theory is the class-AII σ model with $\theta=\pi$ topological term.

The fermionic sector of the corresponding σ-model manifold is $\mathcal{M}_F=\mathrm{O}(4n)/\mathrm{O}(2n)\times\mathrm{O}(2n)$. In fact, for the "minimal" supersymmetric σ model ($n=1$) the second homotopy group is richer:

$$\pi_2[\mathcal{M}_F|_{n=1}]=\mathbb{Z}\times\mathbb{Z},\quad \pi_2[\mathcal{M}_F|_{n\geq2}]=\mathbb{Z}_2. \tag{6.6}$$

For $n=1$ the compact sector of the model is the manifold $(S^2\times S^2)/\mathbb{Z}_2$ (product of the "diffuson" and "Cooperon" 2-spheres divided by $\mathbb{Z}_2$). Thus two topological invariants $N_{1,2}[Q]$, counting the covering of each sphere, emerge in accordance with Eq. (6.6). The most general topological term is $iS_{\rm top}=i\theta_1N_1+i\theta_2N_2$. However, time-reversal symmetry requires that the action is invariant under interchanging the diffuson and Cooperon spheres, which yields $\theta_1=\theta_2\equiv\theta$ where θ is either 0 or π. Hence only a $\mathbb{Z}_2$ subgroup of the whole $\mathbb{Z}\times\mathbb{Z}$ comes into play as expected: the phase diagram of the theory should not depend on n. For the Dirac fermion problem (Ostrovsky *et al.*, 2007a), an explicit expression for the $n=1$ topological term can be written using $\mathbf{u}=T\nabla T^{-1}$ (where the σ-model field $Q=T^{-1}\Lambda T$, see Sec. II.B.1),

$$iS_2[Q]=\frac{\epsilon_{\alpha\beta}}{8}\int d^2r\,\mathrm{Str}[(\Lambda\pm1)\tau_2u_\alpha u_\beta]$$
$$\equiv i\pi(N_1[Q]+N_2[Q]),$$

yielding $\theta=\pi$. The nontrivial value of the topological angle ($\theta=\pi$) holds for higher n as well. It implies that all configurations $Q(\mathbf{r})$ are subdivided into two topologically distinct classes (even and odd); the former give positive and the latter negative contribution to the σ-model partition function. This was confirmed numerically by Ryu, Mudry, Obuse, and Furusaki (2007).

At large conductance g the contribution of topologically nontrivial configurations is exponentially small and can not affect the metallic phase in any essential way. On the other hand, at small g the topological term is expected to suppress localization, similar to its role in the quantum Hall effect (Sec. VI.C) and in the quasi-1D symplectic model (Sec. V.D). This leaves room for two possibilities.

(i) The β function changes sign twice. This would mean that, in addition to the conventional repulsive fixed point of the symplectic class, a new attractive fixed point arises. This scenario was proposed by Ostrovsky *et al.* (2007a). Then, if the RG flow starts with a sufficiently low conductivity, it ends up in this new critical point with a universal conductivity of order unity.

(ii) The β function remains positive everywhere. The RG flow then necessarily leads the system into the ideal-metal fixed point with infinite conductivity.

In view of the strong-coupling nature of the problem, numerical simulations are needed to resolve this dilemma. Recent simulations of disordered graphene (Bardarson *et al.*, 2007; Nomura and MacDonald, 2007; Nomura *et al.*, 2007; Rycerz *et al.*, 2007; Lewenkopf *et al.*, 2008) confirm the suppression of localization in the symplectic class with $\mathbb{Z}_2$ topology. While the results of Nomura and MacDonald (2007) and Rycerz *et al.* (2007) were consistent with the scenario (i), with a critical conductivity $\sim e^2/h$, most recent works (Bardarson *et al.*, 2007; Nomura *et al.*, 2007) appear to favor the second scenario.

It is worth reminding the reader of a different type of $\mathbb{Z}_2$ topology in 2D systems of the symmetry class AII. It arises in the context of the quantum spin Hall (QSH) effect and is related to a nontrivial first homotopy group, $\pi_1(\mathcal{M}_F)=\mathbb{Z}_2$. This enables, as in the 2D situation, a θ term with θ equal to 0 or π also in the 1D case, inducing a $\mathbb{Z}_2$ topological classification of edge states in QSH systems, see Sec. V.D. Therefore these systems possess in addition to the metallic phase two distinct insulating phases, with different edge properties (normal insulator and QSH insulator). An important question is whether there is a direct, quantum-Hall-type transition between these two phases. Recent numerics (Essin and Moore, 2007; Obuse, Furusaki, *et al.*, 2007; Onoda *et al.*, 2007) on some models of QSH systems gives a negative answer: the insulating phases are found to be separated everywhere by the metallic phase. It is interesting to find out whether such a direct transition is generically prohibited, independent of the microscopic model. More activity in this direction is expected in the near future.

C. Integer quantum Hall effect

Our presentation in this section complements the reviews by Huckestein (1995) and Kramer *et al.* (2005).

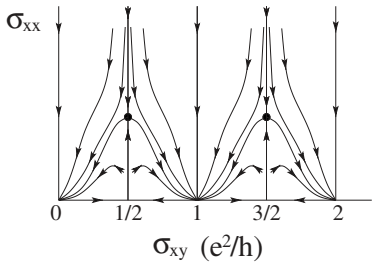

FIG. 20. Two-parameter flow diagram of the Pruisken σ model, as first proposed by Khmelnitskii (1984).

1. Pruisken's σ model

As discovered by von Klitzing *et al.* (1980), the Hall conductivity σ_{xy} of a 2D electron gas in a strong transverse magnetic field develops plateaus at values quantized in units of e^2/h. While the physics of the Hall plateau is fairly well understood by now, the theory of the quantum critical points separating the plateaus—the quantum Hall transition—remains a challenging issue.

From the field-theoretical point of view, the IQHE is described by the σ model (2.16) with a topological term (6.1). It was first derived by Pruisken in the replica formalism (Levine *et al.*, 1983; Pruisken, 1984, 1987); a supersymmetric generalization was obtained by Weidenmüller (1987). The action of the model is given by

$$S[Q]=\frac{1}{8}\int d^2r\,\mathrm{Str}[-\sigma_{xx}(\nabla Q)^2+2\sigma_{xy}Q\nabla_x Q\nabla_y Q], \tag{6.7}$$

where σ_{xx}, σ_{xy} are dimensionless conductivities. The Hall conductivity σ_{xy} is related to the topological angle via $\sigma_{xy}=\theta/2\pi$. There is strong evidence that the corresponding two-parameter flow diagram has the form shown in Fig. 20, as proposed by Khmelnitskii (1984) and Pruisken (1985, 1987). The fixed point at $\theta=(2n+1)\pi$ describes the QH transition. While the theory (6.7) is important for understanding the qualitative features of the problem, it allows one to make only rough predictions on the critical behavior (Pruisken and Burmistrov, 2005). This occurs because a controllable calculation in this framework can only be performed at weak coupling, $\sigma_{xx}\gg 1$, while the fixed points occur at strong coupling, $\sigma_{xx}\sim 1$. In this situation, numerical simulations are particularly important; their results are reviewed in Secs. VI.C.5–VI.C.7.

2. Further analytical approaches

A great deal of effort has been invested in order to solve the problem of the QH transition from the analytical side. In addition to the Pruisken model, Sec. VI.C.1, several other analytical frameworks have been used. While this activity has not led to an ultimate success in the quantitative description of critical behavior, a variety of important connections between the models has been established. In particular, it has been shown that the σ model (6.7) is also obtained as a continuum limit of the

Chalker-Coddington network described in Sec. VI.C.4 (Zirnbauer, 1997). Further, either of these two models can be mapped onto a quantum antiferromagnetic superspin chain (Lee, 1994; Zirnbauer, 1994, 1997; Marston and Tsai, 1999); a mapping onto a Hubbard chain has also been discussed (Lee and Wang, 1996a). Unfortunately, attempts to find an integrable deformation of the above spin chain have failed. A further approach to QH criticality is based on the model of Dirac fermions; this is reviewed in Sec. VI.G.2.

3. Quest for conformal field theory

A related line of activity is the search for a conformal field theory of the QH transition. The guiding principle is inspired by the fact that a relative of Pruisken's model, the O(3) σ model with $\theta=\pi$ topological term, describing a 1D quantum antiferromagnet with half-integer spin, flows under renormalization to a SU(2) WZW model. This means that the target space—which is the 2-sphere $\mathrm{O}(3)/\mathrm{O}(2)=\mathrm{SU}(2)/\mathrm{U}(1)=S^2$ for the O(3) σ model—is promoted to the group SU(2) (isomorphic to the 3-sphere S^3) at criticality. The idea is thus to identify the corresponding critical theory for the QH problem, with a hope that it is of the WZW type and is solvable using conformal field theory. Such a proposal was made by Zirnbauer (1999), along with a detailed analysis of constraints on the sought fixed-point theory. The target space of the theory conjectured by Zirnbauer is a real form of the complex supergroup PSL(2|2). Its base $\mathcal{M}_F\times\mathcal{M}_B$ is a product of the 3-sphere $\mathcal{M}_F=\mathrm{SU}(2)=S^3$ and the 3-hyperboloid $\mathrm{SL}(2,\mathbb{C})/\mathrm{SU}(2)=H^3$. A model of the same type was also proposed by Bhaseen *et al.* (2000) and most recently by Tsvelik (2007). The proposed theories have the form of the WZW model, see Sec. VI.A.5,

$$S[g]=\frac{1}{8\pi t}\int d^2x\ \mathrm{Str}\ \partial_\mu g^{-1}\partial_\mu g+iS_{\mathrm{WZ}}[g], \tag{6.8}$$

where iS_{WZ} is the WZ term (6.2). The peculiarity of the WZW models on the considered manifold is that they are critical at any value of the coupling constant t and level $k\in\mathbb{N}$. While Zirnbauer (1999) argued for $k=1$, Bhaseen *et al.* (2000) considered the model with Kac-Moody symmetry, $k=1/t$. The latter condition restricts $1/t$ to be an integer but facilitates the analysis of the model. Recently Tsvelik (2007) proposed that this model with $k=8$ may be the required fixed-point theory.

Both variants of the theory make a prediction for the statistics of critical eigenfunctions. Specifically, the multifractality spectrum found is exactly parabolic,

$$\Delta_q=\gamma q(1-q), \tag{6.9}$$

$$f(\alpha)=2-(\alpha-\alpha_0)^2/4(\alpha_0-2),\quad \alpha_0=2+\gamma, \tag{6.10}$$

with $\alpha_0-2=4t$ for the case of Zirnbauer (1999) and $\alpha_0-2=2t$ for Bhaseen *et al.* (2000). This prediction of parabolicity of Δ_q and $f(\alpha)$ is indeed consistent with the numerical simulations, Sec. VI.C.7.[12] However, many questions related to the above conjectures remain open. In particular, if there is a whole line of fixed points (parametrized by t), then is there universality at the QH transition? If yes, how is it established? From the numerical point of view, there is no indication of nonuniversality at present.

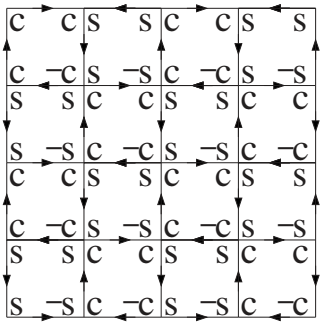

FIG. 21. Chalker-Coddington network model of the IQH transition (Chalker and Coddington, 1988). The symbols $\pm c$, $\pm s$ denote the components $\pm\cos\theta$, $\pm\sin\theta$ of scattering matrices at the nodes of the network.

4. Chalker-Coddington network

The Chalker-Coddington network (CCN) model was introduced by Chalker and Coddington (1988) as an effective description of the IQHE in a smooth random potential. In brief, the model is motivated in the following way. One considers electrons in a Landau level broadened by a potential with large correlation length. Electrons then drift along equipotential lines and tunnel between the lines near saddle points of the random potential. When the energy is sufficiently close to the band center (classical percolation threshold), the tunneling probability becomes ~ 1, and a random network with directed links is formed. At each node of the network two incoming and two ongoing links meet. In the CCN model, this geometrically random structure is replaced by a regular square network, as shown in Fig. 21; the disorder is accounted for by random phases associated with all links. A state Ψ of the network is defined by its amplitudes on the edges of the network. Originally (Chalker and Coddington, 1988) the network was characterized by a transfer matrix, as appropriate for finite-size scaling analysis of the localization length. Later (Klesse and Metzler, 1995) an equivalent description in terms of a scattering matrix was introduced. Each realization of the network is determined by a unitary operator $\mathcal{U}=\mathcal{U}_N\mathcal{U}_E$ acting on states Ψ and modeling the evolution of the state in a time step. Here $\mathcal{U}_N$ is an operator describing the unitary scattering at nodes with amplitudes $\pm\cos\theta$, $\pm\sin\theta$, as shown in Fig. 21. The second factor $\mathcal{U}_E$ is a diagonal operator with random elements $e^{i\phi_e}$ on all edges e of the network. In the simplest formu-

[12]Very recent, ultra-high-precision numerics find deviations from parabolicity; see Note added in proof.

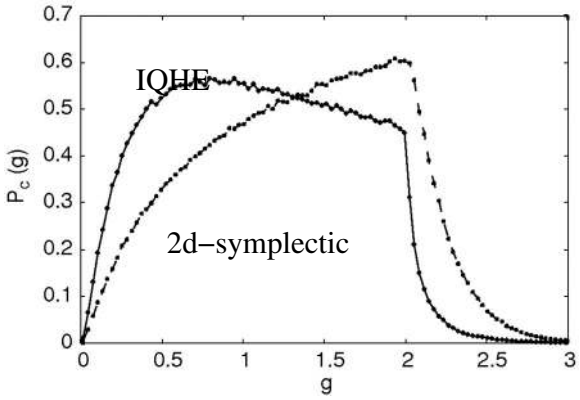

FIG. 22. Conductance distribution at IQH (solid) and 2*d* symplectic (dashed) critical points for periodic boundary conditions and a square sample geometry. Adapted from Ohtsuki *et al.*, 2004.

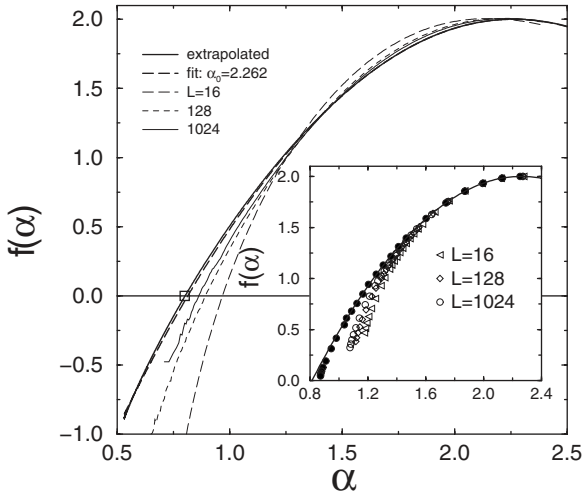

FIG. 23. Multifractal spectrum at the IQH transition. Thick solid line: Numerical results for $f(\alpha)$ obtained from scaling of average IPR after extrapolation to $L\to\infty$. Data for several finite values of $L=16$, 128, and 1024 are also shown. Thick dashed line: Parabolic approximation, Eq. (6.9). Inset: Data points from typical IPR for $L=16$,128, and 1024 (open symbols) and extrapolation to infinite system size (closed circles); data from average IPR are shown by a solid line. From Evers *et al.*, 2001.

lation of the model, the angle θ is the same for all nodes, and the phases ϕ_e are independent random variables distributed uniformly over $[0;2\pi]$. Changing the parameter θ allows one to drive the system through the IQH transition, with the critical point at $\cos^2\theta=1/2$.

The CCN model has been extensively used for numerical simulations of the IQH transition point; it turned out to be particularly well suited for analyzing the statistical properties of energy levels and wave functions. Key results of computer simulations are reviewed below.

The model has been generalized to other symmetry classes. This is most naturally done for counterparts of the IQHE in the superconducting classes C and D, namely, SQHE and TQHE. In these classes the symmetric spaces of the Hamiltonian (Table I) are the groups Sp(N) and O(N), and the required modification amounts to a replacement of the factors $e^{i\phi_e}\in U(1)$ by the elements of $\mathrm{Sp}(2)=\mathrm{SU}(2)$ for the SQHE (in this case the amplitudes are spin doublets) and of O(1) for the TQHE, see Secs. VI.D and VI.E for more detail. For several other symmetry classes nondirected generalizations of the CCN have been constructed and used to study the corresponding critical behavior; specifically, this has been done for the chiral classes AIII, BDI, and CII (Bocquet and Chalker, 2003), Sec. VI.F, and for the symplectic class AII (Merkt *et al.*, 1998; Obuse, Furusaki, *et al.*, 2007) considered in Sec. VI.B.

A further important aspect of the CCN model and its generalizations is that they can serve as a starting point for analytical work. We have already mentioned equivalences between the CCN and other IQH models (Pruisken model and superspin chain) in Sec. VI.C.2. Further, a connection with the models of disordered Dirac fermions has been established (Ho and Chalker, 1996). The network model of the SQHE has led to a number of exact analytical results, see Sec. VI.D.

5. Localization length exponent

Several microscopic models have been used to study numerically the critical properties at the IQH transition. This includes tight-binding models, Landau-space models where the problem is projected on one or several Landau levels, and the CCN models, see Sec. VI.C.4. For a detailed review of the models see Huckestein (1995). The first high-precision determination of the localization length exponent ν was performed employing the Landau-space model (Huckestein and Kramer, 1990; Huckestein *et al.*, 1992; Huckestein, 1995), with the result $\nu=2.35\pm0.03$. Results of later simulations on different models are all in agreement with this value, thus favoring the universality of the IQH critical behavior. At present, the precise value of the leading irrelevant scaling index y is known with much less accuracy. While several authors found values close to $y=0.4$ (Huckestein, 1995; Evers and Brenig, 1998), in some cases values up to $y=0.6$ have been reported (Kramer *et al.*, 2005).

6. Critical conductivity and conductance distribution

In a number of works, the critical conductivity was found numerically in the range 0.5 to 0.6. Specifically, the results are from 0.50 ± 0.03 to 0.55 ± 0.05 for different types of disorder (Huo *et al.*, 1993), 0.50 ± 0.02 (Gammel and Brenig, 1994), and 0.58 ± 0.03 (Schweitzer and Markos, 2005). Results in higher Landau levels are consistent with these values whenever the critical regime (of system sizes) has been reached (Gammel and Evers, 1998).

Several authors also studied the conductance distribution $\mathcal{P}(g)$ of a square sample with periodic boundary conditions in the transverse direction; see Sec. VI.B.3 for a qualitative discussion of $\mathcal{P}(g)$ at criticality. As expected, a scale-invariant distribution was found, see

Fig. 22, with the average $\langle g\rangle = 0.58 \pm 0.03$ and the variance $\mathrm{var}(g) = 0.081 \pm 0.005$ (Wang *et al.*, 1996); similar results were obtained by Cho and Fisher (1997b), Ohtsuki *et al.* (2004), and Kramer *et al.* (2005) where the average was found to be $\langle g\rangle = 0.57 \pm 0.02$, as well as by Schweitzer and Markos (2005); the latter work yields $\langle g\rangle = 0.60 \pm 0.02$.

7. Wave-function multifractality

A high-precision evaluation of the multifractal spectrum at the IQH transition was carried out by Evers *et al.* (2001) for the CCN model of a size $L \times L$ with L ranging from 16 to 1280. Figure 23 shows results for the $f(\alpha)$ spectrum. It is seen that after extrapolation to the thermodynamic limit $L \to \infty$ the $f(\alpha)$ spectrum is well described by the parabolic form (6.10) with $\alpha_0 - 2 = 0.262 \pm 0.003$. One observes that deviations from parabolicity—if they exist—are too small to be resolved in this plot. In Fig. 24 reduced anomalous dimensions $\Delta_q/q(1-q)$ are plotted. This quantity is constant (equal to $\alpha_0 - 2$) for an exactly parabolic spectrum, Eq. (6.9). Observed deviations from the constant are small ($\sim 1\,\%$) and within the error bars.[13] The numerical results are consistent with exact parabolicity of the multifractal spectrum, thus supporting the possibility of a conformal theory of the IQH critical point as discussed in Sec. VI.C.3. If the observed deviations are indeed indicative of true nonparabolicity, then the numerical error bars have to be decreased further by at least a factor of 3 in order to detect them reliably.[14]

A high-precision evaluation of multifractality allows one to test the conformal invariance of the problem via Eq. (6.5). The parameter $\Lambda_c \equiv \xi_M/M$ was found to be $\Lambda_c = 1.22 \pm 0.01$ (Evers and Brenig, 1998; Evers *et al.*, 2001), implying, in combination with the above value of $\alpha_0 - 2$, that Eq. (6.5) is perfectly fulfilled and thus confirming the expectation that the IQH critical theory is conformally invariant.

8. Statistics of the two-point conductance

Closely related to wave-function multifractality is the statistics of two-point conductances, see Sec. II.C.9. Klesse and Zirnbauer (2001) derived a relation between statistical properties of the wave functions and two-point conductances;

$$2\pi\rho\langle y_m f(y_m/y_l)\rangle = \langle F(T_{lm}\rangle,$$

$$F(T) = \int_0^{2\pi} \frac{d\phi}{2\pi} f(T^{-1}|1 - e^{i\phi}\sqrt{1-T}|^2). \tag{6.11}$$

Here $f(x)$ is an arbitrary function, $y_l = |\Psi_l|^2$, $y_m = |\Psi_m|^2$ are wave-function intensities at two links l and m for an eigenstate Ψ of a closed network, and $T_{l,m}$ is the two-point conductance defined for an open network with the edges l and m cut and attached to two terminals. This result was used by Evers *et al.* (2001) to derive the relation (2.62) between the corresponding critical exponents. The parabolic spectrum for wave-function multifractality, Eq. (6.9), translates thus into a parabolic spectrum of exponents X_q for the two-point conductance,

$$X_{q\le 1/2} = X_t q(1-q), \quad X_{q\ge 1/2} = X_t/4, \tag{6.12}$$

with $X_t = 2(\alpha_0 - 2) = 0.524 \pm 0.006$. Earlier (Janßen *et al.*, 1999) an explicit expression for the distribution of the two-point conductance on the CCN was derived assuming the parabolic law (6.12) for X_q. Klesse and Zirnbauer (2001) used this result to test the conformal invariance of the theory, utilizing a numerical analysis of the moments of the two-point conductance in the quasi-1D (cylinder) geometry. The result of Janßen *et al.* (1999) for the distribution of the conductance T between the points $(0,0)$ and (x,y) in this geometry reads

$$\mathcal{P}(T) = \frac{2\pi^{-1/2}\zeta^{-X_t/4}}{T^2(X_t \ln \zeta)^{3/2}} \int_{\mathrm{arcosh}\,1/\sqrt{T}}^{\infty} \frac{e^{-t^2/X_t \ln \zeta}\, t\, dt}{\sqrt{\cosh^2 t - T^{-1}}},$$

$$\zeta = (W/\pi a)|\sinh[\pi(x+iy)/W]|, \tag{6.13}$$

where a is the nonuniversal microscopic scale that sets the length unit. The numerically determined moments of T were in perfect agreement with this formula, thus supporting the conformal invariance. The best fits yielded the values $X_t = 0.54 \pm 0.01$ from the analysis of the moments $\langle T^{n+1/2}\rangle$ and $X_t = 0.57 \pm 0.05$ from the analysis of the typical conductance, $\langle \ln T\rangle$. These values are consistent with the above result $X_t = 0.524 \pm 0.006$.

9. Classical percolation vs quantum Hall effect

If the disorder correlation length is large, there is an intermediate, parametrically broad range of energies where the physics is dominated by classical percolation. On corresponding length scales, tunneling between the percolating contours is exponentially small. This range of energies was studied by Mil'nikov and Sokolov (1988) where the scaling of the localization length with an exponent $\tilde{\nu} = \nu_{\mathrm{perc}} + 1 = 7/3$ was found ($\nu_{\mathrm{perc}} = 4/3$ is the correlation length index of the 2D percolation problem). In this regime quantum interference effects play no role. When energy approaches still closer to the critical point, the probability of tunneling between the contours ceases to be small and quantum interference becomes important—the system enters the true critical regime of the quantum Hall transition. It is this latter regime that is described by the CCN model. While the "quasiclassical QHE" exponent $\tilde{\nu} = 7/3$ is remarkably close to the numerical value of the true QH exponent $\nu = 2.35 \pm 0.03$,

[13] Earlier studies of the IQH multifractality [see references in Evers *et al.* (2001)] gave considerably different results, showing strong deviations from parabolicity. As shown by Evers *et al.* (2001), earlier numerics suffered strongly from the absence of ensemble averaging (its role was explained in Sec. II.C.5) and from finite-size effects. The importance of a careful analysis is illustrated in Fig. 23, where data for a finite-size system are included.

[14] For the most recent developments, see the Note added in proof.

this coincidence is apparently fully accidental, as the physics of the true QH critical regime and the intermediate quasiclassical regime of Mil'nikov and Sokolov (1988) is completely different.

It is worth mentioning that the physics of the intermediate, quasiclassical regime, where the physics is dominated by the vicinity of the percolation fixed point (Mil'nikov and Sokolov, 1988; Evers and Brenig, 1994, 1998; Kratzer and Brenig, 1994; Klesse and Metzler, 1995; Gammel and Brenig, 1996), is interesting in its own right. In particular, quasiclassical time evolution generates a long time tail in the velocity correlation function $\langle v_x(t)v_x(0)\rangle \sim t^{-2}$, which leaves $\sigma_{xx}(\omega)$ with a nonanalytic ω dependence inside an intermediate (quasiclassical) frequency window. The corresponding results may be relevant to experiments if the latter are performed on structures with smooth disorder, in which case the true QH criticality may in fact be totally unobservable for realistic temperatures.

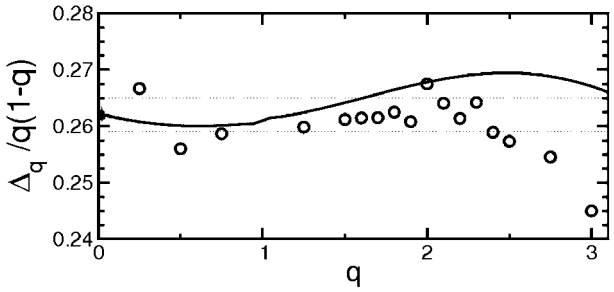

FIG. 24. Anomalous multifractal dimensions Δ_q [divided by $q(1-q)$] at the IQHE critical point, as obtained from extrapolation of the average IPR. In the case of exact parabolicity, the plotted quantity should be constant. The dotted lines indicate the error bars obtained for α_0-2. The circles give $\Delta_q^{\rm typ}/q(1-q)$ as obtained from the typical IPR. As explained in Sec. II.C.5, $\Delta_q^{\rm typ}=\Delta_q$ for $q<q_+$; for IQHE with parabolic spectrum (6.9) and (6.10) we find $q_+=[2/(\alpha_0-2)]^{1/2}\simeq 2.76$. Thus the last two data points for $\Delta_q^{\rm typ}/q(1-q)$ are in the range $q>q_+$, which explains their downward deviations from $\Delta_q/q(1-q)$. Based on data of Evers *et al.*, 2001.

10. Experiment vs theory: Interaction effects

a. Experimental results

The IQH transition and the associated critical properties have been studied in numerous experiments. All basic features—the existence of phase transitions with critical values $\sigma_{xy}=n+1/2$ and $\sigma_{xx}\sim 1$, as well as the power-law scaling behavior—are in agreement with theoretical expectations. The situation with the values of critical exponents is not so simple, as we now discuss. To do this, we have to touch the question of interaction effects, which is left out in the rest of this review, except for Sec. VII.A.

Experiments yield the following results for the critical exponents. First, the index ν of the localization length is $\nu=2.3\pm 0.1$ (Koch *et al.*, 1991); this value was confirmed by Hohls *et al.* (2001) and Hohls, Zeitler, Haug, *et al.* (2002). Second, the width of the critical region (peak in σ_{xx} and plateau transition in σ_{xy}) scales with the temperature T as $\Delta B\propto T^{\kappa}$ where $\kappa=0.42\pm 0.04$ (Wei *et al.*, 1988). While others obtained different values of κ, it was emphasized by van Schaijk *et al.* (2000) that this results from macroscopic inhomogeneities that complicate observation of the true IQH critical behavior with $\kappa\simeq 0.42$. More recent work of the same group (de Visser *et al.*, 2006; Pruisken *et al.*, 2006) favors again $\kappa=0.56\pm 0.02$, however. On the other hand, the impact of density inhomogeneities was reconsidered by Li *et al.* (2005). It was found there that for short-range disorder, when the true IQH criticality can be achieved, $\kappa=0.42\pm 0.01$,whereas the larger value $\kappa=0.58$ was ascribed to impurity clustering. Finally, the frequency scaling of the transition width was found to be $\Delta B\sim\omega^{\zeta}$, with $\zeta=0.41\pm 0.04$ (Engel *et al.*, 1993). A more recent work (Hohls, Zeitler, and Haug, 2002) yielded a result consistent with this value, but with somewhat larger uncertainty, $\zeta=0.5\pm 0.1$. To summarize, the experiments yield ν that agrees with its numerical value (2.35 ± 0.03), as well as the dynamical exponents $z_T\equiv 1/\kappa\nu\simeq 1$ and $z\equiv 1/\zeta\nu\simeq 1$. The remarkable agreement in the value of ν is in fact surprising, in view of the electron-electron interaction.

b. Finite-range interaction

We consider first the case of a finite-range interaction $v(\mathbf{r}-\mathbf{r}')$, following Lee and Wang (1996b); Wang *et al.* (2000). In this case the interaction is irrelevant. Indeed consider the Hartree-Fock interaction between the (close in energy) states α and β, normalized to the level spacing,

$$\lambda=\rho L^2\int d^2r d^2r'\langle[|\psi_\alpha(\mathbf{r})|^2|\psi_\beta(\mathbf{r}')|^2 - \psi_\alpha(\mathbf{r})\psi_\alpha^*(\mathbf{r}')\psi_\beta(\mathbf{r}')\psi_\beta^*(\mathbf{r})]v(\mathbf{r}-\mathbf{r}')\rangle. \tag{6.14}$$

In the σ-model language, see Sec. II.B.1, the scaling of Eq. (6.14) with the system size L is governed by the scaling dimension of the operator

$$Q_{11}^{\rm bb}(\mathbf{r})Q_{22}^{\rm bb}(\mathbf{r})-Q_{12}^{\rm bb}(\mathbf{r})Q_{21}^{\rm bb}(\mathbf{r}). \tag{6.15}$$

While each term in Eq. (6.15) is relevant in the RG sense, having a dominant negative scaling dimension Δ_2 (which governs the IPR scaling, Secs. II.C.1 and VI.C.7), the difference Eq. (6.15), is RG irrelevant (Wegner, 1980), with a scaling dimension $x_2>0$. The numerical value of x_2 at the IQH critical point was estimated to be $x_2=0.66\pm 0.04$ (Lee and Wang, 1996b). With increasing L the interaction (6.14) scales as $\lambda\propto L^{-x_2}$, so that the fixed point is unaffected by it. This implies that the critical index ν of the localization length and the multifractality spectrum Δ_q remain the same as in the noninteracting problem. This is also true for the dynamical exponent z governing the destruction of localization by finite frequency: the corresponding scaling variable is $\omega\xi^z$ with $z=2$. [In general, for a non-interacting transition with finite DOS in d dimensions the scaling variable is ω/q^d

(Wegner, 1976).] The interaction cannot be fully discarded, however (it is said to be *dangerously irrelevant*), as the conductivity at finite T would be zero without the interaction-induced dephasing. The dephasing rate scales as $\tau_\phi^{-1} \propto T^p$ with $p=1+2x_2/z$ (Wang *et al.*, 2000). Thus the dephasing length is $L_\phi \propto \tau_\phi^{1/2} \propto T^{-1/z_T}$ with $z_T = 2/p = 2z/(2x_2+z)$, yielding $z_T \simeq 1.2$ with the above estimate for x_2. Therefore for a system with a metallic gate (which screens the interaction) one expects the exponents $\nu \simeq 2.35$, $z=2$, and $z_T \simeq 1.2$.

c. Coulomb interaction

The situation with $1/r$ Coulomb interaction (as in typical experiments) is much less clear. In this case the interaction is RG relevant and drives the system to a novel fixed point (Lee and Wang, 1996b; Baranov *et al.*, 2002). While the conductivity and the screened compressibility $\partial n/\partial\mu$ remain finite at the transition (Finkelstein, 1990; Belitz and Kirkpatrick, 1994), much less is known theoretically about other critical properties. Several authors (Polyakov and Samokhin, 1998; Wang and Xiong, 2002) have argued that charging effects analogous to those responsible for the linear Coulomb gap in the tunneling DOS of the insulator will lead to $z=z_T=1$ (which is the natural scaling dimension of the $1/r$ interaction). The status of this argumentation is unclear, however, for the following reasons.

(i) These arguments identify z and z_T with a dynamical exponent [z_3 in notations of Belitz and Kirkpatrick (1994)] governing the scaling of the density response function. It is known, however, that in metals the plasmon pole governed by this exponent, $z_3=1$, determines the interaction-induced quantum correction to the tunneling DOS but not to the conductivity (Altshuler and Aronov, 1984), in view of gauge invariance (Finkelstein, 1994). The conductivity correction is governed by the conventional diffusion pole in the *irreducible* density-density response function, which corresponds to the dynamical exponent $z_3^{\rm irr}=2$.

(ii) Each Goldstone mode (or, equivalently, conserved quantity) is in general characterized by a dynamical exponent. For the QH transition this implies that, in addition to the exponents related to the particle number conservation—$z_3=1$ and its irreducible counterpart, $z_3^{\rm irr}=2$—there is another exponent associated with energy conservation. This latter exponent, controlling the renormalization of the frequency term in the σ model, is denoted by ζ in Finkelstein (1990), z_1 in Belitz and Kirkpatrick (1994), and by $2+\gamma^*$ in Baranov *et al.* (2002). This exponent is believed to govern the frequency scaling of the conductivity at the critical point of the Anderson transition in a system with Coulomb interaction and broken spin-rotation invariance in $2+\epsilon$ dimensions (Finkelstein, 1990; Belitz and Kirkpatrick, 1994). One may thus expect that this dynamical exponent plays a central role at the quantum Hall transition as well (Baranov *et al.*, 2002; Burmistrov, 2006).

The problem of finding the index ν of the localization length is also far from being solved. While it was found that ν is equal to its noninteracting value within the Hartree-Fock theory (Yang *et al.*, 1995), it is not clear whether this should be applicable to the true fixed point in the problem with Coulomb interaction. To summarize, in our view, the theoretical problem of the critical behavior in the presence of Coulomb interaction remains open. In particular, it remains to be seen whether the remarkable agreement of ν with its noninteracting value as well as $z=z_T=1$—as suggested by experiments—are indeed exact properties of the interacting problem.

D. Spin quantum Hall effect (class C)

1. Physical realization

The SQHE is a counterpart of the IQHE in superconductors with broken time-reversal but preserved spin-rotation invariance (Gruzberg *et al.*, 1999; Kagalovsky *et al.*, 1999; Senthil *et al.*, 1999). The class C Hamiltonian satisfies the symmetry (4.12) (with τ_y the Pauli matrix in the particle-hole space) and has block structure (4.11). Several possible physical realizations of SQHE systems have been proposed: (i) a d-wave superconductor with complex $d_{x^2-y^2}+id_{xy}$ pairing (Kagalovsky *et al.*, 1999; Senthil *et al.*, 1999) that was conjectured for high-T_c superconductors (Balatsky, 1998; Laughlin, 1998); (ii) granular superconducting film in a magnetic field (Kagalovsky *et al.*, 1999); and (iii) a state of composite fermions at filling fraction $\nu=5/2$ with d-wave pairing (Read and Green, 2000), as proposed by Haldane and Rezayi (1988).

Similar to the case of the IQHE, the key signature of the SQHE is the quantization of the appropriate Hall conductance. Specifically, while the quasiparticle number is not conserved, the spin is, so that the relevant quantity is the spin Hall conductivity $\sigma_{xy}^{\rm s}$, which describes the transverse spin current induced in response to a gradient of the Zeeman field,

$$j_x^z = \sigma_{xy}^{\rm s}[-\partial B^z(y)/\partial y]. \tag{6.16}$$

In the IQHE the step $\Delta\sigma_{xy}$ between the quantized values of the Hall conductivity is e^2/h per spin orientation. In the case of the SQHE, the elementary charge e is replaced by $\hbar/2$, yielding (Senthil *et al.*, 1999)

$$\Delta\sigma_{xy}^{\rm s} = 2n\hbar/8\pi, \tag{6.17}$$

where the factor 2 accounts for the spin and n for the valley degeneracy. In particular, for the case of Dirac fermions in a $d+id$ superconductor ($n=2$), one finds two SQH phases with quantized values

$$\sigma_{xy}^{\rm s} = \pm\hbar/4\pi. \tag{6.18}$$

In the presence of disorder, these two phases become Anderson insulators separated by the SQH transition.

The field theory of this problem is analogous to Pruisken's theory of the IQHE (Sec. VI.C.1)—it is a σ model of the class C with the topological term (6.1), possessing a critical point at $\theta=(2n+1)\pi$ (Senthil *et al.*, 1998, 1999; Read and Green, 2000; Altland *et al.*, 2002). The corresponding flow diagram is expected to have qualitatively the same form as for the IQHE, Fig. 20. The critical behavior at the SQH transition is analyzed below. In the presence of a Zeeman term, the spin-rotation symmetry is broken, and the system crosses over to the symmetry class A of the IQHE transition (Senthil *et al.*, 1998, 1999; Kagalovsky *et al.*, 1999; Cui *et al.*, 2004).

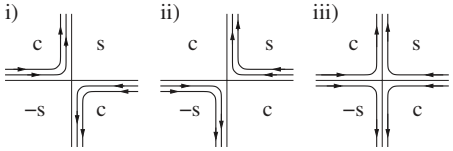

FIG. 25. Possible configurations of paths passing four times through a network node. The symbols c and $\pm s$ denote the elements $\cos\theta$, $\pm\sin\theta$ of the S-matrix at the node. Statement (2) in Sec. VI.D.2 allows one to remove the quantum interference contribution (iii) and to associate with contributions (i) and (ii) weights $\cos^2\theta$ and $\sin^2\theta$, respectively, yielding a mapping to the classical percolation.

2. Mapping to percolation

The network model for the SQHE (Kagalovsky *et al.*, 1999) is the SU(2) version of the Chalker-Coddington IQHE network, see Sec. VI.C.4 and Fig. 21. The directed links of the network carry doublets of complex fluxes representing propagation of the spin-1/2 particle. The scattering at each node is spin independent and defined as in the IQHE. Each realization of the network is characterized by a set of random 2×2 spin matrices U_e associated with all edges e of the network. In view of Eq. (4.12), the evolution operator of the network $\mathcal{U}$ satisfies the symmetry $\mathcal{U}=\tau_y\mathcal{U}^*\tau_y$, implying that $U_e\in\mathrm{SU}(2)$. Starting with this network model, it turns out that one can establish a remarkable property of the SQH transition: some physical observables and critical indices can be calculated exactly via mapping to classical percolation. This was shown for the DOS and the conductance by Gruzberg *et al.* (1999) via supersymmetry; an alternative derivation of these results was presented by Beamond *et al.* (2002). Mirlin *et al.* (2003) extended the mapping to all two- and three-point correlation functions describing, in particular, the wave-function statistics. There was also shown that the mapping breaks down for generic n-point correlation functions with $n>3$.

We briefly sketch the idea of the approach of Beamond *et al.* (2002); Mirlin *et al.* (2003). The primary objects are Green's functions on the network,

$$G(e',e;z)=\langle e'|(1-z\mathcal{U})^{-1}|e\rangle; \tag{6.19}$$

for $z=\exp i(\epsilon\pm i\eta)$ they have a meaning of retarded (G_R, $|z|<1$) and advanced (G_A, $|z|>1$) Green's functions at energy ϵ. The Green's function is straightforwardly represented in the form of a sum over paths

$$G(e,e';z)=\sum_{\text{paths } e'\to e}\cdots zU_{e_j}s_jzU_{e_{j+1}}s_{j+1}\cdots, \tag{6.20}$$

where s_j is the corresponding matrix element ($\cos\theta$, $\sin\theta$, or $-\sin\theta$) of the S matrix between the edges e_j and e_{j+1}. Equation (6.20) generates a convergent expansion in powers of z when $|z|<1$; otherwise, the identity

$$G^\dagger(e,e';z)=\mathbf{1}\cdot\delta_{ee'}-G[e',e;(z^*)^{-1}] \tag{6.21}$$

is to be used. As shown below, each of the sums over paths obtained by substituting Eqs. (6.20) and (6.21) into products of $n\le3$ Green's functions can be reduced after disorder averaging to a sum over classical paths (hulls) in the percolation problem. This reduction crucially relies on the following two statements.

(1) Only paths visiting each edge of the network either 0 or 2 times are to be taken into account; contributions of all remaining paths sum to zero.

(2) Using the statement (1), one can see that each node may be visited 0, 2, or 4 times. The second statement concerns the nodes visited four times. As shown in Fig. 25, there are three possibilities how this may happen; the corresponding contributions have weights (i) $\cos^4\theta$, (ii) $\sin^4\theta$, and (iii) $-\sin^2\theta\cos^2\theta$ from the scattering matrix at this node. The statement is that one can equivalently take into account only contributions (i) and (ii) with weights $\cos^2\theta$ and $\sin^2\theta$, respectively.

After application of statement (2) to all nodes, the network is reduced to a weighted sum over all its possible decompositions in a set of closed loops (such that each edge belongs to exactly one loop). These loops can be viewed as hulls of the bond percolation problem. As a result, the correlation functions (averaged products of Green's functions) are expressed in terms of classical sums over the percolation hulls. The results obtained in this way are listed below.

3. Density of states and localization length

The result for the average of a single Green's function is given by ($|z|<1$) (Beamond *et al.*, 2002)

$$\langle\mathrm{Tr}\,G(e,e,z)\rangle=2-\sum_{N>0}P(e;N)z^{2N}, \tag{6.22}$$

$$\langle\mathrm{Tr}\,G(e,e,z^{-1})\rangle=\sum_{N>0}P(e;N)z^{2N}, \tag{6.23}$$

where $P(e,N)$ is the probability that the edge e belongs to a loop of the length N. [In the bulk of a large system, $L\to\infty$, or for periodic boundary conditions, this probability does not depend on e, $P(e,N)=P(N)$.] This yields the DOS

$$\rho(E)=(1/2\pi)\left[1-\sum_{N>0}P(N)\cos(2NE)\right]. \tag{6.24}$$

In the insulating phases ($t\equiv\cos^2\theta\neq1/2$) this yields

$$\rho(E) \simeq \pi^{-1}\langle N^2\rangle E^2, \tag{6.25}$$

which is the expected behavior of DOS in class C. On approaching the percolation transition point ($t=1/2$) the characteristic diameter of largest loops diverge,

$$\xi \sim |t-1/2|^{-\nu}, \quad \nu = 4/3. \tag{6.26}$$

At the critical point ($t=1/2$)

$$P(N) \sim N^{-2/d_h} = N^{-8/7}, \tag{6.27}$$

where $d_h=7/4$ is the fractal dimension of the percolation hull (Saleur and Duplantier, 1987; Isichenko, 1992), yielding (Gruzberg *et al.*, 1999; Beamond *et al.*, 2002)

$$\rho(E) \sim |E|^{1/7}. \tag{6.28}$$

The characteristic length of loops contributing to Eq. (6.28) is $N_E \sim E^{-1}$, yielding their characteristic "diameter" $\xi_E \sim |E|^{-1/d_h} = |E|^{-4/7}$, which is the localization length of states with energy E. The percolation hull exponent d_h therefore plays a role of the dynamical exponent for the SQH transition.

4. Conductance

To define the two-terminal conductance g, one opens the system by cutting two subsets of links and attaching them to two reservoirs. The average dimensionless conductance is given by

$$\langle g\rangle = 2 \sum_{e\in 1_{\rm out};\ e'\in 2_{\rm in}} P(e,e'), \tag{6.29}$$

where $P(e,e')$ is the probability that a path incident from the second reservoir on the link e' escapes to the first contact via the link e, and the sum goes over all such links. Equation (6.29) was used by Cardy (2000) to calculate the critical conductivity by determining the conductance of a wide sample ($W \gg L$), $\langle g\rangle L/W = \sqrt{3}/2$. A similar result was obtained earlier by numerical evaluation of the Kubo formula, $\sigma_c = 2(0.45\pm 0.01)$ (Evers, 1997). It is worth stressing that, despite the vanishing density of states, the critical conductance is finite. From the point of view of the Einstein relation $\sigma = h\rho D$, this results from a mutual cancellation of the percolation exponents (Ziff *et al.*, 1991; Evers and Brenig, 1994), $\rho(E) \sim N_E/\xi_E^2 \sim E^{2/d_h-1} = E^{1/7}$ and $D(E) \sim \xi_E^2/N_E \sim E^{1-2/d_h} = E^{-1/7}$.

For the average two-point conductance (Sec. II.C.9), Eq. (6.29) yields (Gruzberg *et al.*, 1999)

$$\langle g(e,e')\rangle = 2P(e,e') \sim r^{-1/2}, \tag{6.30}$$

where $r \gg 1$ is the distance between e and e'.

5. Higher correlation functions and multifractality

The results presented in this section were obtained by Mirlin *et al.* (2003). To determine the fractal dimension Δ_2 governing the scaling of two-point correlations of wave functions (2.29) and (2.31), one considers the correlation functions

$$\mathcal{D}(e',e;\gamma) = (2\pi)^{-2}\langle {\rm Tr}[G(e',e;z) - G(e',e;z^{-1})] \times [G(e,e';z) - G(e,e';z^{-1})]\rangle, \tag{6.31}$$

$$\tilde{\mathcal{D}}(e',e;\gamma) = (2\pi)^{-2}\langle {\rm Tr}[G(e,e;z) - G(e,e;z^{-1})] \times {\rm Tr}[G(e',e';z) - G(e',e';z^{-1})]\rangle, \tag{6.32}$$

with a real $z=e^{-\gamma}<1$ and $\gamma \ll 1$ playing a role of the level broadening. Mapping to percolation yields for the averaged products of two Green's functions in Eq. (6.31),

$$\begin{aligned}&\langle {\rm Tr}\, G(e',e;z)G(e,e';z)\rangle \\ &\quad = \langle {\rm Tr}\, G(e',e;z^{-1})G(e,e';z^{-1})\rangle \\ &\quad = -2\sum_N P(e',e;N)z^{2N},\end{aligned} \tag{6.33}$$

$$\langle {\rm Tr}\, G(e',e;z)G(e,e';z^{-1})\rangle = -2\sum_N P_1(e',e;N)z^{2N}, \tag{6.34}$$

where $P(e',e;N)$ and $P_1(e',e;N)$ are probabilities that the edges e and e' belong to the same loop of the length N (respectively with the length N of the part corresponding to the motion from e to e'). According to the classical percolation theory, P and P_1 scale as

$$P(e',e,N),\ P_1(e',e,N) \sim N^{-8/7}r^{-1/4}, \quad r \lesssim N^{4/7} \tag{6.35}$$

and fall off exponentially fast at $r \gg N^{4/7}$, where r is the distance between e and e'. This yields for the correlation functions in Eqs. (6.33) and (6.34) (abbreviated as $\langle G_R G_R\rangle$, $\langle G_A G_A\rangle$, $\langle G_R G_A\rangle$)

$$\begin{aligned}&\langle G_R G_R\rangle = \langle G_A G_A\rangle \simeq \langle G_R G_A\rangle \sim r^{-1/2}, \\ &r \ll \xi_\gamma \equiv \gamma^{-4/7},\end{aligned} \tag{6.36}$$

in agreement with the scaling argument of Gruzberg *et al.* (1999). However, these leading-order terms cancel in Eq. (6.31), and the result is nonzero due to the factors z^{2N} only, implying that relevant N are $N \sim \gamma^{-1}$. As a consequence, $\langle (G_R - G_A)(G_R - G_A)\rangle$ scales different compared to Eq. (6.36),

$$\begin{aligned}\mathcal{D}(e',e;\gamma) &= \frac{1}{\pi^2}\sum_N [P(r,N) - P_1(r,N)](1 - e^{-2N\gamma}) \\ &\sim P(r,\gamma^{-1})\gamma^{-1} \sim (\xi_\gamma r)^{-1/4}, \quad r \lesssim \xi_\gamma.\end{aligned} \tag{6.37}$$

Analysis of the correlation function (6.32) yields similar results. One thus finds the scaling of two-point wave-function correlations for $r \lesssim \xi_E$,

$$\left.\begin{aligned}L^4\langle \psi^*_{i\alpha}(e)\psi_{j\alpha}(e)\psi_{i\beta}(e')\psi^*_{j\beta}(e')\rangle \\ L^4\langle |\psi_{i\alpha}(e)|^2|\psi_{j\beta}|^2\rangle\end{aligned}\right\} \sim \left(\frac{\xi_E}{r}\right)^{1/4}, \tag{6.38}$$

with α,β labeling the spin indices. This implies that the fractal exponent $\Delta_2 \equiv -\eta$ is

$$\Delta_2 = -1/4, \tag{6.39}$$

at variance with what one might naively expect from the $r^{-1/2}$ scaling of the diffusion propagator $\langle G_R G_A\rangle$, Eq.

(6.36). An analogous calculation for three-point correlation functions yields $\Delta_3=-3/4$. For correlation functions of higher orders (determining, in particular, exponents Δ_q with $q>3$) the mapping to percolation breaks down.

The point $q=3$ deserves special attention. It satisfies the relation

$$\Gamma(q) \equiv qx_\rho + \Delta_q = 0, \tag{6.40}$$

where $x_\rho=1/4$ is the scaling dimension of DOS defined by $\rho(E)\sim\xi_E^{-x_\rho}$. It separates two regimes with different scaling of correlation functions. For smaller q, when $\Gamma(q)>0$, the correlation functions

$$\Pi^{(q)}_{s_1\cdots s_q}(e_1,\ldots,e_q;E_1,\ldots,E_q) = \langle \mathrm{Tr}\, G_{s_1}(e_1,e_2;e^{iE_1})\cdots G_{s_q}(e_q,e_1;e^{iE_q})\rangle, \tag{6.41}$$

where $s_j=R$ or A show the scaling

$$\Pi^{(q)}_{s_1\cdots s_q}(e_1,\ldots,e_q;E_1,\ldots,E_q)\sim r^{-qx_\rho} \tag{6.42}$$

and are, to the leading approximation, independent of the indices s_i. However, when one calculates the wave-function correlations,

$$\begin{aligned}\mathcal{D}^{(q)}(e_1,\ldots,e_q;E_1,\ldots,E_q) &= (2\pi)^{-q}\langle \mathrm{Tr}[(G_R-G_A)(e_1,e_2;e^{iE_1}) \\ &\times (G_R-G_A)(e_2,e_3;e^{iE_2})\times\cdots \\ &\times (G_R-G_A)(e_q,e_1;e^{iE_q})]\rangle,\end{aligned} \tag{6.43}$$

these leading-order terms cancel, yielding the multifractal behavior

$$\mathcal{D}^{(q)}(e_1,\ldots,e_q;E_1,\ldots,E_q)\sim (r/\xi_E)^{\Delta_q}\xi_E^{-qx_\rho},\quad r\lesssim\xi_E. \tag{6.44}$$

On the other hand, for $q>3$, when $\Gamma(q)$ is negative, the correlation functions $\Pi^{(q)}_{s_1,\ldots,s_q}$ start to depend in a singular way on the infrared cutoff (ξ_E) and scale in the same way as $\mathcal{D}^{(q)}$, Eq. (6.44) (with a numerical prefactor depending on indices s_i), similar to the conventional Anderson localization transition.

It is instructive to analyze this situation within the field-theoretical approach to the wave-function multifractality (Wegner, 1980, 1985; Duplantier and Ludwig, 1991; Mudry *et al.*, 1996; Bhaseen *et al.*, 2000; Bernard and LeClair, 2002b). In the RG language, $\Gamma(q)$ defined by Eq. (6.40) are scaling dimensions of operators of the type $\mathcal{O}^{(q)}\sim\psi_{s_1}\psi^\dagger_{s_1'}\cdots\psi_{s_q}\psi^\dagger_{s_q'}$, where $\psi,\psi^\dagger$ are electronic fields. Averaged products of Green's functions are expressed as correlation functions of the corresponding operators $\mathcal{O}^{(q)}$; in particular, Eq. (6.41) takes the form

$$\Pi^{(q)}_{s_1\cdots s_q}\sim\langle \mathrm{Tr}\,\mathcal{O}^{(1)}_{s_1s_2}(e_2)\mathcal{O}^{(1)}_{s_2s_3}(e_3)\cdots\mathcal{O}^{(1)}_{s_qs_1}(e_1)\rangle. \tag{6.45}$$

To calculate the scaling behavior of such correlation functions, one applies the operator product expansion (OPE) (Wegner, 1985; Duplantier and Ludwig, 1991; Mudry *et al.*, 1996). Generically, the identity operator will be among those generated by the OPE. Moreover, under the condition $\Gamma(q)>0$ the identity operator will be the most relevant operator and dominate the expansion, leading to the gap scaling $\Pi^{(q)}\sim r^{-q\Gamma(1)}$, in agreement with Eq. (6.42). On the other hand, if $\Gamma(q)<0$, the operator $\mathcal{O}^{(q)}$ will give a dominant contribution to OPE, leading to a multifractal type of scaling, $\Pi^{(q)}\propto r^{-q\Gamma(1)}(r/\xi_E)^{\Gamma(q)}$, as in Eq. (6.44). What is, however, nontrivial from this point of view is that the scaling of the wave-function correlator (6.43) has the multifractal form (6.44) independent of the sign of $\Gamma(q)$. This means that in the regime $\Gamma(q)>0$ the leading (gap scaling) terms (6.42) cancel in the particular combination of the functions $\Pi^{(q)}$ corresponding to $\mathcal{D}^{(q)}$, and subleading terms determine the result (6.44).

A related analysis can also be performed for the moments of the two-point conductance, Eq. (2.61). The corresponding exponents X_q are found to be linked to the wave-function multifractal indices via Eq. (2.63).

6. Numerical results

Numerical simulations of the SQHE network (Mirlin *et al.*, 2003) have allowed us to confirm the analytical predictions (Secs. VI.D.3–VI.D.5) as well as to determine some physical quantities that are not known analytically, most notably, the whole spectrum of multifractality. We present a summary of the numerical results.

In Fig. 26(a) the numerically calculated DOS $\rho(E)$ for different system sizes L is displayed. After a proper rescaling all data collapse onto a single curve. The scale invariance of $\rho(E)$ at criticality is reminiscent of the analogous property of the level statistics at the conventional Anderson or QH transition, see Sec. II.E. At $E\gg\delta$ the critical DOS scales as $|E|^{1/7}$, in agreement with the analytical prediction (6.28). On the other hand, at $E\sim\delta$ one observes an oscillatory structure analogous to the RMT behavior for the class C (Altland and Zirnbauer, 1997).

The anomalous multifractal dimensions Δ_q [divided by $q(1-q)$] are shown by a solid line in the upper panel of Fig. 27. They have been obtained from the scaling of the average IPRs. According to analytical calculations (Sec. VI.D.5), $\Delta_q/q(1-q)=1/8$ for both $q=2$ and 3; this is shown by the dashed line in the figure. The numerical results agree well with the analytical findings at $q=2$ and 3. Furthermore, the parabolic dependence may serve as a numerically good approximation,

$$\Delta_q\simeq q(1-q)/8. \tag{6.46}$$

Nevertheless, Eq. (6.46) is not exact: at $0<q<2$ the numerically found Δ_q values show clear deviations from exact parabolicity (6.46), which are on the order of 10% near $q=0$. In particular, the deviation of the limiting value $\Delta_q/q(1-q)|_{q\to0}=0.137\pm0.003$ from 1/8 well exceeds the estimated numerical uncertainty. The lower panel of Fig. 27 depicts the singularity spectrum $f(\alpha)$. The dashed line represents the parabolic approximation Eq. (2.36) with $\alpha_0-2=1/8$, corresponding to Eq. (6.46). The deviation of $\alpha_0-2=0.137\pm0.003$ from 1/8 highlighted in the inset corresponds to nonparabolicity of τ_q

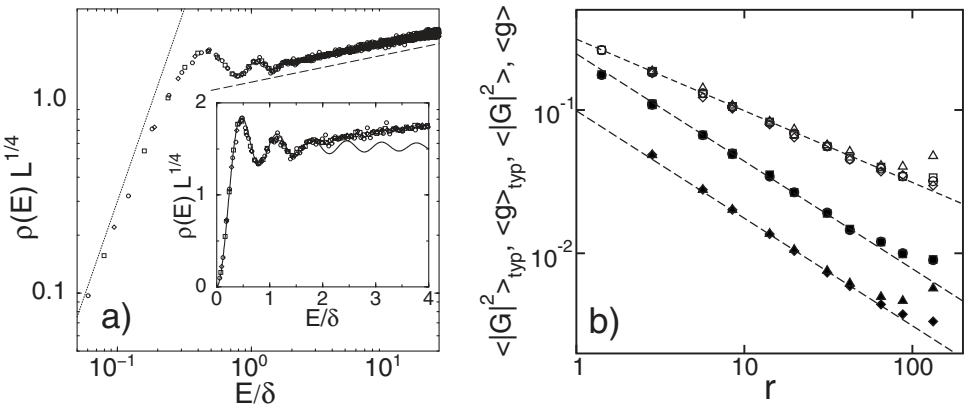

FIG. 26. SQHE criticality. (a) Scaling plot of the DOS for system sizes $L=16$ ($\diamond$), 32 ($\square$), and 96 ($\bigcirc$). Dashed and dotted lines indicate power laws (dashed: $E^{1/7}$, dotted: E^2), $\delta=1/2\pi L^{7/4}$ denotes the level spacing at $E=0$. Inset: Same data on a linear scale and the RMT result (solid curve). From Evers *et al.*, 2003. (b) Scaling of the two-point conductance with distance r between the contacts: average value (empty symbols), $\langle g\rangle$, and typical value (filled symbols), $g_{\rm typ}=\exp\langle\ln g\rangle$, for $L=128$ ($\square$) and $L=196$ ($\bigcirc$). Also shown is scaling of the two-point Green's function $\langle|G|^2\rangle$ and $|G|^2_{\rm typ}=\exp\langle\ln|G|^2\rangle$ [$L=128$ ($\triangle$), $L=196$ ($\diamond$)]. The lines correspond to the $r^{-1/2}$ (dotted) and $r^{-3/4}$ (dashed) power laws. Deviations from power-law scaling at large r are due to the finite system size. From Mirlin *et al.*, 2003.

discussed above. Numerical results for the multifractality at the SQH transition rule out conjectures of critical field theories that predict exactly parabolic spectra (Bernard and LeClair, 2001, 2002b).

In Fig. 26(b) the scaling of the average $\langle g\rangle$ and the typical $g_{\rm typ}=\exp\langle\ln g\rangle$ values of the two-point conductance is shown, along with analogous quantities $\langle|G|^2\rangle$ and $|G|^2_{\rm typ}=\exp\langle\ln|G|^2\rangle$ for a closed system, $|G|^2\equiv-\mathrm{Tr}\,G(e',e;1)G(e,e';1)$. For the average values $\langle g\rangle$ and $\langle|G|^2\rangle$, the numerics fully confirm the theoretical results (6.30) and (6.34) predicting that both quantities scale as $r^{-1/2}$ and, moreover, are equal to each other. A nontrivial character of the equality $\langle g\rangle=\langle|G|^2\rangle$ is well illustrated by data for typical quantities: $g_{\rm typ}$ and $|G|^2_{\rm typ}$ are not equal. Nevertheless, they are found to share a common scaling: $g_{\rm typ},|G|^2_{\rm typ}\sim r^{-X_t}$, confirming the analytical expectations. Furthermore, the numerically obtained value for the exponent, $X_t\simeq 3/4$, is in agreement with the theoretical prediction based on the relation (2.63), $X_t=2x_\rho+2(\alpha_0-2)\simeq 0.774$.

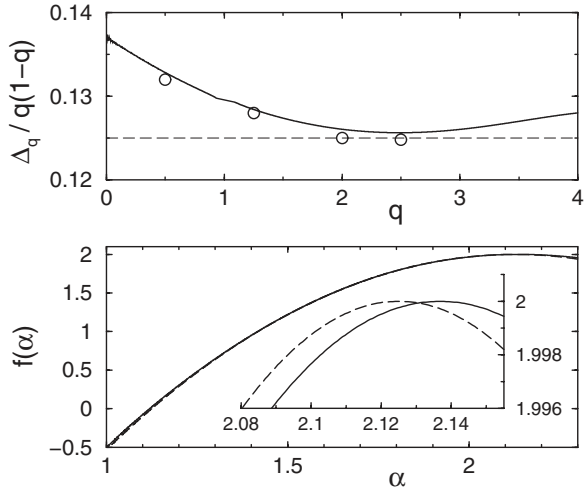

FIG. 27. SQHE multifractality. Upper panel: Anomalous dimensions Δ_q (solid line) and $\Delta_q^{\rm typ}$ (circles) at the SQHE critical point. Numerical results agree well with analytical findings $\Delta_2=-1/4$ and $\Delta_3=-3/4$. Data are presented in the form $\Delta_q/q(1-q)$ emphasizing deviations from exact parabolicity (dashed line). Lower panel: Singularity spectrum $f(\alpha)$ (solid) and the parabolic approximation (dashed). Inset: Magnified view of the apex region. From Mirlin *et al.*, 2003.

E. Thermal quantum Hall effect (class D)

1. Physical realizations and general considerations

Systems belonging to class D are disordered superconductors where both time-reversal and spin-rotation symmetries are broken. The corresponding Hamiltonian has the structure described in Sec. IV.D, see Eqs. (4.8) and (4.9) and following text. Possible physical realizations of this symmetry class include the following: (i) d-wave superconductors with strong spin-orbit scattering, (ii) p-wave paired states of spinless or spin-polarized fermions, e.g., paired states of composite fermions (Read and Green, 2000); (iii) triplet odd-parity (p- or f-wave) superconductors, like $SrRu_3O_4$ (Nelson *et al.*, 2004); and (iv) type-II superconductors in a strong magnetic field in the presence of spin-orbit scattering impurities (Senthil and Fisher, 2000). While neither the quasiparticle number nor spin are conserved for this symmetry class, one still can speak about thermal transport. The TQHE corresponds to the quantization of the ratio κ_{xy}/T of the thermal Hall conductance to the temperature in units of $\pi^2k_B^2/6h$ (Senthil and Fisher, 2000).

For a combination of reasons, class D systems show particularly rich behavior from the point of view of localization, quantum phases, and phase transitions. First, class D allows for two mechanisms of 2D criticality, see Sec. VI.A: (i) a topological θ term associated with a quantum-Hall-type transition and (ii) a metallic phase,

in view of broken spin-rotation invariance. Thus, generically, three phases are possible: metal, insulator, and quantized Hall conductor. A further striking feature of class D is that the type of disorder affects crucially the phase diagram. At the level of the σ model, the reason is believed to be that the relevant target space has two disconnected pieces, and that, depending on the choice of the underlying microscopic model, it may or may not be necessary to consider configurations containing domain walls on which the σ-model field jumps between the two components (Bocquet *et al.*, 2000; Read and Ludwig, 2001; Chalker *et al.*, 2002; Gruzberg *et al.*, 2005). In the following we concentrate on the Cho-Fisher (CF) network model (Cho and Fisher, 1997a) of the TQHE, which is generic in the sense that it displays all three possible phases. Other models of disorder are briefly discussed in the end of Sec. VI.E.2.

2. Network model and phase diagram

To obtain a disordered network model of class D, one can start from the ordered network, Fig. 21, and then allow for independent fluctuations of the node parameters θ_i with some distribution function $\mathcal{P}(\theta)$. The CF model corresponds to the choice

$$\mathcal{P}(\theta) = (1-p)\delta(\theta-\theta_0) + \frac{p}{2}\delta(\theta+\theta_0) + \frac{p}{2}\delta(\theta+\theta_0-\pi), \tag{6.47}$$

implying that disorder is introduced as isolated defects by making the change $\theta \to -\theta$ or $\theta \to \pi-\theta$, for a subset of nodes randomly distributed with a concentration p. This amounts to flipping signs of either both $\sin\theta$ or both $\cos\theta$ associated with such a node. This procedure can be viewed as inserting two additional half-flux lines into two plaquettes adjacent to the node and belonging to the same sublattice. Note that the vortex pair appears with equal probability on the C or S sublattice. This feature is what distinguishes the CF model from the random bond Ising model (RBIM) (Cho and Fisher, 1997a; Merz and Chalker, 2002), which is obtained if all additional vortices are on the same sublattice.

The phase diagram of the CF model was established by Chalker *et al.* (2002), and it was found that all three expected phases are indeed present, see Fig. 28. The DOS in these phases and at transitions between them was studied by Mildenberger, Evers, *et al.* (2007); the results are presented in Secs. VI.E.3 and VI.E.4. It was also checked by Mildenberger, Evers, *et al.* (2007) that the CF model is indeed generic: the same behavior is obtained for a model with a Gaussian distribution $\mathcal{P}(\theta)$.

We discuss now two other disorder models, with properties qualitatively different from the CF model.

(i) A fermionic version of the $\pm J$ RBIM is described by a disordered network model with (Read and Ludwig, 2001; Chalker *et al.*, 2002; Merz and Chalker, 2002)

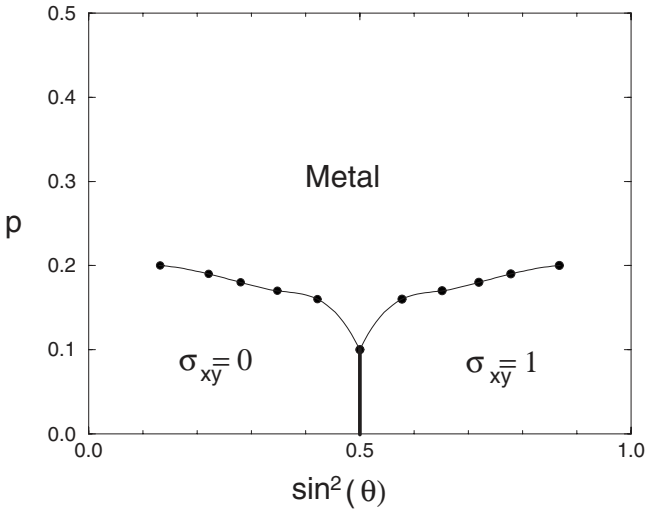

FIG. 28. Phase diagram of the Cho-Fisher model as obtained by Chalker *et al.* (2002) from transfer-matrix calculations. The plane is spanned by the parameters $\sin^2\theta$, the interplaquette tunneling probability, and p, the concentration of vortex disorder: these control the short-distance values of the conductivity components σ_{xy} and σ_{xx}, respectively.

$$\mathcal{P}(\theta) = (1-p)\delta(\theta-\theta_0) + p\,\delta(\theta+\theta_0). \tag{6.48}$$

This implies that all pairs of vortices are inserted in the same sublattice. It has been shown analytically (Read and Ludwig, 2001) and verified numerically (Chalker *et al.*, 2002) that the metallic phase is absent in the RBIM. Two phases with localized states (separated by the TQHE transition) correspond to the paramagnetic and ferromagnetic phases in the Ising spin language. The self-dual state of the disorder-free network ($p=0$, $\sin^2\theta=1/2$) maps onto the critical point of the clean Ising model.

(ii) The $O(1)$ model is obtained if one includes the regular network factors (-1) for propagation along some links, randomly selected with a concentration p. The crucial feature of such a defect (that distinguishes it from the randomness in the nodal parameter such as the vortex pairs in the CF model and the RBIM) is that it cannot be "switched off" by any continuous transformation. Therefore such a defect has the topological character of a vortex. It was found (Read and Ludwig, 2001; Chalker *et al.*, 2002) that such topological defects destroy completely the localization, so that the $O(1)$ model is always in the metallic phase. From the σ-model perspective, it was shown that the effect of vortices is in suppression of the second (disconnected) component of the target space (Bocquet *et al.*, 2000).

3. Thermal metal

The metallic phase can be treated analytically via the σ-model approach. The corresponding RG analysis yields

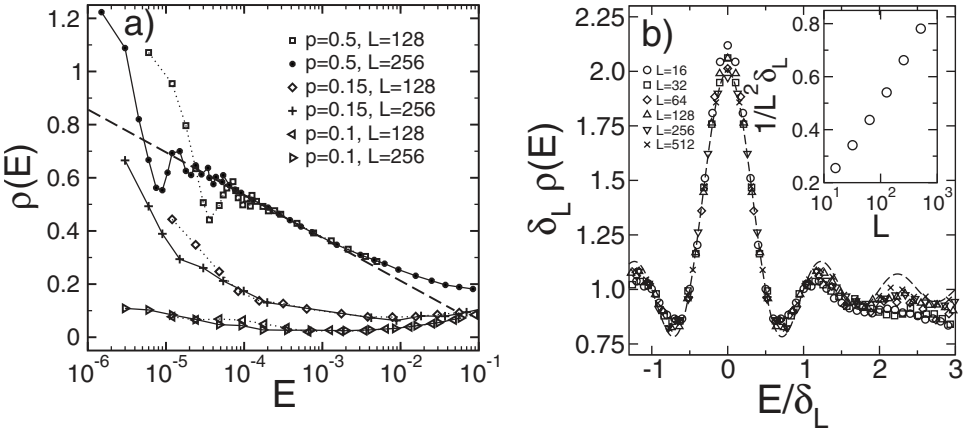

FIG. 29. DOS in the thermal metal phase of the Cho-Fisher model. (a) Low-energy DOS in metallic phase. Parameters (upper curves): $p=0.5$, $\theta=\pi/4$, system sizes $L=128$ (squares) and $L=256$ (full circles). The straight dashed line represents logarithmic asymptotics. For lowest energies the RMT oscillations are clearly visible; they collapse onto a single curve as shown in the right plot. For comparison, results for $p=0.15$ and 0.1 are also shown; the latter point is close to the expected boundary of the metallic phase, see Fig. 28. It can be seen that when the system approaches the phase boundary, the logarithmic increase of the DOS disappears and the RMT oscillations get damped. (b) Renormalized DOS at maximal disorder $p=0.5$ and on the symmetry line $\sin^2\theta=1/2$ for different system sizes vs energy in units of the level spacing δ_L. The RMT result, Eq. (6.53), plotted as a dashed line for comparison. Inset: Logarithmic dependence of $1/L^2\delta_L$ on the system size L, consistent with the data of the left plot. From Mildenberger, Evers, *et al.*, 2007.

$$dt/d\ln L = -t^2, \tag{6.49}$$

where t is the running coupling constant inversely proportional to the dimensionless conductivity, $t=1/\pi g$. The infrared behavior of the system is governed by the perfect-metal fixed point, $t\to 0$. Specifically, the conductance increases logarithmically with system size, $g(L)=g_0+(1/\pi)\ln L/\ell_0$ (ℓ_0 is the mean-free path), justifying the perturbative RG. The RG equation for the second coupling constant ε, whose bare value is the energy E, is given by

$$d\varepsilon/d\ln L = (2+t)\varepsilon, \tag{6.50}$$

leading to a logarithmic increase of DOS (Bocquet *et al.*, 2000; Senthil and Fisher, 2000),

$$\rho(E) = \rho_0 + \frac{1}{4\pi^2 D}\ln\frac{D}{|E|\ell_0^2}, \tag{6.51}$$

where D is the diffusion constant (remaining unrenormalized to this order), $g_0=2\pi\rho_0 D$.

Numerical results for the DOS in the metallic phase are shown in Fig. 29(a). The data exhibit a logarithmic increase of the DOS over almost 3 decades in E for the larger system size, $L=256$. It is worth stressing that the increase continues to be of logarithmic form even though the renormalized DOS at small energies becomes much larger than its bare (large-E) value $\rho_0\simeq 0.1$. This is a signature of the fact that the RG flow is towards weak coupling, so that the one-loop result (6.51) is valid down to arbitrarily low energies in the thermodynamic limit.

At the smallest energies, pronounced oscillations in the DOS are observed. These are RMT oscillations due to finite system size confirming again that we are dealing with a metallic phase. The RMT origin of these oscillations is shown in Fig. 29(b), where the energy is rescaled to the corresponding mean level spacing δ_L. The data collapse onto a single curve, which shows that the renormalized level spacing

$$\delta_L = \frac{1}{L^2\rho(E_{\rm Th})} = \frac{1}{L^2\rho_0[1+t_0\ln(L/\ell_0)]}, \tag{6.52}$$

with $E_{\rm Th}$ the Thouless energy, is indeed the only relevant energy scale in the regime $E\lesssim E_{\rm Th}$ where the RMT is applicable. As further seen in Fig. 29(b), the curve obtained agrees with the RMT prediction,

$$\rho(E) = \frac{1}{L^2\delta_L}\left[1+\frac{\sin(2\pi E/\delta_L)}{2\pi E/\delta_L}\right], \tag{6.53}$$

up to $E/\delta_L\sim 1.5$–2; for larger energies the oscillations are strongly suppressed. This is consistent with the exponential vanishing of the RMT oscillations beyond the Thouless energy, see Mirlin (2000b). With increasing system size, the ratio $E_{\rm Th}/\delta_L$ increases (though only logarithmically), so that the RMT range includes progressively more oscillation periods. This tendency is seen in Fig. 29(b).

4. Localized phases and TQH transition

An analytical approach to the problem alternative to the σ model is based on the model of Dirac fermions with random mass, in the spirit of the analysis of the Ising model by Dotsenko and Dotsenko (1983). Being perturbative in disorder strength, this approach is appropriate for describing the localized phases and the transition between them. The disorder-free system has a transition, driven by tuning a uniform mass through zero, which in the CF model lies at $p=0$, $\sin^2\theta=1/2$ and corresponds to the clean Ising transition. Near the clean

fixed point representing this transition the disorder strength g_M is marginally irrelevant. This implies for the critical DOS a logarithmic correction term of the form (Bocquet *et al.*, 2000; Mildenberger, Evers, *et al.*, 2007)

$$\rho(E) = \frac{|E|}{2\pi}\left(1 + \frac{2g_M}{\pi}\ln\frac{1}{|E|}\right). \tag{6.54}$$

Slightly away from the critical value $\theta=\pi/4$, the system is in a localized phase with a large localization length $\xi \propto |\theta-\pi/4|^{-\nu}$. As the RG flows toward the clean Ising fixed point, the corresponding index should be the same as in the Ising model, $\nu=1$. The behavior of the DOS in the localized phases can be understood using the Dirac fermion RG (Mildenberger, Evers, *et al.*, 2007). Specifically, for energies that are not too small, the behavior will be the same as at criticality, Eq. (6.54). However, for the smallest energies, it is the localization length ξ rather than E that will terminate the RG process. In this sense, the role of ξ is analogous to that of finite system size L at criticality. Thus $\rho(E)$ saturates at the value

$$\rho(E) \sim \frac{\ell_0}{\xi}\left(1 + 2\frac{g_M}{\pi}\ln\frac{\xi}{\ell_0}\right)^{1/2}, \quad E \lesssim E_\xi. \tag{6.55}$$

The energy E_ξ at which the saturation takes place is

$$E_\xi \sim \frac{\ell_0}{\xi}\left(1 + 2\frac{g_M}{\pi}\ln\frac{\xi}{\ell_0}\right)^{-1/2}. \tag{6.56}$$

The Anderson transition from the metallic to a localized phase should therefore be signaled by a transition from logarithmically diverging to finite $\rho(E\to 0)$. This has been verified by numerical simulations by Mildenberger, Evers, *et al.* (2007), Fig. 30.

We comment on the regions of localized phases where the interplaquette coupling is weak ($\sin^2\theta$ close to zero or to unity). As shown by Mildenberger *et al.* (2006), in this situation the DOS of the RBIM acquires a nonuniversal power-law singularity $|E|^{1/z-1}$ with $z>1$ associated with Griffiths strings (Motrunich *et al.*, 2001, 2002). The same mechanism for the formation of divergent DOS in these parts of the localized phases is expected to be operative in the CF model as well.

We turn now to numerical results (Mildenberger, Evers, *et al.*, 2007) on the DOS at the line $\sin^2\theta=1/2$, where the TQH phase boundary is located. These results are shown in Fig. 31. While at sufficiently large p ($p \gtrsim 0.1$) the DOS shows a logarithmic increase characteristic for the metallic phase, for lower p the DOS behavior agrees with Eq. (6.54), as expected for the TQH transition. This is demonstrated in the inset of Fig. 31, where $\rho(E)/|E|$ as a function of $\log|E|$ is plotted for $p=0.05$.

While at moderately low E the DOS at the TQH transition line is in good agreement with the Dirac-fermion RG, Eq. (6.54), the results for the lowest energies obtained by Mildenberger, Evers, *et al.* (2007) constitute a puzzle. Specifically, it was found that the DOS saturates at a low energy scale and even shows a weak upturn. The reason for this behavior is not understood at present; several possible scenarios were proposed by

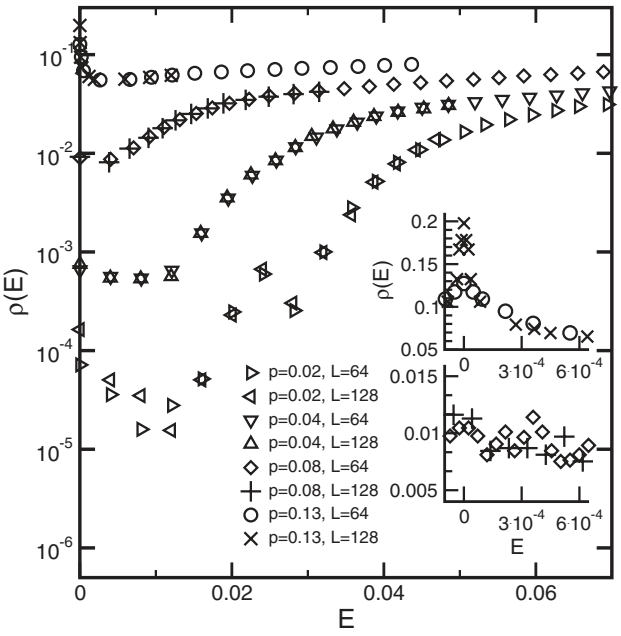

FIG. 30. DOS near $E=0$ for disorder values $p=0.13$, 0.08, 0.04, and 0.02 and for two system sizes $L=64$ and 128 at fixed interplaquette coupling $\sin^2\theta=0.579$. The DOS diverges logarithmically as $E\to 0$ in the metallic phase ($p=0.13$) and remains finite in the localized phase (other values of p). Results for the lowest impurity concentration, $p=0.02$, show an oscillatory feature induced by the band structure of the clean system, as well as strong scatter in the data at the lowest energies, which is due to insufficient ensemble averaging. Upper inset: Low-energy peak at $p=0.13$; its amplitude increases with L, in agreement with Sec. III.A. Lower inset: Low-energy DOS at $p=0.08$. No peak at $E\to 0$ is detected; $\rho(E\to 0)$ is a constant independent on L, indicating that the system is in the insulating phase. Statistical noise in the lower inset is more pronounced than in the upper one due to the smallness of the DOS. From Mildenberger, Evers, *et al.*, 2007.

Mildenberger, Evers, *et al.* (2007): (i) the position p_T of the tricritical point T is in fact not $p_T\simeq 0.1$ as in Fig. 28 but rather considerably smaller, $p_T<0.05$; (ii) in addition to the tricritical point p_T there is a second, repulsive fixed point on the TQH transition line $\sin^2\theta=1/2$, at some $p_N<p_T$. This point would then act as a "flow splitter" which is similar to the Nishimori point in the RBIM; and (iii) the RG treatment of the theory of Dirac fermions with Gaussian random mass is in fact insufficient, and some effects—possibly of nonperturbative origin—eventually drive the system away from the clean Ising fixed point. The clarification of this important issue remains a subject for future research.

F. Chiral classes (AIII, CII, BDI)

We have seen in Sec. V.E that quasi-1D systems of chiral symmetry show a criticality accompanied by a very slow ($L^{-1/2}$) decay of the average conductance and by a Dyson-type singularity ($1/|E\ln^3 E|$) in the DOS. As discussed in the present section, a similar type of criticality takes place in two dimensions.

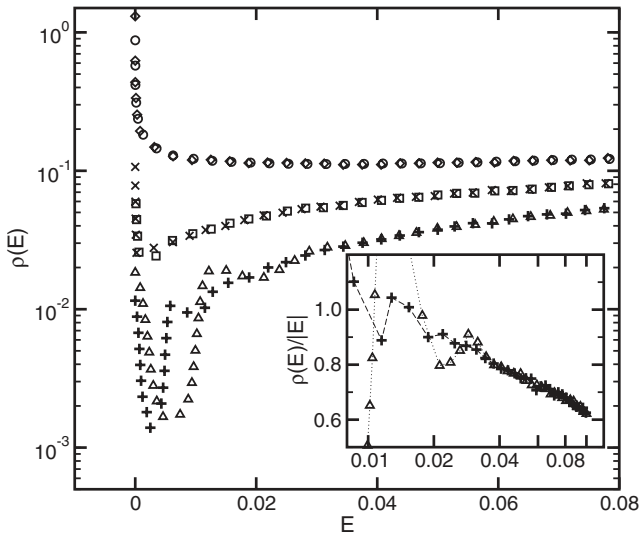

FIG. 31. DOS at low energy on the self-dual line $\sin^2\theta=0.5$ for disorder concentrations $p=0.2$ (○, ◇), 0.1 (□, x), and 0.05 (△, +), where in each case the first symbol is for $L=128$ and the second is for $L=256$. Inset: $\rho(E)/|E|$ at $p=0.05$ on a log-linear scale. The logarithmic correction is clearly observed, in agreement with Eq. (6.54). From Mildenberger, Evers, *et al.*, 2007.

1. Gade-Wegner σ model

In their pioneering works, Gade and Wegner (1991); Gade (1993) derived σ models for systems of the chiral classes and performed their RG analysis at and near two dimensions. They used the fermionic replicas, so that the models are defined on the spaces U(N), U($2N$)/Sp($2N$), and U(N)/O(N) for the chiral unitary, orthogonal, and symplectic classes, respectively. As usual, the supersymmetric generalization (see Table I for the symmetry classes of the corresponding models) is equivalent to the replica version on the level of the perturbation theory. For definiteness, we consider the chiral unitary class (AIII), the results for the other two are similar. The action of the σ model has the form

$$S[Q]=\int d^2r\left\{\frac{1}{16\pi t}\mathrm{Tr}\,\nabla Q^{-1}\nabla Q-\frac{1}{64\pi c}\times[\mathrm{Tr}(Q^{-1}\nabla Q)]^2+i\frac{\pi\rho_0}{4}\varepsilon\mathrm{Tr}\,(Q+Q^{-1})\right\}, \tag{6.57}$$

where $Q\in$ U(N), t and c are two coupling constants, the first of which is related to the conductivity in the usual way, $t^{-1}=2\pi\sigma_{xx}$, ε is the running coupling whose bare value is the energy E (which breaks the chiral symmetry), and ρ_0 is the bare DOS. A special feature of the σ model for chiral classes is the existence of the second term (known as the Gade term), which governs fluctuations of det Q. This σ model was later obtained and analyzed by many authors (Altland and Simons, 1999; Fukui, 1999; Fabrizio and Castellani, 2000; Guruswamy *et al.*, 2000).

The one-loop RG equations in $2+\epsilon$ dimensions are given as

$$-dt/d\ln L=\epsilon t, \tag{6.58}$$

$$-dc/d\ln L=\epsilon c+2c^2, \tag{6.59}$$

$$d\ln\varepsilon/d\ln L=(2+\epsilon)+t^2/2c. \tag{6.60}$$

It is of central importance that in 2D ($\epsilon=0$) the β function (6.58) is identically zero (Gade and Wegner, 1991), i.e., the coupling t (and thus the conductivity) is not renormalized. If one considers a system at nonzero (but small) energy, the chiral symmetry is broken down to that of the unitary Wigner-Dyson class (A), and localization should occur at a sufficiently large scale. To find the scaling of the localization length with energy, one performs the RG transformation until the running energy $\varepsilon(L)$ ceases to be small (i.e., reaches a characteristic scale Δ of the problem; typically, the bandwidth). Beyond this scale, the RG takes the form characteristic for class A, driving the system towards the localized regime. The localization length $\xi(E)$ is thus given by the crossover length $L_c(E)$, up to an energy-independent factor $\sim\exp(1/4t^2)$. Further, the DOS is given by

$$\rho(E)\sim 1/EL_c^2(E). \tag{6.61}$$

Integration of Eqs. (6.59) and (6.60) (with $\epsilon=0$) yields

$$\ln L_c(E)\simeq\frac{1}{2t^2}[\sqrt{B^2+4t^2|\ln(E/\Delta)|}-B], \tag{6.62}$$

where $B=2+t^2/c_0$ and c_0 is the bare value of the coupling c. For asymptotically low energies, $|\ln(E/\Delta)|\gg B^2/4t^2$, this reduces to

$$\xi(E)\propto\exp[t^{-1}|\ln(E/\Delta)|^{1/2}], \tag{6.63}$$

$$\rho(E)\propto E^{-1}\exp[-2t^{-1}|\ln(E/\Delta)|^{1/2}]. \tag{6.64}$$

The last formula is the 2D counterpart of the Dyson singularity. On the other hand, at intermediate energies $|\ln(E/\Delta)|\ll B^2/4t^2$, the behavior is of the power-law type with a nonuniversal exponent,

$$\xi(E)\propto E^{-1/B},\quad \rho(E)\propto E^{-1+2/B}. \tag{6.65}$$

We emphasize that the bare coupling c_0 is of the order of unity even for a system with large conductance ($t\ll 1$). This means that $B\simeq 2$ and the asymptotic behavior (6.63) and (6.64) establishes at exponentially low energies only, $\ln(\Delta/E)\ll 1/t^2$. For this reason it is difficult to reach the true asymptotics in numerical simulations, whereas the intermediate power law regime (6.65) can be well studied; see, e.g., Markos and Schweitzer (2007).

As in the 1D geometry, one can drive the system away from criticality by introducing a staggering in hopping strength ("dimerization") in a lattice model. The DOS in the localized phase was predicted to show a power-law behavior, $\rho(E)\sim E^{-1+2/z}$, governed by the Griffiths mechanism, with a nonuniversal dynamical exponent $z>0$ (Motrunich *et al.*, 2002). Bocquet and Chalker (2003) constructed network models for all chiral classes. A nu-

merical study of the class-AIII network model confirmed the existence of the critical (Gade-Wegner) and localized (Griffiths-type) phases. This study found that the DOS exhibits a nonuniversal $E^{-1+2/z}$ power-law behavior in the localized phase and that z asymptotically tends to infinity with decreasing energy in the critical phase, in agreement with analytical predictions.

2. Dirac fermions approach: Strong-coupling effects

The Gade-Wegner prediction of a critical state with a diverging DOS of the form (6.64) can also be reproduced by starting from a model of disordered Dirac fermions (Guruswamy *et al.*, 2000). Specifically, a model of fermions on a bipartite lattice with π flux and random real hopping (Hatsugai *et al.*, 1997), which belongs to the class BDI, is described by a two-flavor model of Dirac fermions subject to a random vector potential (coupling g_A) and a chiral random mass (g_m). This is a particular type of two-flavor disordered Dirac fermion models considered in Sec. VI.G.4; in notations used there $g_A=\gamma_\perp/2$, $g_m=\beta_z/2$. For this model, exact β functions can be found (Guruswamy *et al.*, 2000) to all orders in g_m:

$$\frac{dg_A}{d\ln L}=\frac{2g_m^2}{(1+2g_m)^2},\quad \frac{dg_m}{d\ln L}=0. \tag{6.66}$$

Further, the dynamical scaling function was found to be

$$\frac{d\ln\varepsilon}{d\ln L}\equiv z=1+\frac{2g_A}{(1+2g_m)^2}+2g_m+O(g_m^2). \tag{6.67}$$

According to Eqs. (6.66), g_m is not renormalized, while g_A grows logarithmically with L. Assuming for simplicity weak disorder, $g_m\ll 1$, we have

$$g_A(L)\simeq g_A^{(0)}+4g_m^2\ln L. \tag{6.68}$$

For sufficiently large L the $\ln L$ term dominates. Substituting the term into Eq. (6.67), one gets

$$\ln\varepsilon(L)\simeq 2g_m^2\ln^2 L. \tag{6.69}$$

This reproduces Eqs. (6.63) and (6.64) for the localization length and the DOS with $t\to g_m\sqrt{2}$.

As shown by Motrunich *et al.* (2002), this result is, however, not completely correct, for the following reason. It is well known that the multifractal spectrum of Dirac fermions in a random vector potential undergoes a transition from a weak-disorder to a strong-disorder phase at $g_A=1$ (freezing transition), see Sec. VI.G.3. As shown by Horovitz and LeDoussal (2002); Motrunich *et al.* (2002), this transition is accompanied by a change of the behavior of the dynamical exponent

$$z=\begin{cases}1+2g_A, & g_A<1\\ 4\sqrt{g_A}-1, & g_A>1.\end{cases} \tag{6.70}$$

In the presence of the second coupling (g_m), $g_A(L)$ will flow according to Eq. (6.68), and z will develop following Eq. (6.70). While the first line of Eq. (6.70) agrees with Eq. (6.67), it is only valid at short distances, $g_A(L)<1$ (which corresponds to the ballistic regime). At sufficiently long (diffusive) scale, where the σ model is applicable, g_A will become larger than unity. Using the second line of Eq. (6.70) instead of Eq. (6.67) yields

$$\rho(E)\sim E^{-1}\exp\{-\tfrac{1}{2}[3g_m^{-1}|\ln(E/\Delta)|]^{2/3}\}. \tag{6.71}$$

Therefore the exponent 1/2 in Eq. (6.63) and in the second (subleading) factor in Eq. (6.64) is replaced by 2/3.

This result was also rederived in the framework of the RG approach. The key point is that, when the running coupling g_A ceases to be weak, it is not sufficient anymore to characterize the disorder by the lowest-order cumulants. Instead, one should take into account an infinite number of couplings. Such a functional RG method was developed by Carpentier and LeDoussal (1999) in the context of a related random XY model. For the problem of Dirac fermions with random mass and vector potential this program was carried out by Mudry *et al.* (2003): the results confirm the conclusion of Motrunich *et al.* (2002), Eq. (6.71). Analogous results were also obtained by Yamada and Fukui (2004); Dell'Anna (2006).

G. Disordered Dirac Hamiltonians

Localization and criticality in models of 2D Dirac fermions subjected to various types of disorder have been extensively studied, including the random bond Ising model (Dotsenko and Dotsenko, 1983), the quantum Hall effect (Ludwig *et al.*, 1994), dirty superconductors with unconventional pairing (Nersesyan *et al.*, 1995; Bocquet *et al.*, 2000; Altland *et al.*, 2002), and some lattice models with chiral symmetry (Guruswamy *et al.*, 2000). Recently, this class of problems has attracted much attention in connection with its application to graphene; see, in particular, Aleiner and Efetov (2006); Khveshchenko (2006); McCann *et al.* (2006); Ostrovsky *et al.* (2006, 2007a, 2007b); Altland (2007).

In the presence of different types of randomness, Dirac Hamiltonians realize all ten symmetry classes of disordered systems; see Bernard and LeClair (2002a) for a detailed symmetry classification. Furthermore, in many cases the Dirac character of fermions induces nontrivial topological properties (θ term or WZ term) of the corresponding field theory (σ model). In Sec. VI.G.1 we review the classification of disorder in a two-flavor model of Dirac fermions describing the low-energy physics of graphene, the RG treatment of the problem, and types of criticality. The emergent critical theories are discussed in Secs. VI.G.2–VI.G.4. In Sec. VI.G.5 we discuss a four-node Dirac fermion model appropriate for a description of dirty d-wave superconductors.

1. Disordered two-node Dirac Hamiltonians: Symmetries of disorder, renormalization group, and types of criticality

The presentation below largely follows the work of Ostrovsky *et al.* (2006, 2007b). We concentrate on a two-flavor model, which is in particular relevant to describing the electronic properties of graphene. Graphene is a semimetal; its valence and conduction bands touch each

TABLE V. Disorder symmetries in graphene. The first five rows represent disorders preserving the time-reversal symmetry T_0; the last four represent those violating T_0. First column: Structure of disorder in the sublattice (σ_μ) and valley (τ_ν) spaces. Second column: Disorder strength according to the notations of Ostrovsky *et al.* (2006, 2007b) used in this review. Third (AE) and fourth (GLL) columns: Disorders considered by Aleiner and Efetov (2006) and Guruswamy *et al.* (2000) and notations used there. The remaining columns indicate which symmetries of the clean Hamiltonian are preserved by disorder (Ostrovsky *et al.*, 2006).

Structure	Coupling	AE	GLL	$\Lambda_\perp$	Λ_z	T_0	$T_\perp$	T_z	C_0	$C_\perp$	C_z	CT_0	$CT_\perp$	CT_z
$\sigma_0\tau_0$	α_0	$\gamma_0/2\pi v^2$		+	+	+	+	+	−	−	−	−	−	−
$\sigma_{\{1,2\}}\tau_{\{1,2\}}$	$\beta_\perp$	$2\beta_\perp/\pi v^2$		−	−	+	−	−	+	−	−	+	−	−
$\sigma_{1,2}\tau_0$	$\gamma_\perp$	$\gamma_\perp/\pi v^2$	$2g_A$	−	+	+	−	+	+	−	+	+	−	+
$\sigma_0\tau_{1,2}$	β_z	$\beta_z/\pi v^2$	$2g_m$	−	−	+	−	−	−	−	+	−	−	+
$\sigma_3\tau_3$	γ_z	$\gamma_z/2\pi v^2$		−	+	+	−	+	−	+	−	−	+	−
$\sigma_3\tau_{1,2}$	β_0		$2g_\mu$	−	−	−	−	+	−	−	+	+	−	−
$\sigma_0\tau_3$	γ_0			−	+	−	+	−	−	+	−	+	−	+
$\sigma_{1,2}\tau_3$	$\alpha_\perp$		$2g_{A'}$	+	+	−	−	−	+	+	+	−	−	−
$\sigma_3\tau_0$	α_z			+	+	−	−	−	−	−	−	+	+	+

other in two conical points K and K' of the Brillouin zone. In the vicinity of these points electrons behave as massless relativistic (Dirac-like) particles. Therefore the effective tight-binding low-energy Hamiltonian of clean graphene is a 4×4 matrix operating in the AB space of the two sublattices and in the K–K' space of the valleys. We introduce the four-component wave function

$$\Psi = \{\phi_{AK}, \phi_{BK}, \phi_{BK'}, \phi_{AK'}\}^T. \tag{6.72}$$

In this representation the Hamiltonian has the form

$$H = v_0\tau_3\boldsymbol{\sigma}\mathbf{k}. \tag{6.73}$$

Here τ_3 is the third Pauli matrix in the K–K' space, $\boldsymbol{\sigma} = \{\sigma_1, \sigma_2\}$ the two-dimensional vector of Pauli matrices in the AB space, and v_0 the velocity ($v_0 \simeq 10^8$ cm/s in graphene). It is worth emphasizing that the Dirac form of the Hamiltonian (6.73) does not rely on the tight-binding approximation but is protected by the symmetry of the honeycomb lattice which has two atoms in a unit cell (Haldane, 1988).

We analyze the symmetries of the clean Hamiltonian (6.73) in the AB and KK' spaces. First, there exists an SU(2) symmetry group in the space of the valleys, with generators (McCann *et al.*, 2006)

$$\Lambda_x = \sigma_3\tau_1, \quad \Lambda_y = \sigma_3\tau_2, \quad \Lambda_z = \sigma_0\tau_3, \tag{6.74}$$

all of which commute with the Hamiltonian. Second, there are two more relevant symmetries of the clean Hamiltonian, namely, time inversion operation (T_0) and chiral symmetry (C_0). Combining T_0, C_0, and isospin rotations $\Lambda_{0,x,y,z}$, one can construct 12 symmetry operations, out of which four (denoted as T_μ) are of time-reversal type, four (C_μ) of chiral type, and four (CT_μ) of Bogoliubov–de Gennes type:

$$T_0\colon A \mapsto \sigma_1\tau_1 A^T \sigma_1\tau_1, \quad C_0\colon A \mapsto -\sigma_3\tau_0 A \sigma_3\tau_0,$$

$$CT_0\colon A \mapsto -\sigma_2\tau_1 A^T \sigma_2\tau_1,$$

$$T_x\colon A \mapsto \sigma_2\tau_0 A^T \sigma_2\tau_0, \quad C_x\colon A \mapsto -\sigma_0\tau_1 A \sigma_0\tau_1,$$

$$CT_x\colon A \mapsto -\sigma_1\tau_0 A^T \sigma_1\tau_0,$$

$$T_y\colon A \mapsto \sigma_2\tau_3 A^T \sigma_2\tau_3, \quad C_y\colon A \mapsto -\sigma_0\tau_2 A \sigma_0\tau_2,$$

$$CT_y\colon A \mapsto -\sigma_1\tau_3 A^T \sigma_1\tau_3,$$

$$T_z\colon A \mapsto \sigma_1\tau_2 A^T \sigma_1\tau_2, \quad C_z\colon A \mapsto -\sigma_3\tau_3 A \sigma_3\tau_3,$$

$$CT_z\colon A \mapsto -\sigma_2\tau_2 A^T \sigma_2\tau_2.$$

It is worth remembering that the C and CT symmetries apply to the Dirac point ($E=0$), i.e., to undoped graphene, and get broken by a nonzero energy E. We assume the average isotropy of the disordered graphene, which implies that Λ_x and Λ_y symmetries of the Hamiltonian are present or absent simultaneously. They are thus combined into a single notation $\Lambda_\perp$; the same applies to $T_\perp$ and $C_\perp$. In Table V all possible matrix structures of disorder along with their symmetries are listed.

To derive the field theory of the problem, one introduces a superfield $\psi(\mathbf{r})$, see Sec. II.B.1 (or, alternatively, its replica counterpart). After the disorder averaging, the action containing all possible disorder structures from Table V is given by ($\bar\psi = \psi^\dagger\Lambda$)

$$\begin{aligned} S[\psi] = \int d^2r \Big(& i\bar\psi(\varepsilon + iv_0\tau_3\boldsymbol{\sigma}\nabla - i0\Lambda)\psi \\ & + \pi\nu_0^2 \Big\{ \alpha_0(\bar\psi\sigma_0\tau_0\psi)^2 + \frac{\alpha_\perp}{2}[(\bar\psi\sigma_1\tau_3\psi)^2 \\ & + (\bar\psi\sigma_2\tau_3\psi)^2] + \alpha_z(\bar\psi\sigma_3\tau_0\psi)^2 + \frac{\beta_0}{2}[(\bar\psi\sigma_3\tau_1\psi)^2 \\ & + (\bar\psi\sigma_3\tau_2\psi)^2] + \frac{\beta_\perp}{4}[(\bar\psi\sigma_1\tau_1\psi)^2 + (\bar\psi\sigma_1\tau_2\psi)^2 \\ & + (\bar\psi\sigma_2\tau_1\psi)^2 + (\bar\psi\sigma_2\tau_2\psi)^2] + \frac{\beta_z}{2}[(\bar\psi\sigma_0\tau_1\psi)^2 \end{aligned}$$

$$+(\bar{\psi}\sigma_0\tau_2\psi)^2]+\gamma_0(\bar{\psi}\sigma_0\tau_3\psi)^2+\frac{\gamma_\perp}{2}[(\bar{\psi}\sigma_1\tau_0\psi)^2 + (\bar{\psi}\sigma_2\tau_0\psi)^2]+\gamma_z(\bar{\psi}\sigma_3\tau_3\psi)^2\Big\}\Big). \quad (6.75)$$

A set of one-loop perturbative RG equations for nine disorder amplitudes and the running energy ε (whose bare value is E) has the form (Ostrovsky *et al.*, 2006)

$$\frac{d\alpha_0}{d\ln L}=2\alpha_0(\alpha_0+\beta_0+\gamma_0+\alpha_\perp+\beta_\perp+\gamma_\perp+\alpha_z+\beta_z+\gamma_z)+2\alpha_\perp\alpha_z+\beta_\perp\beta_z+2\gamma_\perp\gamma_z,$$

$$\frac{d\alpha_\perp}{d\ln L}=2(2\alpha_0\alpha_z+\beta_0\beta_z+2\gamma_0\gamma_z),$$

$$\frac{d\alpha_z}{d\ln L}=-2\alpha_z(\alpha_0+\beta_0+\gamma_0-\alpha_\perp-\beta_\perp-\gamma_\perp+\alpha_z+\beta_z+\gamma_z)+2\alpha_0\alpha_\perp+\beta_0\beta_\perp+2\gamma_0\gamma_\perp,$$

$$\frac{d\beta_0}{d\ln L}=2[\beta_0(\alpha_0-\gamma_0+\alpha_\perp+\alpha_z-\gamma_z)+\alpha_\perp\beta_z+\alpha_z\beta_\perp+\beta_\perp\gamma_0],$$

$$\frac{d\beta_\perp}{d\ln L}=4(\alpha_0\beta_z+\alpha_z\beta_0+\beta_0\gamma_0+\beta_\perp\gamma_\perp+\beta_z\gamma_z),$$

$$\frac{d\beta_z}{d\ln L}=2[-\beta_z(\alpha_0-\gamma_0-\alpha_\perp+\alpha_z-\gamma_z)+\alpha_0\beta_\perp+\alpha_\perp\beta_0+\beta_\perp\gamma_z],$$

$$\frac{d\gamma_0}{d\ln L}=2\gamma_0(\alpha_0-\beta_0+\gamma_0+\alpha_\perp-\beta_\perp+\gamma_\perp+\alpha_z-\beta_z+\gamma_z)+2\alpha_\perp\gamma_z+2\alpha_z\gamma_\perp+\beta_0\beta_\perp,$$

$$\frac{d\gamma_\perp}{d\ln L}=4\alpha_0\gamma_z+4\alpha_z\gamma_0+\beta_0^2+\beta_\perp^2+\beta_z^2,$$

$$\frac{d\gamma_z}{d\ln L}=-2\gamma_z(\alpha_0-\alpha_\perp+\alpha_z-\beta_0+\beta_\perp-\beta_z+\gamma_0-\gamma_\perp+\gamma_z)+2\alpha_0\gamma_\perp+2\alpha_\perp\gamma_0+\beta_\perp\beta_z,$$

$$\frac{d\ln\varepsilon}{d\ln L}=1+\alpha_0+\beta_0+\gamma_0+\alpha_\perp+\beta_\perp+\gamma_\perp+\alpha_z+\beta_z+\gamma_z. \quad (6.76)$$

If all types of disorder are present (i.e., no symmetry is preserved), the RG flow is towards the conventional localization fixed point (unitary Wigner-Dyson class A). If the only preserved symmetry is the time reversal invariance (T_0), again conventional localization (orthogonal Wigner-Dyson class AI) takes place (Aleiner and Efetov, 2006). A nontrivial situation occurs if either (i) one of the chiral symmetries is preserved or (ii) the valleys remain decoupled. In Table VI we list situations when symmetry prevents localization and leads to criticality and nonzero conductivity at $E=0$ (in the case of decoupled nodes—also at nonzero E). Models with decoupled nodes are analyzed in Sec. VI.G.2, and models with a chiral symmetry in Secs. VI.G.3 (C_0 chirality) and VI.G.4 (C_z chirality).

2. Decoupled nodes: Disordered single-flavor Dirac fermions and quantum-Hall-type criticality

If the disorder is of long-range character, the valley mixing is suppressed due to the lack of scattering with large momentum transfer. The couplings that do not mix the valleys are α_0, $\alpha_\perp$, α_z, γ_0, $\gamma_\perp$, and γ_z. For each of the nodes, the system can then be described in terms of a single-flavor Dirac Hamiltonian,

$$H=v_0[\boldsymbol{\sigma}\mathbf{k}+\sigma_\mu V_\mu(\mathbf{r})]. \quad (6.77)$$

Here disorder includes random scalar (V_0) and vector ($V_{1,2}$) potentials and random mass (V_3). The corresponding couplings are $g_V=\alpha_0+\gamma_0$, $2g_A=\alpha_\perp+\gamma_\perp$, and $\tilde{g}_m=\alpha_z+\gamma_z$.[15] The clean single-valley Hamiltonian (6.77) obeys the effective time-reversal invariance $H=\sigma_2H^T\sigma_2$. This symmetry ($T_\perp$) is not the physical time-reversal symmetry (T_0): the latter interchanges the nodes and is of no significance in the absence of internode scattering. The RG equations have the form

$$dg_A/d\ln L=2g_V\tilde{g}_m, \quad (6.78)$$

$$dg_V/d\ln L=2(2g_A+g_V)(g_V+\tilde{g}_m), \quad (6.79)$$

$$d\tilde{g}_m/d\ln L=2(2g_A-\tilde{g}_m)(g_V+\tilde{g}_m), \quad (6.80)$$

$$d\ln\varepsilon/d\ln L=1+2g_A+\tilde{g}_m+g_V. \quad (6.81)$$

Remarkably, single-flavor Dirac fermions are never in the conventional localized phase. More specifically, depending on which of the disorders are present, four different types of criticality take place.

(i) The only disorder is the random vector potential (g_A). This is a special case of the symmetry class AIII. This problem is exactly solvable and has been studied in a great detail; this is discussed in Sec. VI.G.3.

(ii) Only random mass ($\tilde{g}_m$) is present. The system belongs then to class D. The random-mass disorder is marginally irrelevant, and the system flows under RG towards the clean fixed point. This problem is analyzed in Sec. VI.E.3.

(iii) The only disorder is random scalar potential (g_V). The system is then in the Wigner-Dyson symplectic (AII) symmetry class. As found by Ostrovsky

[15](i) The tilde in $\tilde{g}_m$ serves to distinguish it from the chiral random mass coupling g_m, see Table V and Secs. VI.F.2 and VI.G.4; and (ii) our couplings are related to those of Ludwig *et al.* (1994) via $g_A=\Delta_A/2\pi$, $g_V=\Delta_V/2\pi$, $\tilde{g}_m=\Delta_m/2\pi$.

et al. (2007a), the corresponding σ model contains a topological term with $\theta=\pi$, which leads to delocalization. This model is discussed in Sec. VI.B.5.

(iv) At least two types of randomness are present. This is the same as to say that all are present, as the third one will be generated by RG, see Eqs. (6.78)–(6.80). The model belongs to the Wigner-Dyson unitary class A, and it was argued by Ludwig *et al.* (1994) that it flows into the IQH transition fixed point. This is confirmed by the derivation of the corresponding σ model (Altland *et al.*, 2002; Ostrovsky *et al.*, 2007a, 2007b), which contains a topological term with $\theta=\pi$, i.e., is nothing but the Pruisken σ model at criticality. A particular consequence of this is that the conductivity of graphene with this type of disorder is equal to the value σ_U^* of the longitudinal conductivity σ_{xx} at the critical point of the IQH transition multiplied by four (because of spin and valleys). Note that the conclusion of IQH criticality formally holds for arbitrary energy ε, although in reality it only works near half filling; for other ε the critical point would only be approached for unrealistic system sizes and temperatures.

If a uniform transverse magnetic field is applied, the topological angle θ becomes energy dependent. However, at the Dirac point ($E=0$), where $\sigma_{xy}=0$, its value remains unchanged, $\theta=\pi$. This implies the emergence of the half-integer quantum Hall effect, with a plateau transition point at $E=0$.

3. Preserved C_0 chirality: Random Abelian and non-Abelian vector potentials

a. Generalities

Consider a type of disorder which preserves the C_0 chirality, $H=-\sigma_3 H\sigma_3$; according to Table V, the corresponding couplings are $\alpha_\perp$, $\beta_\perp$, and $\gamma_\perp$. The one-loop RG equations are then given by

$$d\alpha_\perp/d\ln L=0, \tag{6.82}$$

$$d\beta_\perp/d\ln L=4\beta_\perp\gamma_\perp, \tag{6.83}$$

$$d\gamma_\perp/d\ln L=\beta_\perp^2. \tag{6.84}$$

The specifics of the C_0 chirality is that it corresponds to the more common meaning of the term "chirality," which refers to a distinction between left and right particles. The model then takes the form of the Euclidean version of 1+1 theory of massless Dirac fermions coupled to a gauge field. Indeed, according to Eq. (6.73) the matrices $\sigma_1\tau_3$ and $\sigma_2\tau_3$ play the role of Dirac γ matrices, and the matrix σ_3 determining the C_0 chirality is γ_5. Depending on further symmetries, three different C_0 chiral models arise.

(i) The only coupling present is $\alpha_\perp$, which corresponds to the random Abelian vector potential. In this case the nodes are decoupled, and the Hamiltonian decomposes in two copies of a model of the class AIII. This model has already been mentioned in Sec.VI.G.2.

(ii) If the time-reversal symmetry T_0 is preserved, only the couplings $\beta_\perp$ and $\gamma_\perp$ are allowed, and the problem is in the symmetry class CI. The model describes then fermions coupled to a SU(2) non-Abelian gauge field and is a particular case of analogous SU(N) models.

(iii) All three couplings are present. This describes Dirac fermions coupled to both Abelian U(1) and non-Abelian SU(2) gauge fields. This model is in the AIII symmetry class.

Remarkably, these critical C_0 chiral models are exactly solvable: one can calculate exactly the spectra of multifractal exponents, the critical index of the DOS, and the value of conductivity. They have been much studied and we summarize the key ideas and results.

b. Abelian vector potential

The model of 2D Dirac fermions moving in a random vector potential,

$$H=v_0\sigma_\mu(i\partial_\mu-A_\mu), \tag{6.85}$$

is exactly solvable at zero energy and characterized by a line of fixed points (Ludwig *et al.*, 1994). Decomposing the vector potential into longitudinal (pure gauge) and transverse parts,

$$A_\nu=\epsilon_{\nu\rho}\partial_\rho\phi(\mathbf{r})+\partial_\nu\chi(\mathbf{r}), \tag{6.86}$$

and assuming that the total magnetic flux is zero,[16] one can explicitly write the zero-energy wave functions (Ludwig *et al.*, 1994; Castillo *et al.*, 1997):

$$\Psi_+(\mathbf{r})=\begin{pmatrix}0\\ \psi_+(\mathbf{r})\end{pmatrix},\quad \Psi_-(\mathbf{r})=\begin{pmatrix}\psi_-(\mathbf{r})\\ 0\end{pmatrix}, \tag{6.87}$$

$$\psi_\pm(\mathbf{r})=B_\pm^{-1/2}e^{-i\chi(\mathbf{r})}e^{\pm\phi(\mathbf{r})}, \tag{6.88}$$

where $B_\pm=\int d^2\mathbf{r}e^{\pm 2\phi(\mathbf{r})}$ is the normalization factor. We consider the first of the functions (6.87) for definiteness and analyze the statistical properties of $|\psi_+(\mathbf{r})|^2$. They are governed by fluctuations of $\phi(\mathbf{r})$. Assuming a white-noise distribution of the random vector potential with $\langle A_\mu(\mathbf{r})A_\nu(\mathbf{r}')\rangle=2\pi g_A\delta_{\mu\nu}\delta(\mathbf{r}-\mathbf{r}')$, one gets the following statistics for $\phi(\mathbf{r})$:

$$\mathcal{P}[\phi]\propto\exp\left\{-\frac{1}{4\pi g_A}\int d^2\mathbf{r}(\nabla\phi)^2\right\}. \tag{6.89}$$

Equation (6.89) implies that $\phi(\mathbf{r})$ is a free massless bosonic field characterized by the correlation function

$$\langle\phi(\mathbf{r})\phi(\mathbf{r}')\rangle=g_A\ln(L/|\mathbf{r}-\mathbf{r}'|). \tag{6.90}$$

[16]For a nonzero total flux there will be additional zero modes, in view of the Atiyah-Singer index theorem; see, e.g., Aharonov and Casher (1979).

TABLE VI. Possible types of disorder in graphene leading to criticality. [A further possible mechanism of delocalization is generation of the metallic phase due to broken spin- (or isospin-) rotation invariance, see Sec. VI.A.1. If the only preserved symmetry is T_z, the system is in class AII, while if only CT_0 or CT_z invariance is preserved, the system belongs to class D. (No topological term arises in these situations.) In both classes, the system flows towards a perfect-metal fixed point if the bare conductivity is above the localization threshold.] First column: Preserved symmetries. Second column: Symmetry class. Third column: Type of criticality. The first three rows correspond to C_z chiral symmetry leading to Gade-Wegner-type criticality, see Sec. VI.G.4. The next three rows contain models with C_0 chiral symmetry (random gauge fields), inducing a WZ term in the σ-model action, see Sec. VI.G.3. The last four rows correspond to the case of decoupled valleys (long-range disorder), see Sec. VI.G.2; from top to bottom: random vector potential, scalar potential, mass, and any of their combinations. For these models (except for the random vector potential, which is C_0 chiral at the same time) the σ model acquires a topological term with $\theta=\pi$. Adapted from Ostrovsky *et al.*, 2007.

Symmetries	Class	Criticality	Conductivity
C_z, T_0	BDI	Gade	$\approx 4e^2/\pi h$
C_z	AIII	Gade	$\approx 4e^2/\pi h$
C_z, T_z	CII	Gade	$\approx 4e^2/\pi h$
C_0, T_0	CI	WZW	$4e^2/\pi h$
C_0	AIII	WZW	$4e^2/\pi h$
Λ_z, C_0	$2\times$AIII	WZW	$4e^2/\pi h$
Λ_z, $T_\perp$	$2\times$AII	$\theta=\pi$	$4\sigma_{Sp}^{**}$ or ∞ (?)
Λ_z, $CT_\perp$	$2\times$D	$\theta=\pi$	$4e^2/\pi h$
Λ_z	$2\times$A	$\theta=\pi$	$4\sigma_U^*$

c. Multifractality

To find the multifractal spectrum, one considers the moments $\langle|\psi_+(\mathbf{r})|^{2q}\rangle$, see Sec. II.C.1. For not too strong disorder ($g_A \leq 1$), it turns out to be sufficient to average separately the exponential $e^{2q\phi(\mathbf{r})}$ and each of the q normalization factors $\int d^2\mathbf{r} e^{\pm 2\phi(\mathbf{r})}$. The resulting spectrum (Ludwig *et al.*, 1994)

$$\tau_q = 2(q-1)(1-g_A q) \tag{6.91}$$

has an exactly parabolic form. The corresponding $f(\alpha)$ spectrum is given by Eq. (2.36) with $d=2$, $\gamma=2g_A$:

$$f(\alpha) = 2-(\alpha-2-2g_A)^2/8g_A. \tag{6.92}$$

In view of the exact parabolicity, the spectrum contains a termination point at $\alpha=0$, see Sec. II.C.7. The corresponding value of q is $q_c=(1+g_A)/2g_A$. Thus Eq. (6.91) is only valid for $q\leq q_c$; for larger q the exponent τ_q saturates at a constant value, $\tau_{q\geq q_c}=-f(0)=(1-g_A)^2/2g_A$.

It is worth recalling that we consider the spectrum describing the ensemble-averaged IPRs, $\langle P_q\rangle$, see Sec. II.C.5. If one looks at the scaling of the typical IPR, P_q^{typ}, the information about rare events encoded in the part of the spectrum with $f(\alpha)<0$ gets lost, and only the range $\alpha_+<\alpha<\alpha_-$ is probed, where $\alpha_\pm=2(g_A^{1/2}\mp 1)^2$. The corresponding τ_q^{typ} spectrum reproduces τ_q in the range $q_-<q<q_+$, where $q_\pm=g_A^{-1/2}$, and becomes linear outside this range, see Eq. (2.41). This behavior was found for the random vector potential problem by Chamon *et al.* (1996); Castillo *et al.* (1997); Carpentier and LeDoussal (2001) where the spectrum τ_q^{typ} was studied (there the notation q_c is used for our q_+).

d. Freezing

As was found by Chamon *et al.* (1996); Castillo *et al.* (1997); Carpentier and LeDoussal (2001), with increasing disorder the system undergoes a phase transition (freezing) at $g_A=1$. In the strong disorder phase, $g_A>1$, the spectrum takes the form

$$\tau(q) = -2(1-g_A^{1/2}q)^2, \quad q<q_c=g_A^{-1/2}; \tag{6.93}$$

$$f(\alpha) = \alpha(8g_A^{1/2}-\alpha)/8g_A. \tag{6.94}$$

In this phase $f(0)=0$, which implies that there is a probability of order unity to find a point in the sample where the wave function is of order unity. Correspondingly, the saturation value of τ_q for $q>q_c$ is $\tau_{q>q_c}=0$. At first sight, this may seem to imply that the wave functions are localized. The situation is, however, not so simple: a nontrivial multifractal spectrum shows a complex wave-function structure. Further, it can be shown that the probability to find a secondary spike in the wave function of approximately the same magnitude as the main one and separated by a distance comparable to the system size L is of order unity (Carpentier and LeDoussal, 2001; Fukui, 2003). The nature of these "quasilocalized" wave functions is therefore similar to that of critical states in 1D systems of chiral symmetry, see Sec. V.E.

e. Density of states

The scaling of the DOS is governed by the dynamical exponent z via

$$\rho(E) \propto E^{(2-z)/z}. \tag{6.95}$$

In the weak-disorder phase ($g_A<1$) the value of z is $z=1+2g_A$ (Ludwig *et al.*, 1994; Nersesyan *et al.*, 1995; Altland *et al.*, 2002). However, as discussed in Sec. VI.F.2, freezing has also impact on the dynamical exponent; in the strong-disorder phase z is given by the second line of Eq. (6.70).

f. Non-Abelian random gauge field

The problem remains exactly solvable in the case of a SU(N) non-Abelian gauge field. However, in contrast to the Abelian case, where one finds a line of fixed points, the theory flows now into an isolated fixed point, which is a WZW theory on the level $k=-2N$ (Nersesyan *et al.*, 1995; Mudry *et al.*, 1996; Caux, 1998; Caux *et al.*, 1998). The spectrum of multifractality is parabolic with $\gamma=(N-1)/N^2$ and is given by Eqs. (6.91) and (6.92) with $2g_A$ replaced by $(N-1)/N^2$. The DOS is given by Eq. (6.95) with a dynamical exponent $z=2-1/N^2$. In the case N

$=2$ that arises in the two-node model one thus finds $z=7/4$, yielding the DOS scaling $\rho(E)\propto E^{1/7}$.

When both Abelian and non-Abelian random gauge fields are present, they contribute additively to the exponents (in the nonfrozen regime), as the two sectors of the theory decouple. This yields (Mudry *et al.*, 1996) the multifractal scaling (6.91) and (6.92) with $\gamma=2g_A\to 2g_A+(N-1)/N^2$ and the DOS scaling (6.95) with $z=1+2g_A+(N^2-1)/N^2$.

g. Conductivity

A further remarkable feature of the models with C_0 chiral randomness is the independence of conductivity on the disorder strength. We sketch the proof of this statement given by Ostrovsky *et al.* (2006). The conductivity is given by the Kubo formula

$$\sigma=-\frac{1}{2\pi\hbar}\mathrm{Tr}[j^x(G^R-G^A)j^x(G^R-G^A)], \tag{6.96}$$

where Tr includes both the matrix trace and the spatial integration. The chiral symmetry implies the identity

$$\sigma_3 G^{R(A)}(E)\sigma_3=-G^{A(R)}(-E), \tag{6.97}$$

allowing one to present the conductivity at zero energy in terms of retarded Green's functions. Further, in view of the Dirac character of the spectrum, the components of the current operator are related via

$$\sigma_3 j^x=-j^x\sigma_3=ij^y. \tag{6.98}$$

By making use of Eqs. (6.97) and (6.98) the Kubo formula can be cast in the following form:

$$\sigma(E=0)=-\frac{1}{\pi\hbar}\sum_{\alpha=x,y}\mathrm{Tr}[j^\alpha G^R j^\alpha G^R]. \tag{6.99}$$

At first glance, this expression may be thought to be zero due to gauge invariance. Indeed, the right-hand side of Eq. (6.99) is proportional to the second derivative of the partition function $Z[\mathbf{A}]=\mathrm{Tr}\log G^R[\mathbf{A}]$ (or, equivalently, first derivative of the current $\mathrm{Tr}\, j^\alpha G^R[\mathbf{A}]$) with respect to the constant vector potential $\mathbf{A}$. Since a constant vector potential does not affect gauge-invariant quantities, the derivative is zero. This argument is, however, not fully correct, in view of a quantum anomaly. The elimination of $\mathbf{A}$ amounts technically to a shift in the momentum space $\mathbf{k}\to\mathbf{k}-e\mathbf{A}$, which naively does not change the momentum integral. If we consider a formal expansion in the disorder strength, this argument will indeed hold for all terms involving disorder but not for the zero-order contribution. The momentum integral $\int d^2k\,\mathrm{Tr}\, j^\alpha G_0^R(\mathbf{k})$ is ultraviolet divergent and the shift of variable is illegitimate. This anomaly was first identified by Schwinger (1962) for (1+1)-dimensional massless Dirac fermions. In the Schwinger model, the polarization operator is not affected by an arbitrary external vector potential $\mathbf{A}(x,t)$ and is given by the anomalous contribution, yielding a photon mass in the 1+1 electrodynamics (Schwinger, 1962; Peskin and Schroeder, 1995). In the present context, the role of $\mathbf{A}(x,t)$ is played by the chiral disorder. Explicit calculation of the disorder-free diagram yields (including a factor of 2 accounting for spin)

$$\sigma=-\frac{8e^2v_0^2}{\pi\hbar}\int\frac{d^2k}{(2\pi)^2}\frac{\delta^2}{(v_0^2k^2+\delta^2)^2}=\frac{4e^2}{\pi h}. \tag{6.100}$$

Therefore the dimensionless conductivity acquires the universal value $4/\pi$, with no corrections at any order in the disorder strength. This result was obtained earlier by Ludwig *et al.* (1994) for the Abelian case and Tsvelik (1995) for a certain model of non-Abelian gauge field.

4. Disorders preserving C_z chirality: Gade-Wegner criticality

We now turn to disorder which preserves the C_z chirality, $H=-\sigma_3\tau_3 H\sigma_3\tau_3$; according to Table V, the corresponding coupling constants are β_0, $\alpha_\perp$, $\gamma_\perp$, and β_z. If no time-reversal symmetries are preserved, the system belongs to the chiral unitary (AIII) class. The combination of C_z chirality and time-reversal invariance T_0 (only couplings $\gamma_\perp$ and β_z are present) corresponds to the chiral orthogonal symmetry class BDI; this model was discussed in Sec. VI.F.2. Finally, the combination of C_z chirality and T_z symmetry (couplings $\gamma_\perp$ and β_0) falls into the chiral symplectic symmetry class CII. The RG flow and DOS in these models have been analyzed by Guruswamy *et al.* (2000) using notations $g_A=\gamma_\perp/2$, $g_m=\beta_z/2$, $g_\mu=\beta_0/2$, and $g_{A'}=\alpha_\perp/2$. In all cases, the resulting theory is of the Gade-Wegner type, see Sec. VI.F.

In contrast to random gauge field models (C_0 chirality), the proof of the universality of the conductivity based on gauge-invariance argument does not apply to models with C_z chirality. Nevertheless, the zero-energy conductivity is found to have the same universal value, $\sigma=4e^2/\pi h$, in the limit of weak disorder (Ostrovsky *et al.*, 2006; Ryu, Mudry, Furusaki, and Ludwig, 2007). In this case, however, there are corrections to this value perturbative in the disorder strength. In particular, the leading correction is found in the second order (Ostrovsky *et al.*, 2006), $\delta\sigma^{(2)}=(e^2/\pi h)(\beta_0-\beta_z)^2$.

The following comment (applicable to both C_0 and C_z chiral models) on infrared regularization of the problem is in order here. This role is played in Eq. (6.100) by δ, which is an infinitesimal imaginary part in the denominator of the Green's function. Physically, it has a meaning of the inverse electron lifetime or, alternatively, a dephasing rate, and can be thought of as modeling processes of escape of electrons in some reservoir or some dephasing mechanism. As discussed by Ostrovsky *et al.* (2006), for a different type of the infrared regularizations (i.e., by finite frequency) the critical conductivity will take a different value, while still of order e^2/h.

5. Dirac Hamiltonians for dirty *d*-wave superconductors

We discuss the application of Dirac fermion theory to disordered *d*-wave spin-singlet superconductors with $d_{x^2-y^2}$ symmetry. In such systems the superconducting gap vanishes at four points in the Brillouin zone, and the

TABLE VII. Criticality and DOS in d-wave superconductors with preserved spin-rotation invariance and different types of randomness. First column: Number of nodes coupled. Second column: Presence or absence of time-reversal invariance. Third column: Symmetry class. Fourth column: Type of criticality. Fifth column: Low-energy scaling of DOS.

Nodes coupled	T	Class	Criticality	DOS
1	+	AIII	WZW	$\|E\|^{(1-2g_A)/(1+2g_A)}$
2	+	CI	WZW	$\|E\|^{1/7}$
4	+	CI		$\|E\|$
1	−	A	θ term	Noncritical
2	−	C	θ term	$\|E\|^{1/7}$
4	−	C		E^2

dispersion relation near these points is of the Dirac type. One is thus led to analyze the low-energy physics of the problem in terms of a four-flavor Dirac Hamiltonian. Investigation of symmetries of this problem in the presence of different types of impurities and the corresponding RG treatment were pioneered by Nersesyan *et al.* (1995); for a recent analysis, see Altland *et al.* (2002). The main physical quantity of interest for this problem is the low-energy behavior of DOS.

Following Nersesyan *et al.* (1995) and Altland *et al.* (2002) we focus on potential disorder, assume that the spin-rotation invariance is preserved, but allow for a possibility of time-reversal symmetry breaking (e.g., by magnetic field in vortices in type-II superconductors). In analogy with the two-flavor model (Sec. VI.G.1) it is crucial whether the disorder couples the nodes or not. Depending on the range of disorder and the interval of energies considered, one can distinguish three different situations: (i) short-range disorder: all four nodes are coupled; (ii) long-range disorder: internode scattering is negligible, and nodes are decoupled; the problem then acquires single-node character; and (iii) each node is coupled to the opposite one but not to the other two. The system then decomposes into two parts—each of them describing a pair of the oppositely located nodes. Nersesyan *et al.* (1995) showed that, in view of strong anisotropy of nodal Dirac Hamiltonians, there is an intermediate energy range where this model becomes physically justified.

Combining these three types of disorder with possibilities of preserved or broken time-reversal invariance, one gets six distinct models. Their symmetries, emerging types of criticality, and the corresponding behavior of DOS are summarized in Table VII. When all four nodes are coupled, the system is in the conventional localized regime of symmetry classes CI and C describing spin-singlet superconductors (Senthil and Fisher, 1999; Senthil *et al.*, 1998). When only opposite nodes are coupled, the T-invariant problem becomes a model of non-Abelian random gauge field, and the theory acquires the WZ term, leading to the $E^{1/7}$ scaling of the DOS, see Sec. VI.G.3. For broken T invariance, the two-node problem is described by the class C σ model with the $\theta=\pi$ topological term, i.e., it is in the SQH transition universality class, see Sec. VI.D. The DOS scales as $E^{1/7}$ in this case as well. Finally, if the nodes are completely decoupled, the Hamiltonian for each of them takes the form analyzed in Sec. VI.G.2. More specifically, when T invariance is preserved, the problem reduces to the class AIII model of random Abelian vector potential (Sec. VI.G.3) with the DOS following the nonuniversal power law (6.95), $\rho(E)\sim|E|^{(1-2g_A)/(1+2g_A)}$. In case of broken T invariance, the problem belongs to class A and is described by the Pruisken σ model with a topological term, i.e., it is in the universality class of the IQH critical point. In the latter situation, the DOS is uncritical.

We also mention two additional types of disorder that have been studied in detail. In the case of magnetic impurities both T-invariance and spin rotation symmetry are broken and thus the system belongs to class D (Bocquet *et al.*, 2000; Senthil and Fisher, 2000), see Sec. VI.E. For the case of perfect nesting, where the chemical potential $\mu=0$, and very strong potential scatterers one encounters the symmetry class AIII leading to the Gade phase (Altland, 2002).

VII. CONCLUDING REMARKS

This concludes our review of the physics of Anderson transitions between localized and metallic phases in disordered electronic systems and of associated critical phenomena. Recently a detailed understanding of these transitions has emerged, including such salient features as symmetry and topology classification, mechanisms of criticality in quasi-1D and 2D systems, and wave-function multifractality. We have given a systematic exposition of these issues and hope that this will help interested researchers to navigate in this rich field.

For several reasons, including limits in space, time, and—last but not least—our expertise, we were not able to discuss all aspects of the problem. The selection of presented material certainly reflects our perspective of the field. We apologize to all researchers whose work is not sufficiently discussed. Probably, the most important issue largely left out is electron-electron interactions. (This was only briefly discussed in Sec. VI.C in the context of the IQH transition.) This by itself is a rich and complicated problem; we restrict ourselves to just a few remarks and references.

A. Interaction effects

Physically, the impact of interaction effects onto low-temperature transport and localization in disordered electronic systems can be subdivided into two distinct effects: (i) renormalization and (ii) dephasing.

1. Renormalization

The renormalization effects, which are governed by virtual processes, become increasingly more pronounced with lowering temperature. The importance of such effects in diffusive low-dimensional systems was demon-

strated by Altshuler and Aronov (1984). To resum the arising singular contributions, Finkelstein (1990) developed the RG approach based on the σ model for an interacting system. This made possible an analysis of the critical behavior at the localization transition in $2+\epsilon$ dimensions in the situations when spin-rotation invariance is broken (by spin-orbit scattering, magnetic field, or magnetic impurities). However, in the case of preserved spin-rotation symmetry it was found that the strength of the interaction in the spin-triplet channel scales to infinity at certain RG scale. This was interpreted as magnetic instability of the system; for a detailed exposion of proposed scenarios see Belitz and Kirkpatrick (1994).

Recently, the problem has attracted much attention in connection with experiments on high-mobility low-density 2D electron structures (Si MOSFETs) giving evidence in favor of a metal-insulator transition (Abrahams *et al.*, 2001). Whether these results are due to a true metallic phase existing in these systems or, else, are explained by interaction effects at intermediate ("ballistic") temperatures remains a debated issue. In a recent work (Punnoose and Finkel'stein, 2005) the RG for the σ model of interacting 2D electrons with a number of valleys $N>1$ was analyzed on the two-loop level. It was shown that in the limit of a large number of valleys N (in practice, $N=2$ as in Si is already sufficient) the temperature of magnetic instability is suppressed to unrealistically low values, and a metal-insulator transition emerges.

The interaction-induced renormalization effects become extremely important for correlated 1D systems (Luttinger liquids). While 1D systems provide a paradigmatic example of strong Anderson localization, a sufficiently strong attractive interaction can lead to delocalization in such systems. An RG treatment of the corresponding localization transition in a disordered interacting 1D systems was developed by Giamarchi and Schulz (1988); see also Giamarchi (2004).

2. Dephasing

We turn now to effects of dephasing governed by inelastic processes of electron-electron scattering at finite temperature T. Dephasing has been much studied for metallic systems where it provides a cutoff for weak localization effects (Altshuler and Aronov, 1984). As to the Anderson transitions, they are quantum (zero-T) phase transitions, and dephasing contributes to their smearing at finite T. This was discussed in Sec. VI.C.10 in the context of dynamical scaling at the IQH transition. There is, however, an interesting situation when dephasing processes can create a localization transition. We mean the systems where all states are localized in the absence of interaction, such as wires or 2D systems. At high temperatures, when dephasing is strong so that the dephasing rate $\tau_\phi^{-1}(T)$ is larger than the mean level spacing in the localization volume, the system is a good metal and its conductivity is given by the quasiclassical Drude conductivity with a relatively small weak localization correction (Altshuler and Aronov, 1984). With lowering temperature dephasing gets progressively less efficient, the localization effects proliferate, and eventually the system becomes an Anderson insulator. What is the nature of this state? A natural question to ask is whether the interaction of an electron with other electrons will be sufficient to provide a thermal bath that would assist the variable-range hopping transport (Fleishman *et al.*, 1978), as occurs in the presence of a phonon bath. The answer to this question was given by Fleishman and Anderson (1980), and it is negative. Fleishman and Anderson found that at low T the interaction of a "short-range class" (which includes a finite-range interaction in any dimensionality d and Coulomb interaction in $d<3$) is not sufficient to delocalize otherwise localized electrons, so that the conductivity remains strictly zero. In combination with the Drude conductivity at high T this implies the existence of a transition at some temperature T_c.

This conclusion was recently corroborated by an analysis (Gornyi *et al.*, 2005; Basko *et al.*, 2006) in the framework of the idea of Anderson localization in Fock space (Altshuler *et al.*, 1997). In these works the temperature dependence of conductivity $\sigma(T)$ in systems with localized states and weak electron-electron interaction was studied. It was found that with decreasing T the system first shows a crossover from the weak-localization regime into that of "power-law hopping" over localized states (where σ is a power-law function of T), and then undergoes a localization transition. The transition is obtained within both a self-consistent Born approximation (Basko *et al.*, 2006) and an approximate mapping onto a model on the Bethe lattice (Gornyi *et al.*, 2005). The latter also yields critical behavior for $\sigma(T)$ above T_c, which has a non-power-law form $\ln \sigma(T) \sim (T-T_c)^{-1/2}$ characteristic for the Bethe lattice, see Sec. II.D. Up to now, this transition has not been observed in experiments,[17] which indicates instead a smooth crossover from the metallic to the insulating phase with lowering T (Hsu and Valles, 1995; Van Keuls *et al.*, 1997; Khavin *et al.*, 1998; Minkov *et al.*, 2007). The reason for this discrepancy remains unclear. A recent attempt to detect the transition in numerical simulations also did not give clear confirmation of the theory (Oganesyan and Huse, 2007), possibly because of strong restrictions on the size of an interacting system that can be numerically diagonalized.

B. Experimental studies of localization transitions

Of all localization transitions, the best studied experimentally is the IQH transition. We have discussed the corresponding experimental findings in Sec. VI.C.10. Its superconducting counterparts (SQH and TQH transi-

[17]Of course, in a real system phonons are always present and provide a bath necessary to support the hopping conductivity at low T, so that there is no true transition. However, when the coupling to phonons is weak, this hopping conductivity will have a small prefactor, yielding a "quasitransition."

tions) have not been observed yet, although several physical realizations were proposed, see Secs. VI.D.1 and VI.E.1. Much effort has been invested in research on strongly interacting disordered 2D systems in zero magnetic field but it remains controversial whether what is observed there is a true metal-insulator transition, see Sec. VII.A.

Below we review the experimental observation of the Anderson transition in 3D electronic and optical systems. For electronic systems (doped semiconductors, see Sec. VII.B.1) the localization transition has been observed unambiguously. However, a theoretical analysis is complicated by the presence of the Coulomb interaction, which modifies the critical behavior. As a result, one cannot expect that the experimentally extracted critical exponents agree with numerical values obtained from computer simulations on noninteracting systems. Localization of light (Sec. VII.B.2) has an advantage in this respect, since the photon-photon interaction is negligibly small. However, it turns out that implementation of sufficiently strong disorder so as to reach the Anderson transition and strong localization of light in 3D is a complicated endeavor. The second major difficulty is posed by the absorption.

1. Anderson transition in doped semiconductors

The 3D localization transition was studied on doped semiconductor systems, such as Si:P, Si:B, Si:As, and Ge:Sb. In most work, samples with a substantial degree of compensation [i.e., acceptors in addition to donors, e.g., Si:(P,B)] were used, which allows one to vary the amount of disorder and the electron concentration independently. Of these samples, values of the conductivity exponent s in the vicinity of $s \approx 1$ were reported (Thomas *et al.*, 1982; Zabrodskii and Zinovéva, 1984; Field and Rosenbaum, 1985; Hirsch *et al.*, 1988) with scattering of values and the uncertainties of the order of 10%. A similar result was obtained for an amorphous material Nb_xSi_{1-x}. [Recall that s is expected to be equal in 3D to the localization length exponent ν according to the scaling relation $s=\nu(d-2)$.]

On the other hand, the early study of the transition in undoped Si:P (Paalanen *et al.*, 1982; Rosenbaum *et al.*, 1983; Thomas *et al.*, 1983) gave an essentially different result, $s \approx 0.5$. A resolution of this discrepancy was proposed by Stupp *et al.* (1993, 1994) who found that the actual critical region in an uncompensated Si:P is rather narrow and that the scaling analysis restricted to this range yields $s \approx 1.3$. A more recent study (Waffenschmidt *et al.*, 1999), which employed uniaxial stress to tune through the transition [as used by Paalanen *et al.* (1982); Rosenbaum *et al.* (1983); Thomas *et al.* (1983)], has essentially confirmed these conclusions, yielding $s = 1.0 \pm 0.1$, in agreement with the values obtained for samples with compensation. Further, in this work dynamical scaling near the transition with varying temperature was demonstrated; the corresponding dynamical exponent was $z = 2.94 \pm 0.3$. Good scaling was also observed in a similar experiment on uncompensated Si:B (Bogdanovich, 1999), however, with somewhat different critical exponents ($s \approx 1.6$, $z \approx 2$). A possible explanation for the discrepancy is that the temperatures reached in this work were not sufficiently low. Another possibility is that Si:B belongs to a different universality class, in view of stronger spin-orbit scattering.

The fact that the most common experimental value $s \approx 1$ found differs from what one would expect based on numerical studies for noninteracting systems is not surprising, since the Coulomb interaction affects the critical exponents. For a discussion of the experimental data and their comparison with theoretical expectations for the Anderson transitions in the presence of Coulomb interaction see Belitz and Kirkpatrick (1994).

2. Anderson localization of light

Experimental efforts to observe the Anderson localization with light turned out to be challenging. The main difficulty is that the characteristic signature of wave localization, the exponential decrease $e^{-\xi/L}$ of the transmission with the system size L, is often hard to disentangle from another exponential $e^{-\ell_a/L}$ originating from photon absorption.

Garcia and Genack (1991); Genack and Garcia (1991) studied the transmission of microwave radiation through a random mixture of aluminum and Teflon spheres inside a copper tube. In the vicinity of the localization transition, they reported power-law scaling of the effective diffusion constant $D(L) \sim L^{-1}$. The presence of strong absorption in the microwave system makes it complicated to interpret the data that were reported as evidence for the localization of light.

To diminish photon losses, Wiersma *et al.* (1997) used a powder from μm GaAs crystals employing near infrared radiation. However, still the exponential signal of localization reported in this work is not undisputed, again due to the presence of residual absorption (Scheffold *et al.*, 1999). A similar study in silicon powders did not show any hint of localization (Rivas *et al.*, 1999).

In order to overcome the problem of separating localization from absorption, a proposal has been made by Chabanov *et al.* (2000). Localization is accompanied by large mesoscopic fluctuations in the spectral function which also carry over to the frequency-dependent transmission function $T(\omega)$. Hence the measurement of the statistical properties of $T(\omega)$, e.g., its variance, could provide a sensitive means to uncover quantum interference effects. Using this method they were able to confirm localization in quasi-one-dimensional waveguides; an application to a three-dimensional system, a mixture of aluminum spheres, did not show signatures of strong localization.

To summarize, up to now a convincing demonstration for the Anderson localization and transition in 3D systems appears to be absent. However, Störzer *et al.* (2006) reported the observation of an anomalous time dependency of the light diffusion in a TiO_2 powder indicating the vicinity of the Anderson critical point. Another promising research direction has appeared with the ad-

vent of photonic crystals (Busch *et al.*, 2007), where in the presence of disorder a localization transition should take place for states near a photonic band edge (John, 1984, 1987; Busch and John, 1999).

Note added in proof. Recently, several important developments occurred.

(i) Ultra-high-precision numerical simulations of multifractality at the IQH transition (Evers *et al.*, 2008; Obuse, Subramaniam, *et al.*, 2008) have shown that the multifractality spectrum is not exactly parabolic (even though deviations are small, Sec. VI.C.7). Furthermore, boundary multifractality was found to show much more pronounced nonparabolicity. These results rule out WZW-type theories of the IQH critical point that predict parabolic multifractality, Sec. VI.C.3.

(ii) Obuse, Furusaki, *et al.* (2008) studied boundary multifractality (Sec. II.C.8) in 2D systems of symplectic symmetry (Sec. VI.B), at transitions from metallic phase to normal insulator and to SQH insulator (Secs. V.D and VI.B.5). It was found that boundary multifractality in these two cases is distinctly different, while bulk properties are the same. Thus, boundary multifractality may distinguish transitions which are in the same bulk universality class but have different topological characteristics.

(iii) Recent experiment on HgTe/(Hg,Cd)Te quantum wells (Koenig *et al.*, 2007) showed formation of a 2D QSH insulator characterized by two counterpropagating edge states (Sec. V.D). Further, Hsieh *et al.* (2008) found evidence of an analogous 3D topological insulator in a system with strong spin-orbit interaction (BiSb crystal). The boundary of this system is believed to be a "topological metal" characterized by a symplectic-class 2D σ model with topological term, see Sec. VI.B.5. Complete classification of 3D topological insulators was developed by Schnyder *et al.* (2008).

(iv) Recent experiments on Bose-Einstein condensates of ultracold atomic gases (Billy *et al.*, 2008; Roati *et al.*, 2008) showed Anderson localization in 1D geometry. These systems, allowing for a control of disorder and interaction strength, open a new perspective for experimental exploration of localization and, in particular, of Anderson transitions (Sec. VII.B).

ACKNOWLEDGMENTS

We express our gratitude to J. Chalker, Y. Fyodorov, I. Gornyi, I. Gruzberg, A. Ludwig, R. Narayanan, P. Ostrovsky, D. Polyakov, A. Subramaniam, and, especially, A. Mildenberger for enjoyable collaborations over many years on the topics included in this review. We are grateful to Y. Fyodorov, I. Gornyi, I. Gruzberg, A. Mildenberger, A. Subramaniam, and P. Wölfle for reading the manuscript and many valuable comments. In addition, this review has benefited from discussions with I. Burmistrov, K. Busch, and A. Finkelstein. Finally, we thank many of our colleagues, especially A. Altland, D. Belitz, M. Feigelman, M. Janßen, V. Kagalovsky, R. Klesse, V. Kravtsov, C. Mudry, L. Schweitzer, A. Tsvelik, P. Wölfle, and M. Zirnbauer, for numerous illuminating discussions over the past years. This work has received support from the Center for Functional Nanostructures of the Deutsche Forschungsgemeinschaft.

REFERENCES

Abou-Chacra, R., P. W. Anderson, and D. J. Thouless, 1973, J. Phys. C **6**, 1734.
Abou-Chacra, R., and D. J. Thouless, 1974, J. Phys. C **7**, 65.
Abrahams, E., P. W. Anderson, D. C. Licciardello, and T. V. Ramakrishnan, 1979, Phys. Rev. Lett. **42**, 673.
Abrahams, E., S. V. Kravchenko, and M. P. Sarachik, 2001, Rev. Mod. Phys. **73**, 251.
Aharonov, Y., and A. Casher, 1979, Phys. Rev. A **19**, 2461.
Aleiner, I. L., and K. B. Efetov, 2006, Phys. Rev. Lett. **97**, 236801.
Altland, A., 2002, Phys. Rev. B **65**, 104525.
Altland, A., 2007, Phys. Rev. Lett. **97**, 236802.
Altland, A., and B. D. Simons, 1999, Nucl. Phys. B **562**, 445.
Altland, A., and B. Simons, 2006, *Condensed Matter Field Theory* (Cambridge University Press, Cambridge, England).
Altland, A., B. D. Simons, and M. R. Zirnbauer, 2002, Phys. Rep. **359**, 283.
Altland, A., and M. R. Zirnbauer, 1997, Phys. Rev. B **55**, 1142.
Altshuler, B. L., and A. G. Aronov, 1984, in *Electron-Electron Interaction in Disordered Systems*, edited by M. Pollak and A. Efros (North-Holland, Amsterdam), p. 1.
Altshuler, B. L., Y. Gefen, A. Kamenev, and L. S. Levitov, 1997, Phys. Rev. Lett. **78**, 2803.
Altshuler, B. L., V. E. Kravtsov, and I. V. Lerner, 1986, Sov. Phys. JETP **64**, 1352.
Altshuler, B. L., I. K. Zharakeshev, S. A. Kotochigova, and B. I. Shklovskii, 1988, Sov. Phys. JETP **67**, 625.
Anderson, P. W., 1958, Phys. Rev. **109**, 1492.
Ando, T., 1989, Phys. Rev. B **40**, 5325.
Ando, T., and H. Suzuura, 2002, J. Phys. Soc. Jpn. **71**, 2753.
Asada, Y., K. Slevin, and T. Ohtsuki, 2002, Phys. Rev. Lett. **89**, 256601.
Asada, Y., K. Slevin, and T. Ohtsuki, 2004, Phys. Rev. B **70**, 035115.
Balatsky, A. V., 1998, Phys. Rev. Lett. **80**, 1972.
Balents, L., and M. P. A. Fisher, 1997, Phys. Rev. B **56**, 12970.
Baranov, M. A., I. S. Burmistrov, and A. M. M. Pruisken, 2002, Phys. Rev. B **66**, 075317.
Bardarson, J. H., J. Tworzydlo, P. W. Brouwer, and C. W. J. Beenakker, 2007, Phys. Rev. Lett. **99**, 106801.
Basko, D. M., I. L. Aleiner, and B. L. Altshuler, 2006, Ann. Phys. (N.Y.) **321**, 1126.
Beamond, E. J., J. Cardy, and J. T. Chalker, 2002, Phys. Rev. B **65**, 214301.
Beenakker, C. W. J., 1997, Rev. Mod. Phys. **69**, 731.
Belitz, D., and T. Kirkpatrick, 1994, Rev. Mod. Phys. **66**, 261.
Berezinsky, V. L., 1974, Sov. Phys. JETP **38**, 620.
Bernard, D., and A. LeClair, 2001, Phys. Rev. B **64**, 045306.
Bernard, D., and A. LeClair, 2002a, J. Phys. A **35**, 2555.
Bernard, D., and A. LeClair, 2002b, Nucl. Phys. B **628**, 442.
Bernevig, B. A., T. L. Hughes, and S.-C. Zhang, 2006, Science

314, 1757.
Bhaseen, M. J., I. I. Kogan, O. A. Soloviev, N. Taniguchi, and A. M. Tsvelik, 2000, Nucl. Phys. B **580**, 688.
Billy, J., V. Josse, Z. Zuo, A. Bernard, B. Hambrecht, P. Lugan, D. Clément, L. Sanchez-Palencia, P. Bouyer, and A. Aspect, 2008, Nature (London) **453**, 891.
Bocquet, M., and J. T. Chalker, 2003, Phys. Rev. B **67**, 054204.
Bocquet, M., D. Serban, and M. R. Zirnbauer, 2000, Nucl. Phys. B **578**, 628.
Bogdanovich, S., M. P. Sarachik, and R. N. Bhatt, 1999, Phys. Rev. Lett. **82**, 137.
Bouchaud, J. P., and A. Georges, 1990, Phys. Rep. **195**, 127.
Brezin, E., and S. Hikami, 1997, Phys. Rev. B **55**, R10169.
Brouwer, P. W., and K. Frahm, 1996, Phys. Rev. B **53**, 1490.
Brouwer, P. W., A. Furusaki, I. A. Gruzberg, and C. Mudry, 2000, Phys. Rev. Lett. **85**, 1064.
Brouwer, P. W., A. Furusaki, and C. Mudry, 2003, Phys. Rev. B **67**, 014530.
Brouwer, P. W., C. Mudry, and A. Furusaki, 2000, Nucl. Phys. B **565**, 653.
Brouwer, P. W., C. Mudry, B. D. Simons, and A. Altland, 1998, Phys. Rev. Lett. **81**, 862.
Bundschuh, R., C. Cassanello, D. Serban, and M. R. Zirnbauer, 1998, Nucl. Phys. B **532**, 689.
Burmistrov, I., 2006, Ph.D. thesis (University of Amsterdam), http://dare.uva.nl/document/23446.
Busch, K., and S. John, 1999, Phys. Rev. Lett. **83**, 967.
Busch, K., G. von Freymann, S. Linden, S. F. Mingaleev, L. Tkeshelashvili, and M. Wegener, 2007, Phys. Rep. **444**, 101.
Cardy, J., 2000, Phys. Rev. Lett. **84**, 3507.
Carpentier, D., and P. LeDoussal, 1999, Nucl. Phys. B **588**, 565.
Carpentier, D., and P. LeDoussal, 2001, Phys. Rev. E **63**, 026110.
Caselle, M., 1996, e-print arXiv:cond-mat/9610017v2.
Caselle, M., and U. Magnea, 2004, Phys. Rep. **394**, 41.
Caselle, M., and U. Magnea, 2006, J. Stat. Mech.: Theory Exp. **0601**, P013.
Castellani, C., and L. Peliti, 1986, J. Phys. A **19**, L429.
Castilla, G. E., and S. Chakravarty, 1993, Phys. Rev. Lett. **71**, 384.
Castillo, H. E., C. de C. Chamon, E. Fradkin, P. M. Goldbart, and C. Mudry, 1997, Phys. Rev. B **56**, 10668.
Caux, J.-S., 1998, Phys. Rev. Lett. **81**, 4196.
Caux, J.-S., N. Taniguchi, and A. M. Tsvelik, 1998, Nucl. Phys. B **525**, 621.
Chabanov, A. A., M. Stoytchev, and A. Z. Genack, 2000, Nature (London) **404**, 850.
Chalker, J. T., 1990, Physica A **167**, 253.
Chalker, J. T., and P. D. Coddington, 1988, J. Phys. C **21**, 2665.
Chalker, J. T., N. Read, V. Kagalovsky, B. Horovitz, Y. Avishai, and A. W. W. Ludwig, 2002, Phys. Rev. B **65**, 012506.
Chalker, J. T., and S. Siak, 1990, J. Phys.: Condens. Matter **2**, 2671.
Chamon, C. d. C., C. Mudry, and X.-G. Wen, 1996, Phys. Rev. Lett. **77**, 4194.
Chayes, J. T., L. Chayes, D. S. Fisher, and T. Spencer, 1986, Phys. Rev. Lett. **57**, 2999.
Cho, S., and M. P. A. Fisher, 1997a, Phys. Rev. B **55**, 1025.
Cho, S., and M. P. A. Fisher, 1997b, Phys. Rev. B **55**, 1637.
Cuevas, E., 2003a, Phys. Rev. B **68**, 024206.
Cuevas, E., 2003b, Phys. Rev. B **68**, 184206.
Cuevas, E., 2005, Phys. Rev. B **71**, 024205.
Cuevas, E., M. Ortuno, V. Gasparian, and A. Perez-Garrido, 2002, Phys. Rev. Lett. **88**, 016401.
Cui, Q., X. Wan, and K. Yang, 2004, Phys. Rev. B **70**, 094506.
Dell'Anna, L., 2006, Nucl. Phys. B **750**, 213.
Derkachov, S. E., and A. N. Manashov, 1997, Phys. Rev. Lett. **79**, 1423.
de Visser, A., L. A. Ponomarenko, G. Galistu, D. T. N. de Lang, A. M. M. Pruisken, U. Zeitler, and D. Maude, 2006, J. Phys.: Conf. Ser. **51**, 379.
Dorokhov, O. N., 1982, JETP Lett. **36**, 318.
Dotsenko, V. S., and V. S. Dotsenko, 1983, Adv. Phys. **32**, 129.
Duplantier, B., and A. W. W. Ludwig, 1991, Phys. Rev. Lett. **66**, 247.
Dyson, F., 1953, Phys. Rev. **92**, 1331.
Dyson, F. J., 1962, J. Math. Phys. **3**, 140.
Efetov, K. B., 1983, Adv. Phys. **32**, 53.
Efetov, K. B., 1985, Sov. Phys. JETP **61**, 606.
Efetov, K. B., 1987, Sov. Phys. JETP **65**, 360.
Efetov, K. B., 1990, Physica A **167**, 119.
Efetov, K. B., 1997, *Supersymmetry in Disorder and Chaos* (Cambridge University Press, Cambridge, England).
Efetov, K. B., and A. I. Larkin, 1983, Sov. Phys. JETP **58**, 444.
Efetov, K. B., A. I. Larkin, and D. E. Khmeniskii, 1980, Sov. Phys. JETP **52**, 568.
Eggarter, T. P., and R. Riedinger, 1978, Phys. Rev. B **18**, 569.
Engel, L. W., D. Shahar, C. Kurdak, and D. C. Tsui, 1993, Phys. Rev. Lett. **71**, 2638.
Essin, A. M., and J. E. Moore, 2007, Phys. Rev. B **76**, 165307.
Evangelou, S. N., 1995, Phys. Rev. Lett. **75**, 2550.
Evangelou, S. N., and T. Ziman, 1987, J. Phys. C **20**, L235.
Evers, F., 1997, Phys. Rev. E **55**, 2321.
Evers, F., and W. Brenig, 1994, Z. Phys. B: Condens. Matter **94**, 155.
Evers, F., and W. Brenig, 1998, Phys. Rev. B **57**, 1805.
Evers, F., A. Mildenberger, and A. D. Mirlin, 2001, Phys. Rev. B **64**, 241303(R).
Evers, F., A. Mildenberger, and A. D. Mirlin, 2003, Phys. Rev. B **67**, 041303.
Evers, F., A. Mildenberger, and A. D. Mirlin, 2008, Phys. Rev. Lett. **101**, 116803.
Evers, F., and A. D. Mirlin, 2000, Phys. Rev. Lett. **84**, 3690.
Fabrizio, M., and C. Castellani, 2000, Nucl. Phys. B **583**, 542.
Fal'ko, V. I., and K. B. Efetov, 1995a, Europhys. Lett. **32**, 627.
Fal'ko, V. I., and K. B. Efetov, 1995b, Phys. Rev. B **52**, 17413.
Fendley, P., 2001, in *New Theoretical Approaches to Strongly Correlated Systems*, edited by A. M. Tsvelik (Kluwer, Dordrecht), p. 141.
Field, S. B., and T. F. Rosenbaum, 1985, Phys. Rev. Lett. **55**, 522.
Finkelstein, A. M., 1990, Sov. Sci. Rev., Sect. A **14**, 1.
Finkelstein, A. M., 1994, Physica B **197**, 636.
Fisher, D., 1995, Phys. Rev. B **51**, 6411.
Fleishman, L., and P. W. Anderson, 1980, Phys. Rev. B **21**, 2366.
Fleishman, L., D. C. Licciardello, and P. W. Anderson, 1978, Phys. Rev. Lett. **40**, 1340.
Fukui, T., 1999, Nucl. Phys. B **562**, 477.
Fukui, T., 2003, Phys. Rev. B **68**, 153307.
Fyodorov, Y. V., 1995, in *Mesoscopic Quantum Physics (Les Houches 1994)*, edited by E. Akkermans, G. Montambaux, J.-L. Pichard, and J. Zinn-Justin (North-Holland, Amsterdam), p. 493.
Fyodorov, Y. V., 2003, JETP Lett. **78**, 250.
Fyodorov, Y. V., and A. D. Mirlin, 1994, Int. J. Mod. Phys. B **8**,

3795.
Fyodorov, Y. V., and A. D. Mirlin, 1995, Phys. Rev. B **51**, 13403.
Fyodorov, Y. V., A. D. Mirlin, and H.-J. Sommers, 1992, J. Phys. I **2**, 1571.
Fyodorov, Y. V., and H.-J. Sommers, 1997, J. Math. Phys. **38**, 1918.
Gade, R., 1993, Nucl. Phys. B **398**, 499.
Gade, R., and F. Wegner, 1991, Nucl. Phys. B **360**, 213.
Gammel, B. M., and W. Brenig, 1994, Phys. Rev. Lett. **73**, 3286.
Gammel, B. M., and W. Brenig, 1996, Phys. Rev. B **53**, R13279.
Gammel, B. M., and F. Evers, 1998, Phys. Rev. B **57**, 14829.
Garcia, N., and A. Z. Genack, 1991, Phys. Rev. Lett. **66**, 1850.
Garcia-Garcia, A. M., 2006, Phys. Rev. E **73**, 026213.
Garcia-Garcia, A. M., and E. Cuevas, 2007, Phys. Rev. B **75**, 174203.
Garcia-Garcia, A. M., and K. Takahashi, 2004, Nucl. Phys. B **700**, 361.
Garcia-Garcia, A. M., and J. J. Verbaarschot, 2003, Phys. Rev. E **67**, 046104.
Genack, A. Z., and N. Garcia, 1991, Phys. Rev. Lett. **66**, 2064.
Giamarchi, T., 2004, *Quantum Physics in One Dimension* (Oxford University Press, Oxford, 2004).
Giamarchi, T., and H. Schulz, 1988, Phys. Rev. B **37**, 325.
Girvin, S. M., and M. Jonson, 1980, Phys. Rev. B **22**, 3583.
Gopar, V. A., K. A. Muttalib, and P. Wölfle, 2002, Phys. Rev. B **66**, 174204.
Gor'kov, L. P., A. I. Larkin, and D. Khmel'nitskii, 1979, JETP Lett. **30**, 248.
Gornyi, I. V., A. D. Mirlin, and D. G. Polyakov, 2005, Phys. Rev. Lett. **95**, 206603.
Gruzberg, I. A., N. Read, and A. W. W. Ludwig, 1999, Phys. Rev. Lett. **82**, 4524.
Gruzberg, I. A., N. Read, and S. Vishveshwara, 2005, Phys. Rev. B **71**, 245124.
Guhr, T., A. Müller-Gröling, and H. A. Weidenmüller, 1998, Phys. Rep. **299**, 189.
Guruswamy, S., A. LeClair, and A. W. W. Ludwig, 2000, Nucl. Phys. B **583**, 475.
Haldane, F. D. M., 1988, Phys. Rev. Lett. **61**, 2015.
Haldane, F. D. M., and E. H. Rezayi, 1988, Phys. Rev. Lett. **60**, 956; **60**, 1886(E) (1988).
Halsey, T. C., M. H. Jensen, L. P. Kadanoff, I. Procaccia, and B. I. Shraiman, 1986, Phys. Rev. A **33**, 1141.
Hatsugai, Y., X.-G. Wen, and M. Kohmoto, 1997, Phys. Rev. B **56**, 1061.
Heinzner, P., A. Huckleberry, and M. R. Zirnbauer, 2005, Commun. Math. Phys. **257**, 725.
Helgason, S., 1978, *Differential Geometry, Lie Groups, and Symmetric Spaces* (Academic, New York).
Hikami, S., 1981, Phys. Lett. **98B**, 208.
Hikami, S., 1983, Nucl. Phys. B **215**, 555.
Hirsch, M. J., U. Thomanschefsky, and D. F. Holcomb, 1988, Phys. Rev. B **37**, 8257.
Ho, C.-M., and J. T. Chalker, 1996, Phys. Rev. B **54**, 8708.
Hohls, F., U. Zeitler, and R. J. Haug, 2001, Phys. Rev. Lett. **86**, 5124.
Hohls, F., U. Zeitler, and R. J. Haug, 2002, Phys. Rev. Lett. **88**, 036802.
Hohls, F., U. Zeitler, R. J. Haug, R. Meisels, K. Dybko, and F. Kuchar, 2002, Phys. Rev. Lett. **89**, 276801.
Horovitz, B., and P. LeDoussal, 2002, Phys. Rev. B **65**, 125323.
Hsieh, D., D. Qian, L. Wray, Y. Xia, Y. S. Hor, R. J. Cava, and M. Z. Hasan, 2008, Nature (London) **452**, 970.
Hsu, S.-Y., and J. M. Valles, Jr., 1995, Phys. Rev. Lett. **74**, 2331.
Huckestein, B., 1995, Rev. Mod. Phys. **67**, 357.
Huckestein, B., and B. Kramer, 1990, Phys. Rev. Lett. **64**, 1437.
Huckestein, B., B. Kramer, and L. Schweitzer, 1992, Surf. Sci. **263**, 125.
Huo, Y., R. E. Hetzel, and R. N. Bhatt, 1993, Phys. Rev. Lett. **70**, 481.
Isichenko, M. B., 1992, Rev. Mod. Phys. **64**, 961.
Ivanov, D. A., 2002a, in *Vortices in Unconventional Superconductors and Superfluids*, edited by R. P. Huebener, N. Schopol, and G. E. Volovik (Springer, Berlin), p. 253.
Ivanov, D. A., 2002b, J. Math. Phys. **43**, 126.
Janßen, M., 1994, Int. J. Mod. Phys. B **8**, 943.
Janßen, M., 1998, Phys. Rep. **295**, 1.
Janßen, M., M. Metzler, and M. R. Zirnbauer, 1999, Phys. Rev. B **59**, 15836.
John, S., 1984, Phys. Rev. Lett. **53**, 2169.
John, S., 1987, Phys. Rev. Lett. **58**, 2486.
Jüngling, K., and R. Oppermann, 1980, Z. Phys. B: Condens. Matter **38**, 93.
Kagalovsky, V., B. Horovitz, Y. Avishai, and J. T. Chalker, 1999, Phys. Rev. Lett. **82**, 3516.
Kane, C. L., and E. J. Mele, 2005a, Phys. Rev. Lett. **95**, 226801.
Kane, C. L., and E. J. Mele, 2005b, Phys. Rev. Lett. **95**, 146802.
Khavin, Y. B., M. E. Gershenson, and A. L. Bogdanov, 1998, Phys. Rev. B **58**, 8009.
Khmelnitskii, D. E., 1984, JETP Lett. **38**, 552.
Khveshchenko, D. V., 2006, Phys. Rev. Lett. **97**, 036802.
Klesse, R., and M. Metzler, 1995, Europhys. Lett. **32**, 229.
Klesse, R., and M. Zirnbauer, 2001, Phys. Rev. Lett. **86**, 2094.
Koch, S., R. J. Haug, K. v. Klitzing, and K. Ploog, 1991, Phys. Rev. Lett. **67**, 883.
Koenig, M., S. Wiedmann, C. Bruene, A. Roth, H. Buhmann, L. W. Molenkamp, X.-L. Qi, and S.-C. Zhang, 2007, Science **318**, 766.
Kogan, I. I., C. Mudry, and A. M. Tsvelik, 1996, Phys. Rev. Lett. **77**, 707.
Kondev, J., and J. B. Marston, 1997, Nucl. Phys. B **497**, 639.
Kottos, T., 2005, J. Phys. A **38**, 10761.
Kramer, B., and A. MacKinnon, 1993, Rep. Prog. Phys. **56**, 1469.
Kramer, B., T. Ohtsuki, and S. Kettemann, 2005, Phys. Rep. **417**, 211.
Kratzer, P., and W. Brenig, 1994, Z. Phys. B: Condens. Matter **94**, 147.
Kravtsov, V. E., I. V. Lerner, and V. I. Yudson, 1988, Sov. Phys. JETP **67**, 1441.
Kravtsov, V. E., and K. A. Muttalib, 1997, Phys. Rev. Lett. **79**, 1913.
Kravtsov, V. E., and A. M. Tsvelik, 2000, Phys. Rev. B **62**, 9888.
Kravtsov, V. E., O. Yevtushenko, and E. Cuevas, 2006, J. Phys. A **39**, 2021.
Laughlin, R. B., 1998, Phys. Rev. Lett. **80**, 5188.
Lee, D. H., 1994, Phys. Rev. B **50**, 10788.
Lee, D.-H., and Z. Wang, 1996a, Philos. Mag. Lett. **73**, 145.
Lee, D.-H., and Z. Wang, 1996b, Phys. Rev. Lett. **76**, 4014.
Lee, P. A., and T. V. Ramakrishnan, 1985, Rev. Mod. Phys. **57**, 287.
Lerner, I. V., and F. Wegner, 1990, Z. Phys. B: Condens. Matter **81**, 95.
Levine, H., S. B. Libby, and A. M. M. Pruisken, 1983, Phys. Rev. Lett. **51**, 1915.

Levitov, L. S., 1990, Phys. Rev. Lett. **64**, 547.
Levitov, L. S., 1999, Ann. Phys. **8**, 697.
Lewenkopf, C. H., E. R. Mucciolo, and A. H. Castro Neto, 2008, Phys. Rev. B **77**, 081410(R).
Li, W., G. A. Csathy, D. C. Tsui, L. N. Pfeiffer, and K. W. West, 2005, Phys. Rev. Lett. **94**, 206807.
Ludwig, A. W. W., M. P. A. Fisher, R. Shankar, and G. Grinstein, 1994, Phys. Rev. B **50**, 7526.
Mandelbrot, B. B., 1974, J. Fluid Mech. **62**, 331.
Markos, P., 2006, Acta Phys. Slov. **56**, 561.
Markos, P., and L. Schweitzer, 2006, J. Phys. A **39**, 3221.
Markos, P., and L. Schweitzer, 2007, Phys. Rev. B **76**, 115318.
Marston, J. B., and S.-W. Tsai, 1999, Phys. Rev. Lett. **82**, 4906.
Mathur, H., 1997, Phys. Rev. B **56**, 15794.
McCann, E., K. Kechedzhi, V. I. Fal'ko, H. Suzuura, T. Ando, and B. L. Altshuler, 2006, Phys. Rev. Lett. **97**, 146805.
McKenzie, R. H., 1996, Phys. Rev. Lett. **77**, 4804.
Mello, P. A., P. Pereyra, and N. Kumar, 1988, Ann. Phys. (N.Y.) **181**, 290.
Mendez-Bermudez, J. A., and T. Kottos, 2005, Phys. Rev. B **72**, 064108.
Mendez-Bermudez, J. A., and I. Varga, 2006, Phys. Rev. B **74**, 125114.
Merkt, R., M. Janssen, and B. Huckestein, 1998, Phys. Rev. B **58**, 4394.
Merz, F., and J. T. Chalker, 2002, Phys. Rev. B **65**, 054425.
Mildenberger, A., and F. Evers, 2007, Phys. Rev. B **75**, 041303(R).
Mildenberger, A., F. Evers, and A. D. Mirlin, 2002, Phys. Rev. B **66**, 033109.
Mildenberger, A., F. Evers, A. D. Mirlin, and J. T. Chalker, 2007, Phys. Rev. B **75**, 245321.
Mildenberger, A., F. Evers, R. Narayanan, A. D. Mirlin, and K. Damle, 2006, Phys. Rev. B **73**, 121301(R).
Mildenberger, A., A. R. Subramaniam, R. Narayanan, F. Evers, I. A. Gruzberg, and A. D. Mirlin, 2007, Phys. Rev. B **75**, 094204.
Mil'nikov, G. V., and I. M. Sokolov, 1988, JETP Lett. **48**, 536.
Minkov, G. M., A. V. Germanenko, O. E. Rut, A. A. Sherstobitov, and B. N. Zvonkov, 2007, Phys. Rev. B **75**, 235316.
Mirlin, A. D., 2000a, in *New Directions in Quantum Chaos (Proceedings of the International School of Physics "Enrico Fermi" Course CXLIII)*, edited by G. Casati, I. Guarneri, and U. Smilansky (IOS, Amsterdam), p. 493.
Mirlin, A. D., 2000b, Phys. Rep. **326**, 259.
Mirlin, A. D., and F. Evers, 2000, Phys. Rev. B **62**, 7920.
Mirlin, A. D., F. Evers, and A. Mildenberger, 2003, J. Phys. A **36**, 3255.
Mirlin, A. D., and Y. V. Fyodorov, 1991, Nucl. Phys. B **366**, 507.
Mirlin, A. D., and Y. V. Fyodorov, 1994a, Phys. Rev. Lett. **72**, 526.
Mirlin, A. D., and Y. V. Fyodorov, 1994b, J. Phys. I **4**, 655.
Mirlin, A. D., Y. V. Fyodorov, F.-M. Dittes, J. Quezada, and T. H. Seligman, 1996, Phys. Rev. E **54**, 3221.
Mirlin, A. D., Y. V. Fyodorov, A. Mildenberger, and F. Evers, 2006, Phys. Rev. Lett. **97**, 046803.
Mirlin, A. D., A. Müller-Groeling, and M. R. Zirnbauer, 1994, Ann. Phys. (N.Y.) **236**, 325.
Moshe, M., H. Neuberger, and B. Shapiro, 1994, Phys. Rev. Lett. **73**, 1497.
Motrunich, O., K. Damle, and D. Huse, 2001, Phys. Rev. B **63**, 224204.
Motrunich, O., K. Damle, and D. A. Huse, 2002, Phys. Rev. B **65**, 064206.
Mudry, C., P. W. Brouwer, and A. Furusaki, 1999, Phys. Rev. B **59**, 13221.
Mudry, C., P. W. Brouwer, and A. Furusaki, 2000, Phys. Rev. B **62**, 8249.
Mudry, C., C. Chamon, and X.-G. Wen, 1996, Nucl. Phys. B **466**, 383.
Mudry, C., S. Ryu, and A. Furusaki, 2003, Phys. Rev. B **67**, 064202.
Muttalib, K. A., Y. Chen, and M. E. H. Ismail, 2001, in *Symbolic Computation, Number Theory, Special Functions, Physics and Combinatorics*, edited by F. G. Garvan and M. E. H. Ismail (Kluwer, Dordrecht), p. 199.
Muttalib, K. A., Y. Chen, M. E. H. Ismail, and V. N. Nicopoulos, 1993, Phys. Rev. Lett. **71**, 471.
Muttalib, K. A., and P. Wölfle, 1999, Phys. Rev. Lett. **83**, 3013.
Muttalib, K. A., P. Wölfle, and V. A. Gopar, 2003, Ann. Phys. **308**, 156.
Nelson, K., Z. Mao, Y. Maeno, and Y. Liu, 2004, Science **306**, 1151.
Nersesyan, A. A., A. M. Tsvelik, and F. Wenger, 1995, Nucl. Phys. B **438**, 561.
Nomura, K., M. Koshino, and S. Ryu, 2007, e-print arXiv:0705.1607.
Nomura, K., and A. H. MacDonald, 2007, Phys. Rev. Lett. **98**, 076602.
Novoselov, K. S., A. K. Geim, S. V. Morozov, D. Jiang, M. I. Katsnelson, I. V. Grigorieva, S. V. Dubonos, and A. A. Firsov, 2005, Nature (London) **438**, 197.
Novoselov, K. S., A. K. Geim, S. V. Morozov, D. Jiang, Y. Zhang, S. V. Dubonos, I. V. Grigorieva, and A. A. Firsov, 2004, Science **306**, 666.
Obuse, H., A. Furusaki, S. Ryu, and C. Mudry, 2007, Phys. Rev. B **76**, 075301.
Obuse, H., A. Furusaki, S. Ryu, and C. Mudry, 2008, Phys. Rev. B **78**, 115301.
Obuse, H., A. R. Subramaniam, A. Furusaki, I. A. Gruzberg, and A. Ludwig, 2007, Phys. Rev. Lett. **98**, 156802.
Obuse, H., A. R. Subramaniam, A. Furusaki, I. A. Gruzberg, and A. W. W. Ludwig, 2008, Phys. Rev. Lett. **101**, 116802.
Oganesyan, V., and D. A. Huse, 2007, Phys. Rev. B **75**, 155111.
Ohtsuki, T., K. Slevin, and B. Kramer, 2004, Physica E (Amsterdam) **22**, 248.
Onoda, M., Y. Avishai, and N. Nagaosa, 2007, Phys. Rev. Lett. **98**, 076802.
Oppermann, R., 1987, Nucl. Phys. B **280**, 753.
Oppermann, R., 1990, Physica A **167**, 301.
Ossipov, A., and Y. V. Fyodorov, 2005, Phys. Rev. B **71**, 125133.
Ostrovsky, P. M., I. V. Gornyi, and A. D. Mirlin, 2006, Phys. Rev. B **74**, 235443.
Ostrovsky, P. M., I. V. Gornyi, and A. D. Mirlin, 2007a, Phys. Rev. Lett. **98**, 256801.
Ostrovsky, P. M., I. V. Gornyi, and A. D. Mirlin, 2007b, Eur. Phys. J. Spec. Top. **148**, 63.
Paalanen, M. A., T. F. Rosenbaum, G. A. Thomas, and R. N. Bhatt, 1982, Phys. Rev. Lett. **48**, 1284.
Peskin, M. E., and D. V. Schroeder, 1995, *An Introduction to Quantum Field Theory* (Westview, Boulder).
Polyakov, D. G., and K. V. Samokhin, 1998, Phys. Rev. Lett. **80**, 1509.
Potempa, H., and L. Schweitzer, 2002, Phys. Rev. B **65**, 201105.
Prigodin, V. N., and B. L. Altshuler, 1998, Phys. Rev. Lett. **80**,

1944.
Pruisken, A. M. M., 1984, Nucl. Phys. B **235**, 277.
Pruisken, A. M. M., 1985, Phys. Rev. B **32**, 2636.
Pruisken, A. M. M., 1987, in *The Quantum Hall Effect*, edited by R. Prange and S. Girvin (Springer, Berlin).
Pruisken, A. M. M., and I. S. Burmistrov, 2005, Ann. Phys. **316**, 285.
Pruisken, A. M. M., D. T. N. de Lang, L. A. Ponomarenko, and A. de Visser, 2006, Solid State Commun. **137**, 540.
Punnoose, A., and A. M. Finkel'stein, 2005, Science **310**, 289.
Read, N., and D. Green, 2000, Phys. Rev. B **61**, 10267.
Read, N., and A. W. W. Ludwig, 2001, Phys. Rev. B **63**, 024404.
Rivas, J. G., R. Sprik, C. M. Soukoulis, K. Busch, and A. Lagendijk, 1999, Europhys. Lett. **48**, 22.
Roati, G., C. D'Errico, L. Fallani, M. Fattori, C. Fort, M. Zaccanti, G. Modugno, M. Modugno, and M. Inguscio, 2008, Nature (London) **453**, 895.
Rodriguez, A., L. J. Vasquez, and R. A. Roemer, 2008, e-print arXiv:0807.2209.
Rosenbaum, T. F., R. F. Milligan, M. A. Paalanen, G. A. Thomas, R. N. Bhatt, and W. Lin, 1983, Phys. Rev. B **27**, 7509.
Rycerz, A., J. Tworzydlo, and C. W. J. Beenakker, 2007, Europhys. Lett. **79**, 57003.
Ryu, S., C. Mudry, A. Furusaki, and A. W. W. Ludwig, 2007, Phys. Rev. B **75**, 205344.
Ryu, S., C. Mudry, H. Obuse, and A. Furusaki, 2007, Phys. Rev. Lett. **99**, 116601.
Sakai, H., and Y. Takane, 2005, J. Phys. Soc. Jpn. **74**, 1521.
Saleur, H., and B. Duplantier, 1987, Phys. Rev. Lett. **58**, 2325.
Schaefer, L., and F. Wegner, 1980, Z. Phys. B: Condens. Matter **38**, 113.
Scheffold, F., R. Lenke, R. Tweer, and G. Maret, 1999, Nature (London) **398**, 206.
Schnyder, A. P., S. Ryu, A. Furusaki, and A. W. W. Ludwig, 2008, e-print arXiv:0803.2786.
Schreiber, M., and H. Grussbach, 1996, Phys. Rev. Lett. **76**, 1687.
Schweitzer, L., and P. Markos, 2005, Phys. Rev. Lett. **95**, 256805.
Schweitzer, L., and H. Potempa, 1999, Physica A **266**, 486.
Schweitzer, L., and I. K. Zharekeshev, 1997, J. Phys.: Condens. Matter **9**, L441.
Schwinger, J., 1962, Phys. Rev. **128**, 2425.
Seiberg, N., 1990, Prog. Theor. Phys. Suppl. **102**, 319.
Senthil, T., and M. P. A. Fisher, 1999, Phys. Rev. B **60**, 6893.
Senthil, T., and M. P. A. Fisher, 2000, Phys. Rev. B **61**, 9690.
Senthil, T., M. P. A. Fisher, L. Balents, and C. Nayak, 1998, Phys. Rev. Lett. **81**, 4704.
Senthil, T., J. B. Marston, and M. P. A. Fisher, 1999, Phys. Rev. B **60**, 4245.
Shapiro, B., 1982, Phys. Rev. Lett. **48**, 823.
Shapiro, B., 1987, Philos. Mag. B **56**, 1031.
Sheng, L., D. N. Sheng, C. S. Ting, and F. D. M. Haldane, 2005, Phys. Rev. Lett. **95**, 136602.
Shklovskii, B. I., B. Shapiro, B. R. Sears, P. Lambrianides, and H. B. Shore, 1993, Phys. Rev. B **47**, 11487.
Slevin, K., and T. Nagao, 1993, Phys. Rev. Lett. **70**, 635.
Slevin, K., and T. Ohtsuki, 1999, Phys. Rev. Lett. **82**, 382.
Störzer, M., P. Gross, C. M. Aegerter, and G. Maret, 2006, Phys. Rev. Lett. **96**, 063904.
Stupp, H., M. Hornung, M. Lakner, O. Madel, and H. v. Löhneysen, 1993, Phys. Rev. Lett. **71**, 2634.
Stupp, H., M. Hornung, M. Lakner, O. Madel, and H. v. Löhneysen, 1994, Phys. Rev. Lett. **72**, 2122.
Subramaniam, A. R., I. A. Gruzberg, A. W. W. Ludwig, F. Evers, A. Mildenberger, and A. D. Mirlin, 2006, Phys. Rev. Lett. **96**, 126802.
Suzuura, H., and T. Ando, 2002, Phys. Rev. Lett. **89**, 266603.
Takane, Y., 2004a, J. Phys. Soc. Jpn. **73**, 9.
Takane, Y., 2004b, J. Phys. Soc. Jpn. **73**, 2366.
Takane, Y., 2004c, J. Phys. Soc. Jpn. **73**, 1430.
Thomas, G. A., Y. Ootuka, S. Katsumoto, S. Kobayashi, and W. Sasaki, 1982, Phys. Rev. B **25**, 4288.
Thomas, G. A., M. Paalanen, and T. F. Rosenbaum, 1983, Phys. Rev. B **27**, 3897.
Thouless, D., 1974, Phys. Rep., Phys. Lett. **13**, 93.
Thouless, D., 1977, Phys. Rev. Lett. **39**, 1167.
Titov, M., P. W. Brouwer, A. Furusaki, and C. Mudry, 2001, Phys. Rev. B **63**, 235318.
Tsvelik, A. M., 1995, Phys. Rev. B **51**, 9449.
Tsvelik, A. M., 2007, Phys. Rev. B **75**, 184201.
Van Keuls, F. W., H. Mathur, H. W. Jiang, and A. J. Dahm, 1997, Phys. Rev. B **56**, 13263.
van Schaijk, R. T. F., A. de Visser, S. M. Olsthoorn, H. P. Wei, and A. M. M. Pruisken, 2000, Phys. Rev. Lett. **84**, 1567.
Varga, I., 2002, Phys. Rev. B **66**, 094201.
Vasquez, L. J., A. Rodriguez, and R. A. Roemer, 2008, e-print arXiv:0807.2217.
Verbaarschot, J. J. M., H. A. Weidenmüller, and M. R. Zirnbauer, 1985, Phys. Rep. **129**, 367.
Verbaarschot, J. J. M., and I. Zahed, 1993, Phys. Rev. Lett. **70**, 3852.
Vollhardt, D., and P. Wölfle, 1980, Phys. Rev. B **22**, 4666.
von Klitzing, K., G. Dorda, and M. Pepper, 1980, Phys. Rev. Lett. **45**, 494.
Waffenschmidt, S., C. Pfleiderer, and H. v. Löhneysen, 1999, Phys. Rev. Lett. **83**, 3005.
Wakabayashi, K., Y. Takane, and M. Sigrist, 2007, Phys. Rev. Lett. **99**, 036601.
Wang, Z., M. P. A. Fisher, S. M. Girvin, and J. T. Chalker, 2000, Phys. Rev. B **61**, 8326.
Wang, Z., B. Jovanovic, and D.-H. Lee, 1996, Phys. Rev. Lett. **77**, 4426.
Wang, Z., and S. Xiong, 2002, Phys. Rev. B **65**, 195316.
Wegner, F., 1976, Z. Phys. B **25**, 327.
Wegner, F., 1979, Z. Phys. B **35**, 207.
Wegner, F., 1980, Z. Phys. B **36**, 209.
Wegner, F., 1985, in *Localisation and Metal Insulator transitions*, edited by H. Fritzsche and D. Adler (Plenum, New York), p. 337.
Wegner, F., 1987, Nucl. Phys. B **280**, 210.
Wegner, F., 1989, Nucl. Phys. B **316**, 663.
Wegner, F., 1990, Z. Phys. B: Condens. Matter **78**, 36.
Wei, H. P., D. C. Tsui, M. A. Paalanen, and A. M. M. Pruisken, 1988, Phys. Rev. Lett. **61**, 1294.
Weidenmüller, H., 1987, Nucl. Phys. B **290**, 87.
Wiersma, D. S., P. Bartolini, A. Lagendijk, and R. Righini, 1997, Nature (London) **390**, 671.
Wigner, E. P., 1951, Ann. Math. **53**, 36.
Witten, E., 1984, Commun. Math. Phys. **92**, 455.
Wölfle, P., and R. N. Bhatt, 1984, Phys. Rev. B **30**, 3542.
Yamada, H., and T. Fukui, 2004, Nucl. Phys. B **679**, 632.
Yang, S.-R. E., A. H. MacDonald, and B. Huckestein, 1995, Phys. Rev. Lett. **74**, 3229.
Yevtushenko, O., and V. E. Kravtsov, 2003, J. Phys. A **36**, 8265.
Yevtushenko, O., and V. E. Kravtsov, 2004, Phys. Rev. E **69**,

026104.
Zabrodskii, A. G., and K. Zinov'eva, 1984, Sov. Phys. JETP **59**, 425.
Zamolodchikov, A. B., and A. B. Zamolodchikov, 1996, Nucl. Phys. B **477**, 577.
Zhang, Y., Y.-W. Tan, H. L. Stormer, and P. Kim, 2005, Nature (London) **438**, 201.
Ziff, R. M., X. P. Kong, and E. G. D. Cohen, 1991, Phys. Rev. A **44**, 2410.
Ziman, T. A. L., 1982, Phys. Rev. Lett. **49**, 337.
Zirnbauer, M. R., 1986a, Phys. Rev. B **34**, 6394.
Zirnbauer, M. R., 1986b, Nucl. Phys. B **265**, 375.
Zirnbauer, M. R., 1992, Phys. Rev. Lett. **69**, 1584.
Zirnbauer, M. R., 1994, Ann. Phys. **3**, 513.
Zirnbauer, M. R., 1996, J. Math. Phys. **37**, 4986.
Zirnbauer, M. R., 1997, J. Math. Phys. **38**, 2007.
Zirnbauer, M. R., 1999, e-print arXiv:hep-th/9905054v2.
Zirnbauer, M. R., 2004, e-print arXiv:math-ph/0404057.